Sorption/Desorption and Photodegradation of Dispersed Oil Components in Marine Ecosystem

by

Xiao Zhao

A dissertation submitted to the Graduate Faculty of
AuburnUniversity
in partial fulfillment of the
requirements for the Degree of
Doctor of Philosophy

Auburn, Alabama
August 1, 2015

Keywords: Oil dispersants, SedimentSorption,
Polycyclic Aromatic Hydrocarbon, Photodegradation, Photocatalyst

Approved by

Dongye Zhao, Chair, Professor of Environmental Engineering
Mark Barnett, Professor of Environmental Engineering
Prabhakar Clement, Professor of Environmental Engineering
Xinyu Zhang, Associate Professor of Polymer and Fiber Engineering
Anne Gorden, Associate Professor of Chemistry and Biochemistry

Abstract

This effects of a prototype oil dispersant on solubilization, sorption, and desorption of three model Polycyclic aromatic hydrocarbons (PAHs) in sediment-seawater systems were investigated. Increasing dispersant dosage linearly enhanced solubility for all PAHs. Conversely, the dispersant enhanced the sediment uptake of the PAHs, and induced significant desorption hysteresis. Such contrasting effects (adsolubilization vs. solubilization) of dispersant were found dependent of the dispersant concentration and PAH hydrophobicity. The dual-mode models adequately simulated the sorption kinetics and isotherms, and quantified dispersant-enhanced PAH uptake. Sorption of naphthalene and 1-methylnaphthalen by sediment positively correlated with uptake of the dispersant, while sorption of pyrene dropped sharply when the dispersant exceeded critical micelle concentration (CMC). The deepwater conditions diminished the dispersant effects on solubilization, but enhanced uptake of the PAHs, albeit sorption of the dispersant was lowered. The information may aid in understanding roles of dispersants on distribution, fate and transport of petroleum PAHs in marine systems.

Fate of dispersed petroleum hydrocarbons in marine systems were investigated and the effects of typical weathering process including dispersion, sorption and photodegradation on distribution of representative petroleum hydrocarbons were examined in this work. Corexit 9500A was used to prepare dispersed water accommodated oil (DWAO) under varied dispersant-oil-ratios (DORs). Higher doses of dispersant can disperse more *n*-alkanes and PAHs

into thewater column. Some petroleum with lower molecular weight was dispersed more favorably, while the solubilization of longer chained alkanes (C30-C40) and PAHs with 5-6 rings were not enhanced even with a high DOR of 1:2. Three dispersants (Corexit 9500A, Corexit 9527A and SPC 1000) were compared for dispersing the petroleum hydrocarbons. For *n*-alkanes, the Corexit 9500A disperse both C11-C18 and C19-C28 effectively, and Corexit 9527A favored to disperse short chained alkanes (C10-C16). SPC 1000 was the most effective dispersant which can disperse a broader range of alkanes (C12-C28). Further addition of 180 mg/L of dispersant into the DWAO can enhance the solubilization effect thereby loweringthe uptake of both PAHs and *n*-alkanes onto a loamy sand. In the DWAO, both *n*-alkanes and PAHs were readily photo-degraded under typical marine surface sunlight. Intensive alkylation of PAHs was observed in Day 3 and the concentrations of alkylated PAHs reached themaximumvalues in Day 3, subsequentlyfollowed by a rapiddecay in Day 4- continuing until Day 14.

We prepared and characterized a new type of photocatalyst, referred to as cobalt-doped titanate nanotubes (Co-TNTs), using TiO_2 (P25) as the precursor through a two-step process (hydrothermal reaction at 150 ºC followed by calcination at 600 °C). The optimal catalyst (Co-TNTs-600) was obtained at a Co loading of 2.26 wt.% and calcination temperature of 600 ºC. The catalyst effectively catalyzes photodegradation of phenanthrene (a model polycyclic aromatic hydrocarbon) under simulated solar light. The pseudo first-order rate constant was determined to be 0.39 h^{-1}, about 10 times that of the conventional photocatalyst TiO_2. TEM, XRD and XPS analyses indicate that Co-TNTs-600 is a composite nanomaterial containing titanate, anatase and CoO crystals. The hydrothermal treatment converts TiO_2 into tubular, multilayered titanate nanotubes, allowing for incorporation Co(II) ions on the matrices. The subsequent calcination partially transforms titanate into anatase and the adsorbed Co^{2+} ions into

CoO. UV-vis DRS spectra suggest that the absorption edge of Co-TNTs-600 shifts to the visible light region compared to P25 and un-calcined titanate nanotubes (TNTs), and the new catalyst displays a narrower optical energy band of 2.8 eV compared to 3.2 eV for P25 and 3.4 eV for TNTs. The incorporated CoO acts as an electron transfer mediator, which prevents the recombination of hole-electron pairs created mainly by anatase under solar irradiation. In addition, the Co-TNTs-600 exhibits good reusability and can be gravity-separated and reused in multiple cycles of operations for phenanthrene photodegradation. This new catalyst appears promising for catalyzing photodegradation of persistent PAH.

Acknowledgments

I would never have been able to finish my dissertation without the help and support of my committee members, friends, and family.

First and foremost, I would like to express my deepest gratitude to my major advisor, Dr. Dongye Zhao, for his guidance, inspiration, patience, motivation, and friendship. He taught me not only how to design and conduct experiments, but also to think creatively. With his continuous and unconditional help, I developed the research ideas and wrapped up all of them into this dissertation. I have learned a lot from his expertise of environmental engineering and chemistry and I thank him for everything he has done for me.

Additional thanks to Drs. Mark Barnett, Prabhakar Clement, Xinyu Zhang and Anne Gorden for their support and services on my Ph.D. committee. Their valuable advice, enlightening guidance, and inspiring comments all make this dissertation into a better shape. Sincere appreciation is also extended to Dr. Yucheng Feng, who served in the committee as my outside reader and also helped a lot on several analytical instrumentations. Thanks to Jinling Zhuang for assistance in the lab and technical guidance. Thanks to my fellow students in the environmental engineering program for their friendship, helps, and creating a happy environment. Special thanks go to my roommate Wenbo for his help and careduring the past 5 years. I deeply appreciate Dr. Wen Liu for all the support and I really enjoyed the discussing moments over our lunch.

Finally, I would like to thank my wife and parents for their endless love and unconditional support.

Table of Contents

List of Tables

List of Figures

List of Abbreviations

CMC	Critical Micelle Concentration
CPI	Carbon Preference Index
DOM	Dissolved Organic Matter
DOR	Dispersant Oil Ratio
DWAO	Dispersed Water Accommodated Oil
DwH	Deepwater Horizon
LSC	Louisiana Sweet Crude
PAHs	Polycyclic Aromatic Hydrocarbons
SER	Surfactant Enhanced Remediation
SOM	Soil Organic Matter
SPM	Suspended Particulate Matter
TNTs	Titanate nanotubes
WAO	Water Accommodated Oil

Chapter 1. General Introduction

1.1.Introduction of 2010 Deepwater Horizon (DwH) oil spill

With growing demands for energy and global industrialization of petroleum exploitation, frequent oil spill accidents have occurred worldwide during last 50 years(Wang and Fingas 1997). The released oil can damage the natural ecosystem and become persistent, thereby threatening to the health ofcoastal creatures and human beings even several years after the spill. During the catastrophic 2010 Deepwater Horizon (DwH) spill, massive and unprecedented amounts of liquid petroleum and methane gas were released into the water column from the Macondo well at a depth of about 1500 m (Diercks et al. 2010). Between the blowout on April 20th and the final closure on July 15th, the estimated total leakage of crude oil was 7.94×10^8 to 1.11×10^9 L with a maximum expression coverage of 62159 km^2(Reddy et al. 2012, Sammarco et al. 2013). As part of the remediation process, approximately 8.21×10^6 L chemical dispersant was applied, 5.30×10^6 L of them (both Corexit EC9500A and Corexit 9527A) was sprayed to the surface and 2.91×10^6 L (Corexit EC9500A only) was injected into the oil stream at the wellhead (Kujawinski et al. 2011),and it is noteworthy that this markedthe first time to use chemical dispersant at such depth. The spilled Louisiana Sweet Crude (LSC) oil contained saturated *n*-alkanes, polycyclic aromatic hydrocarbons (PAHs), and their alkylated homologues with over 50% as low-molecular-weight petroleum hydrocarbons (methane and C2-C11) (Ryerson et al. 2012). During the spill, the elevated concentration of oil components such as *n*-alkanes, PAHs (both parent PAHs and alkylated ones), benzene, toluene, ethylbenzene and xylene (BTEX) were detected both in surface water samples and deepwater samples (Camilli et al. 2010, Diercks et al. 2010a, Sammarco et al. 2013, Wade et al. 2011). During the one-year period after the DwH incident, the reported PAHs levels in all the tested seafood samples (fish,

shrimp, crab, and oyster samples collected from the Mississippi Gulf Coast areas) were far below the public health Levels of Concern (LOC) established jointly by the NOAA/FDA/Gulf Coast states, and the fishing areas were reopened later (Xia et al. 2012);however, based on a field study tracking gill tissues of larval and adult fish in the Louisiana area, aberrant protein expression, physiological and reproductive impairment was observed (Whitehead et al. 2011). In addition, a recent study conducted at municipal Pensacola Beach, FL, revealed that the spilled oil had a profound impact on both abundance and community composition of indigenous bacteria in marine system (Kostka et al. 2011). Overall, the long-term effects of this environmental disaster is still unfolding, and researchers have suggested the use of a range of plausible risk parameters and long-term monitoring strategies for metals as well as PAHs to determine the safety of seafood in related area (Gohlke et al. 2011).

1.2.Effects of dispersants on the sorption/desorption behaviors of PAHs

PAHs are one of the key components in crude oil and also the products of incomplete combustion, such as an explosion or the in-situ burning process in oil spill accidents. Due to their toxic, mutagenic, carcinogenic and persistent properties, PAHs represent the most toxic contaminants associated with oil spills and are a major environmental concern to federal agencies (Nam et al. 2008). Elevated concentrations of EPA listed PAHs, like naphthalene, phenanthrene, pyrene, chrysene, and benzo(a)pyrene were detected in Gulf of Mexico during and after the 2010 DwH oil spill. The spilled oil contains about 3.9% of PAHs by weight and a total of 2.1×10^{10} g of PAHs was released into water column in DWH oil spill (Reddy et al. 2012).

In marine systems, the fate and transport of PAHs are associated with the processes of solubilization, biodegradation, sorption on, and desorption from the sediments and suspended

particulate matter (SPM) and dilution into the water column. The vertical transportation of SPM combined with deep-sea blowout makes the PAHs more easily incorporated to the bottom sediments, more resistant to biotic or abiotic degradation resulting in long-time persistency(Gearing et al. 1980, Yamada et al. 2003). In addition, the horizontal SPM movement with the current could transport PAHs into the open ocean or to places away from the local contamination site (Tremblay et al. 2005).

In a soil/sediment-water system, distributions of PAHs aremainly governed by the soil organic matter (SOM) content and the properties of the PAHs. SOM usually exerts the greatest thermodynamic affinity for hydrophobic compounds, and the soil with higher SOM level usually provides higher sorption capacity (White and Pignatello 1999, Zhao et al. 2001). The PAHs with molecular weight are less soluble and more favorable to sorption sites on SOM. Temperature, salinity, and dissolved organic matter (DOM) are also potential factors affecting the PAHs sorption to soil/sediments. Researchers have reported an inverse relationship between temperature and sorption coefficient, and have attributed the phenomenon to factors such as the exothermic nature of the adsorption, lowered solubility of PAHs, and alternation of SOM structure at lower temperature (Tremblay et al. 2005, Zhang et al. 2009). Yu, et al. (Yu, et al. 2011) observed that the presence of DOM in soil systems inhibits sorption of PAHs and increases desorption. In all these cases, water solubility is considered a key factor affecting the sorption behavior of PAHs (Rivas 2006).

Dispersants are usually applied as remediation in response to anoil spill aiming to lower the interfacial tension between oil and water and break oil slicks to small (<100μm) and dispersed micelles, which are easier to be dissolved into the water column and degraded (Kujawinski et al. 2011). Besides organic solvents, the essential components in dispersant formulations are

surfactants, which contain both lipophilic/hydrophobic and hydrophilic groups. Commonly used dispersant components are a mixture of two nonionic surfactants, sorbitan monooleate (Span 80) and ethoxylated sorbitan monooleate (Tween 80), together with an anionic surfactant dioctyl sodium sulfosuccinate (DOSS) (Thibodeaux et al. 2011). For example, the Corexit 9527 and 9500 series dispersants contain the same surfactants, i.e. Span 80, Tween 80, Tween 85, but with different solvents (Scelfo and Tjeerdema 1991). Corexit 9527 contains the hydrocarbon solvent ethylene glycol monobutylether (17%), and both non-ionic (48%) and anionic (35%) surfactants. Corexit 9500 is a more recent formulation with better penetration and emulsion fighting properties and same surfactants (Mitchell and Holdway 2000).

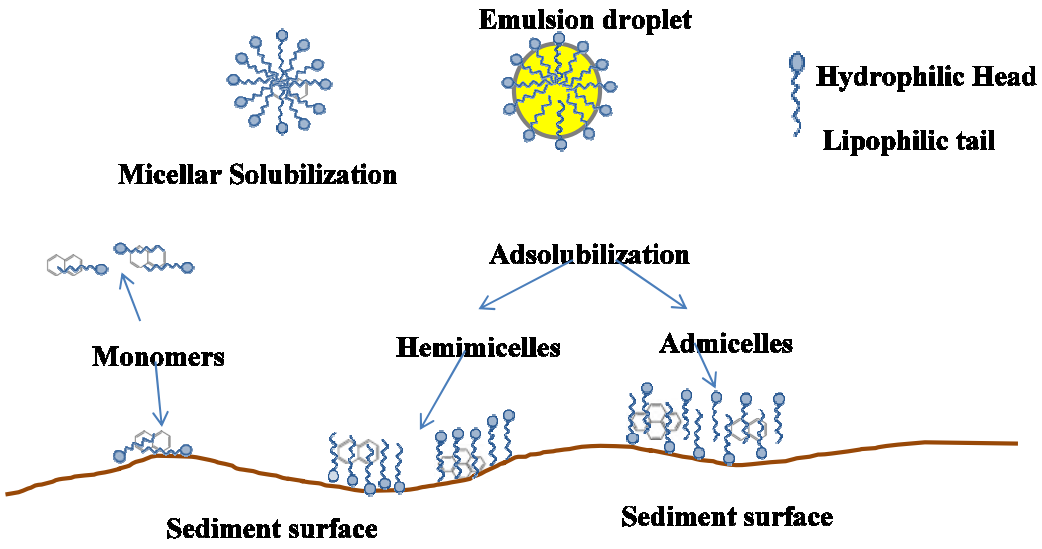

Fig. 1-1. Surfactant effects on sorption and dispersion of PAHs in sediment/water systems.

Even though the dispersants have been applied as a response measure in oil spills for decades, limited research has investigated their effects on PAHs fate, transportation and sorption/desorption behavior in marine system. As the key components of dispersants, surfactants were reported to have contrasting effects on the sorption of PAHs by sediments. As

depicted in Fig. 1-1, the surfactants can exist in several types of forms: micelles, monomers, hemimicelles and admicells. On one hand, the partitioning of PAHs into surfactants micelles or monomers can increase the apparent solubility of PAHs therefore enhance their mobility. This process is usually termed “solubilization” or “micellar solubilization”. Many studies reported the increase of solubilities of PAHs after adding anionic, nonionic or anionic-nonionic surfactant mixtures due to the PAH-cored micelle formation, and *in-situ* surfactant-enhanced remediation (SER) technology was widely used to mobilize the retarded PAHs in sediments by adding certain surfactants (Zhao et al. 2005). On the other hand, the surfactants can also be adsorbed by the soil matrix and provide additional sorption sites for PAHs, thereby enhancingthe PAHs retardation (Ko et al. 1998). This process is named “adsolubilization”. The sorbed surfactants molecules can assemble and form the aggregate termed “hemimicelles” or “admicelles”, which can serve as strong absorbents for PAHs.

In addition, in the oil spill accidents, since released oil can serve as solvent for PAHs due to high hydrophobicity, the PAHs distribution will be significantly influenced after the introduction of crude oil or dispersed oil. Walter et al. (2000) investigated distribution of 9 PAHs in oil contaminated soil systems and found that oil phase in the system drastically decreased the amount of PAHs associated with the soil surface and in the aqueous phase, resulting in more PAHs distributed in the adsorbed and liquid oil phases. As for the DwH oil spill case, the blowout site was located deep, and so far there is no fundamental study on the PAHs behavior under such deepwater conditions. For environmental study, deepwater conditions are referred to high pressure (usually higher than 16 MPa, even up to 100 Mpa), low temperature (-1 to 4 °C), little or no light, constant salinity (3.5%), sluggish currents (<0.25 knots), and slow sediment accumulation rates (0.1-10 cm per thousands of years) (Glover and Smith 2003). As yet no

fundamental studies have explored the PAHs sorption/desorption behavior under deepwater conditions, especially combined with the introduction of dispersant.

1.3.Fate of dispersed petroleum hydrocarbons in marine system: dispersion, sorption and photodegradation

The overall chemical fate of spills in the DwH accident is unclear, not only because of the unprecedented amount of both spilled oil and dispersants applied, but also owing to the fact that the spilled oil experienced a unique series of processes following their release at a depth of 1500 m (Reddy et al. 2012). The released oil was subjected to a variety of weathering processes including evaporation, dissolution, dispersion, photochemical oxidation, water-oil emulsification, bio-degradation and adsorption onto suspended particulate materials (Wang and Fingas 1997). Based on the oil budget calculator developed by Department of Interior (DOI) and National Oceanic and Atmospheric Administration (NOAA), the direct recovery from the wellhead, burning and skimming removed 17%, 5% and 3% of spilled oil, respectively (Lubchenco 2010). And 25% of the oil was naturally evaporated or dissolved during the travel from wellhead to gulf surface/shoreline. Chemical dispersion and natural dispersion processes accounted for 8% and 16% removal of total oil respectively. The residual amount (26%) included the oil on/below the surface in forms of light sheen or tar balls under other natural degrading processes.

Both dissolution and dispersion are important processes governing the fate of released oil and they are two different concepts. Dissolution is the process by which oil hydrocarbons are dissolved into water forming a solution. While dispersion is the processes by which oil are broken down into smaller droplets and dispersed into water column (Lubchenco 2010). The petroleum hydrocarbons are sparingly soluble due to its high hydrophobicity, while the

dispersion processes can enhance the dissolution of hydrocarbons into water column and increase their bioavailability. The *n*-alkanes are extremely insoluble, for instance the solubility of *n*-decane ($C_{10}H_{22}$) is only 51 μg/L and the solubility gets lower for longer chained *n*-alkanes (Diallo et al. 1994). PAHs are considerably more soluble and are believed the major soluble fraction of petroleum,withnaphthalene asthe most soluble one with a solubility as high as 30 mg/L (Fu et al. 2014, Zhao et al. 2015). Both*n*-alkanes and PAHs can be effectively solubilized *via* commonly used surfactants (Bruheim et al. 1999, Edwards et al. 1991). Surfactants can originate from eithernatural or anthropogenic sources. Microorganisms can produce extracellular biosurfactants to promote the formation of oil emulsions thereby enhancing the dispersion of spilled oil (Desai and Banat 1997), at the same time, the fatty acid moieties of biosurfactants can also boost the growth of bacteria on the surface of oil droplets (Rosenberg et al. 1979). Dispersants are mainly composed of surfactants and have been used for oil spill mitigation for more than 50 years (Board 2005). Both surfactants and solvents in dispersants are responsible for solubilizing the petroleum hydrocarbons. Typical light crude and heavy crude have solubility of 10-50 and 5-30 mg/L, respectively (Fingas 2012). After examining 8 EPA approved dispersants, researchers observed that the total petroleum hydrocarbons (TPHs) ranges from 6.8 mg/L for JD-2000 to 1800 mg/L for ZI-400 in water column with a dispersant-oil ratio (DOR) of 1:10. By using Corexit 9500A at a DOR of 1:100, researchers observed the total *n*-alkanes increased by 75 fold (Özhan et al. 2014). Dispersant Corexit EC9500A can also effectively solubilize both parent PAHs and their alkylated homologous (Gong et al. 2014b, Zhao et al. 2015);however, there is limited data available onthe effects of DORs on the distribution of dispersed petroleum hydrocarbons. Furthermore, the information on the mechanism of dispersion for individual dispersants and how they interact with the components of petroleum is required to make the best

selection of dispersant for a particular remediation.The sorption of petroleum hydrocarbons onto suspended particulate matter or sediments is recognized as an important process for oil transport and studies have revealed that the interactions between oil and sediments play an crucial role in dispersion and degradation of spilled oil (Fu et al. 2014). In a sediment-water system, the distribution of petroleum hydrocarbons are mainly governed *via* soil organic matter (SOM) content and properties of hydrocarbons. The introduction of dispersant into the system will cause contrasting effects and alter the sorption behavior of oil components in two ways: on one hand, the dispersant can enhance the solubilization of petroleum hydrocarbons thereby favoring the desorption process; on the other hand, the surfactants molecules can also be sorbed on soil surface then serve as stronger sorption sink for petroleum hydrocarbons resulting in more petroleum hydrocarbons sorption into soil matrix.

Photo-degradation mediated by sunlight is another important process for transformation/decay of petroleum hydrocarbons in marine system, and yet, it is important to note that the effects sunlight irradiation are different for different petroleum hydrocarbons. The *n*-alkanes are readily bio-degraded, but they are almost totally unaffected by sunlight irradiation due to their lack of ability to absorb UV (Tjessem and Aaberg 1983). It has also been reported that the photo-degradation of *n*-alkanes were enhanced with increasing amounts of photo-sensitizer (commonly used were quinones or PAH-alcohols, such as anthraquinone or 1-naphthol) present (Boukir et al. 2001, Guiliano et al. 1997). Theoretically, PAHs should beintrinsically stable considering the π electrons delocalized over the aromatic rings, but they are highly photo-reactive owing to their ability to absorb light in UV region, thus, direct photolysis is the main mechanism associated with the degradation of linear PAHs (Plata et al. 2008). When researchers investigate the photolysis of mixture of PAHs and *n*-alkanes (1:100 mole/mole)

under UV, they observed photoalkylation occurred readily and significant amount of alkylated PAHs were formed within 5h of irradiation and nearly 47% of *n*-hexadecane was alkylated (Mahajan et al. 2003). How the dispersed petroleum hydrocarbons will transform under a typical sunlight irradiation is still unknown. The overall processes can be depicted in Fig. 1-2.

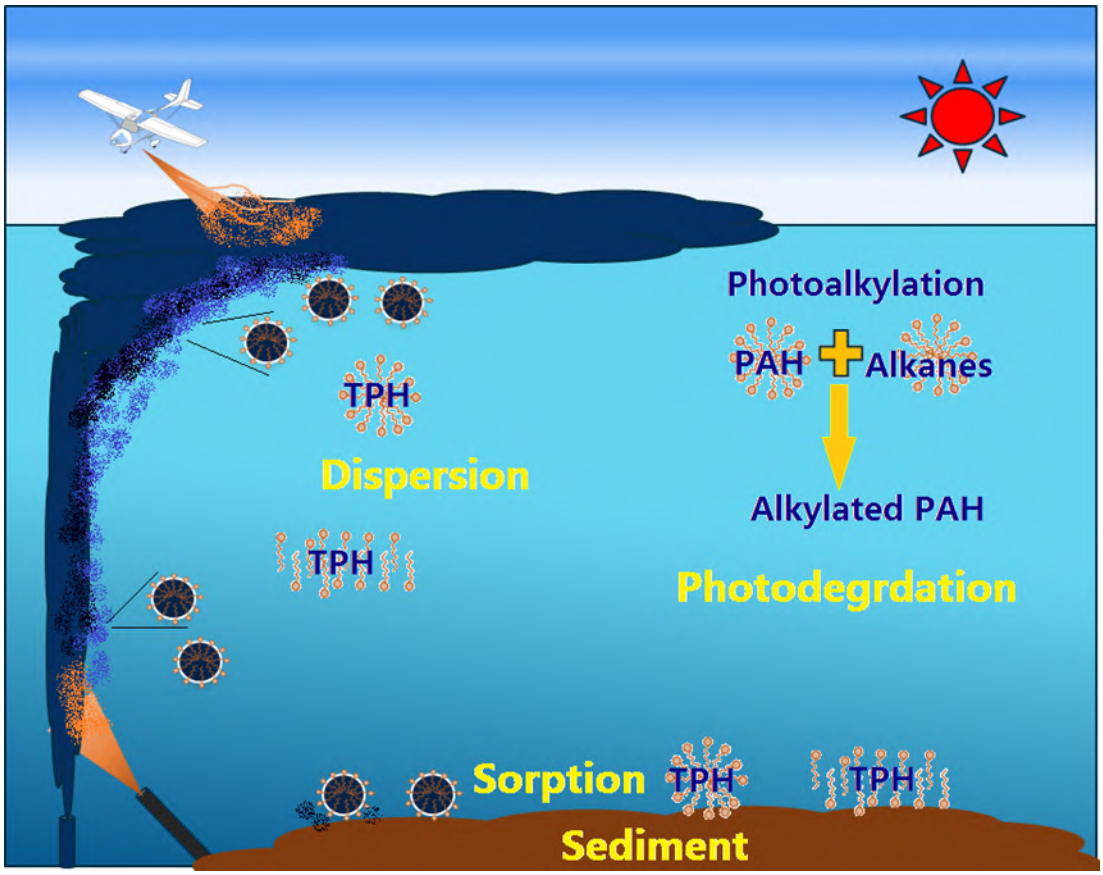

Fig. 1-2. Overall fate of dispersed petroleum hydrocarbons

1.4.New materials for enhanced photocatalytic degradation of PAHs

In recent years, water pollution and the lack of clean and cost-effective energy sources are seen as key challenges on a global scale (Shannon et al. 2008). Since the energy of the sun can be harnessed for sustainable use through photocatalysis, green and efficient photocatalysts are a great choice for water decontamination (Schneider et al. 2014). TiO_2-devised materials have attracted tremendous interest for this applicationdue to their utility in solar-driven hydrogen

production, in photocatalytic decomposition of organic contaminants, and in absorbents for environmental remediation (Chen and Burda 2008, Chen and Mao 2007, Liu et al. 2013b, Pelaez et al. 2012, Tan et al. 2014). TiO_2 is typical an *n*-type semiconductor with relatively large band gap,its three main crystal phases are anatase, rutile and brookite, withe band gaps of ca. 3.2, 3.0 and 3.2 eV respectively(Pelaez et al. 2012). Even though TiO_2 can effectively utilize UV light, its large band gap limits its optical absorption in the solar spectrum, which consists primarily of UV, visible and infrared (IR) radiation with relative energy distribution of ~5%, 43% and 55% respectively (Chen et al. 2015, Shankar et al. 2015). Thereforeresearchers have pursued means toimprove the visible light absorption of TiO_2. Further complicating this problem, poor aggregation and sedimentation characteristics limit the separation and reuse of the nanoparticles ofTiO_2(Liu et al. 2013a).

To date, one-dimensional (1D) titanate nanotubes (TNTs) synthesized usinghydrothermal methodsand TiO_2 as precursor have gained significant scientific interest. The TNTs can serve as excellent adsorbents for heavy metals owing to their high specific area, great ion-exchange properties and abundant functional groups (Liu et al. 2013b, Wang et al. 2013a, Xiong et al. 2011b). However, TNTs aredemonstrated to be poor photocatalysts despite their higher surface area and good crystallized structure, and the main reason is addressed to the high electron-hole recombination rate after excitation under illumination (Kim et al. 2012, Lee et al. 2007, Yu et al. 2006a). Therefore, increasing numbers of researchers have attempted to enhance the photocatalytic activity of TNTs. Some commonly used modification approach includes calcination (Lin et al. 2008, Yu et al. 2006b), H_2O_2 treatment (Khan et al. 2006), acid treatment (Chen et al. 2015a), and surface modification using non-metal such as F and P (Kim et al. 2012), and metals including Cu, Pd, W (Chen et al. 2013, Grandcolas et al. 2013). Among these

approaches, metal doping is quite promising due to the fact that appropriate dopant can not only absorb visible light, but also inhibit the recombination of electron holes pairs. Compared to the intensive work associated with precious metal doping, the exploration of the use of less expensive transitionmetalshas beenlimited. Cobalt is one of the commonly used metal for making oxide/TiO_2 composites, and cobalt oxide has been found to narrow band gaps (with CoO and Co_3O_4 have band gaps of ~2.4 and 2.19 eV respectively), which may be of benefit in extending the utility of the material into the visible wavelengths (Dahl et al. 2014). When compared to the P25 or bare TiO_2, cobalt oxide/TiO_2 composite showed considerable improvement on organic compound photo-oxidation and H_2 production rate (Dai et al. 2013, Wang et al. 2013b, Zhang et al. 2012). Thus, cobalt is a potential alternative dopant for enhancing the photocatalytic activities of TNTs for PAH degradation.

1.5.Objectives

The overall goal of this dissertation is to: 1) investigate the effects of a model oil dispersant (Corexit EC9500A) on the solubilization, sorption and desorption of two model parent PAHs (naphthalene and pyrene) and one alkylated PAH (1-methylnaphthalene) in sediment-seawater systems; 2) investigate the dispersant-facilitated dissolution, sorption/desorption and photodegradation of petroleum hydrocarbons in marine water-sediment systems; and 3) develop and test a new type of cobalt-doped TNTs (Co-TNTs) for efficient photodegradation of PAHs under solar light.

The specific objectives are to:

- ✧ Investigate effects of the dispersant on solubilization of the PAHs;

- ✧ Examine sediment sorption and desorption behaviors of the dispersant under surface water and deepwater conditions;
- ✧ Determine the effects of the dispersant and dispersed oil on sediment sorption and desorption of the PAHs and elucidate the underlying mechanisms;
- ✧ Test the PAH-sediment interactions under deepwater conditions in the presence of the dispersant
- ✧ Investigate the effects of three model dispersants on dispersion of various types and fractions of petroleum hydrocarbons;
- ✧ Determine the effects of dispersants on sediment sorption of dispersed petroleum hydrocarbons;
- ✧ Explore the photodegradation patterns of dispersed petroleum hydrocarbons under simulated solar irradiation;
- ✧ Develop an optimized hydrothermal-calcination method for preparing the desired catalyst;
- ✧ Test the effectiveness of the catalyst for phenanthrene photodegradation;
- ✧ Elucidate the mechanisms for enhanced photocatalytic activity by characterizing the morphology, crystal phases and compositions of Co-TNTs.

1.6.Organizations

This dissertation includes five chapters. Except for Chapter 1 (General Introduction) andChapter 5 (Conclusions and Suggestions for Future Research), each chapter is formatted in the style of Water Research. **Chapter 1** gives a general introduction of the background and outlines the objectives of this dissertation. **Chapter 2** investigates effects and mechanisms of a model oil dispersant (Corexit EC9500A) on sorption/desorption of representative PAHs

(naphthalene, 1-methylnaphthalene, pyrene) with two Gulf Coast marine sediments. This chapter is based on the information that has been published in Marine Pollution Bulletin (Zhaoet al., 2015). **Chapter 3** describes the fate of dispersed petroleum hydrocarbons in marine systems, and the detailed investigation includes the processes of dispersion, sorption and photodegradation of dispersed petroleum hydrocarbons. **Chapter 4** evaluates the effectiveness of a new type of cobalt-doped titanate nanotubes for enhanced photocatalytic degradation of phenanthrene. **Chapter 5** gives a summary of key conclusions of all the research and suggestions for future work.

Chapter 2. Effects of oil dispersant on solubilization, sorption and desorption of polycyclic aromatic hydrocarbons in sediment-seawater-oil system

This chapter describes the effects of dispersant on environmental fate of PAHs in sediment-seawater-oil systems. Typical processes including solubilization, sorption and desorption of three representative PAHs with two marine sediments were studied. Sediment sorption behaviors of the dispersant under surface water and deepwater conditions were also investigated and compared. The PAHs sorption/desorption behaviors were explored with varied amount of dispersant under both surface water condition and simulated deep-water conditions. Dual-mode was employed to fit the kinetic results of PAH sorption. A series of distribution coefficients were calculated to help unveil the mechanisms of dispersant enhanced/suppressed sorption of PAHs.This chapter is based on the information that has been published in Marine Pollution Bulletin (Zhao et al., 2015)

2.1.Introduction

Oil spill accidents have been a major challenge to the petroleum industry (Wang and Fingas 1997b). Oil spills often cause serious ecological and health consequences. For example, oil components such as polycyclic aromatic hydrocarbons (PAHs) can persist in the environment and pose long-term threat to the environmental and ecological health (Gong et al. 2014a).

The 2010 Deepwater Horizon (DwH) oil spill gushed an estimated 7.94×10^8 to 1.11×10^9 L of crude oil into the Gulf of Mexico (Reddy et al. 2012, Sammarco et al. 2013). To mitigate the environmental impacts, approximately 8.21×10^6 L chemical dispersants (Corexit EC9500A and Corexit 9527A) was applied, of which 5.30×10^6 L was sprayed at the surface and 2.91×10^6 L (Corexit EC9500A only) was injected into the oil stream at the wellhead (Kujawinski et al. 2011).

Crude oil is a mixture of more than 17,000 hydrocarbon compounds with varying volatility, solubility and toxicity (Sammarco et al. 2013). The light molecular weight hydrocarbons are relatively more soluble in water, such as PAHs, monoaromatic hydrocarbons, phenols and nitrogen- and sulfur-containing heterocyclic compounds, which are often of priority concern due to their high mobility and toxicity (Gong et al. 2014a).PAHs are important oil components, and can also result from incomplete combustion of fuels. PAHs represent a major environmental concern associated with oil spill, discharge and seepage (Nam et al. 2008). In addition, alkylated-PAHs often outweigh the parent-PAHs in concentration and in bio-toxicity. EPA (2003) has regulated 34 PAHs, including 18 parent-PAHs and 16 groups of alkylated PAHs (Choi et al. 2012). The DwH oil contained about 3.9% of PAHs by weight and a total of 2.1×10^4 tons of PAHs was released into the water column (Reddy et al. 2012). During and after the DwH oil spill, elevated concentrations of PAHs and alkylated PAHs were detected, including naphthalene, 1-methylnaphthalene, phenanthrene, pyrene, chrysene, and benzo(a)pyrene in the Gulf of Mexico. At the time of the accident, up to 0.13 μg/L of naphthalene and 0.34 μg/L of pyrene were detected on the sea surface near the site, and 1.22 mg/L and 0.02 μg/L, respectively, near the wellhead. The alkylated naphthalene concentration reached 0.71 μg/L in the surface water and 32.1 μg/L near the wellhead (Diercks et al. 2010b).

In marine eco-systems, PAHs undergo various physical and chemical processes, including solubilization, chemical and biological transformation, sorption to sediments and suspended particulate matter (SPM), and dispersion in the water column. Interactions with sediment particles or SPM can alter the fate and transport of PAHs. For example, association of PAHs with SPM can facilitate formation of marine oil snow and result in vertical transport of PAHs, and sediment-sorbed PAHs are more resistant to biotic or abiotic degradation(Gearing et al.

1980b, Yamada et al. 2003). In addition, the horizontal SPM movement with the ocean current may spread PAHs to the open sea (Tremblay et al. 2005).

Sediment organic matter (SOM) often plays a governing role in sorption of hydrophobic hydrocarbons including PAHs (White and Pignatello 1999, Zhao et al. 2001). PAHs of higher molecular weight are subject to stronger sorption on SOM. Temperature and salinity can also affect the sorption rate and extent. For example, temperature inversely affect the PAH uptake due to the exothermic nature of the sorption (Tremblay et al., 2005; Zhang et al., 2009).

Oil dispersants are designed to disperse oil in the water column, enhance biodegradation and mitigate the impacts on near-shore ecosystems (Kujawinski et al. 2011b). Corexit EC9527A and EC9500A are among the most commonly used oil dispersants. The key components in the dispersants include three nonionic surfactants (Span 80, Tween 80, and Tween 85), and one anionic surfactant dioctyl sodium sulfosuccinate (DOSS) (Thibodeaux et al. 2011). Corexit EC9527A contains 48 wt.% of the non-ionic surfactants and 35 wt.% of the anionic surfactant and 17% of solvents (Scelfo and Tjeerdema 1991). Corexit 9500A is a more recent formulation with improved penetration and emulsion properties and lower toxicity (Mitchell and Holdway 2000). Corexit 9500A shares the same surfactants as Corexit 9527A, but it does not include 2-butoxy ethanol as a solvent.

While surfactants are known to affect the sorption of PAHs by soil and sediment, little is known on the effects of oil dispersants. In water-sediment systems, surfactant molecules can exist as micelles, monomers, hemimicelles and admicelles, depending on the surfactant concentration. Partitioning of oil or PAHs into surfactant micelles or monomers can increase the apparent solubility, thereby dispersing or solubilizing more oil/PAHs in the water column (Diallo et al. 1994). On the other hand, the surfactants can also be adsorbed on the particles to form

hemimicelles or admicelles, providing additional capacity to adsolubilize PAHs (Ko et al. 1998). Gong et al. (2014b) reported that Corexit 9500A enhanced the uptake of phenanthrene onto a sandy loam sediment.

The presence of oil or dispersed oil may significantly alter the distribution of PAHs in sediment-water systems. Walter et al. (2000) investigated distribution of 9 PAHs in an oil-contaminated soil system and observed that more PAHs were distributed in the adsorbed oil and liquid oil phases than the ones dissolved in water phase; however, there has been little reported on the effects oil dispersants and dispersed oil.

During the DwH oil spill, Corexit EC9500A was applied at the 1500 m deep wellhead. The deepwater conditions are characterized by high pressure (~16 MPa), low temperature (~4 °C), little or no light, constant salinity (3.5%), and sluggish currents (<0.25 knots) (Glover and Smith 2003). More importantly, the oil plumes may contain large amount of suspended organic matter including methane/oil mixtures, methane gas, methane gas hydrates, waxy solid (formed by hydrocarbons beyond C14) and so on (Gong et al. 2014a). Good quality data and information on the sorption/desorption behaviors of oil dispersants and PAHs under typical physical conditions (high pressure, high salinity and low temperature) has not been described previously.

The goal of this study was to investigate effects of a model oil dispersant (Corexit EC9500A) on the solubilization, sorption and desorption of two model parent PAHs (naphthalene and pyrene) and one alkylated PAH (1-methylnaphthalene) in sediment-seawater systems. The specific objectives were to: 1) investigate effects of the dispersant on solubilization of the PAHs, 2) examine sediment sorption and desorption behaviors of the dispersant under surface water and deepwater conditions, 3) determine the effects of the dispersant and dispersed oil on sediment sorption and desorption of the PAHs and elucidate the underlying mechanisms,

and 4) test the PAH-sediment interactions under deepwater conditions in the presence of the dispersant.

2.2.Materials and methods

2.2.1. Chemicals

All chemicals were of analytical grade or higher. Naphthalene, 1-methylnaphthalene, and pyrene were purchased from Alfa Aesar (Ward Hill, MA, USA). Table 2-1 summarizes salient physicochemical properties of these PAHs. ^{14}C-radiolabeled naphthalene (specific activity: 52 mCi/mmol) and pyrene (60 mCi/mmol) were purchased from Moravek Biochemicals Inc. (Brea, CA, USA). Sodium azide (NaN_3) and sodium chloride (NaCl) were obtained from Fisher Scientific (Fair lawn, NJ, USA). Ecoscint cocktail was purchased from National diagnostics (Atlanta, GA, USA). Corexit EC9500A was acquired from Nalco Company (Naperville, IL, USA). Table 2-2 shows the compositions of this dispersant. A surrogate Louisiana sweet crude oil was obtained from the BP Company (Houston, TX, USA).

Table 2-1. Physicochemical properties of PAHs[a]

Compound	Molecular formula	Chemical Structure	Molecular weight (g/mol)	Solubility in water at 25 °C(mg/L)	Melting point °C	logK_{ow}
Naphthalene	$C_{10}H_8$	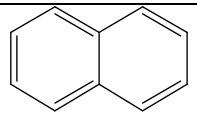	128.16	30-34	80	3.36
1-methylnaphthalene	$C_{11}H_{10}$	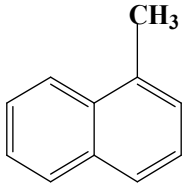	142.2	25.8	-22	3.87
Pyrene	$C_{16}H_{10}$	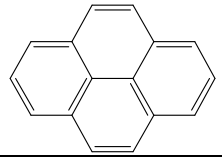	202.25	0.16	145	5.18

[a]Data for naphthalene and pyrene from Lan Chun et al.(2002) , and for 1-methylnaphthalene from Eganhouse and Calder (1976).

Table 2-2. Chemical constituents of dispersant Corexit EC9500A[a]

Name	CAS number	Ionic property	Synonym	Molecular formula	Average MW (g/mol)	CMC (mg/L)	Chemical structure
Span 80	1338-43-8	Neutral surfactant	Sorbitan, mono-(9Z)-9-octadecenoate	$C_{24}H_{44}O_6$	428.61	N\A	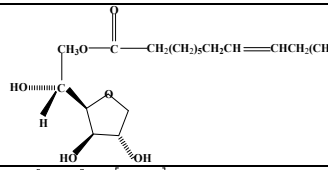
Tween 80	9005-65-6	Neutral surfactant	Sorbitan, mono-(9Z)-9-octadecenoate, poly(oxy-1,2-ethanediyl) derivs.	$C_{64}H_{124}O_{26}$	1310	14	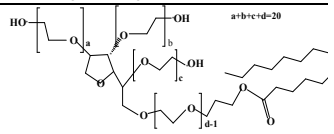
Tween 85	9005-70-3	Neutral surfactant	Sorbitan, tri-(9Z)-9-octadecenoate, poly(oxy-1,2-ethanediyl) derivs	$C_{60}H_{108}O_8 \cdot (C_2H_4O)n$	1838.57	23	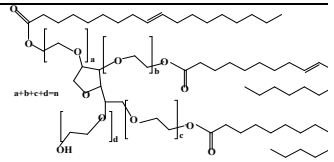
DOSS	577-11-7	Anionic surfactant	Butanedioic acid, 2-sulfo-, 1,4-bis(2-ethylhexyl) ester, sodium salt (1:1)	$C_{20}H_{37}SO_7Na$	444.57	578	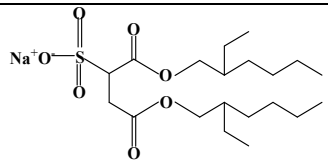
DPnB	29911-28-2	Solvent	Propanol, 1-(2-butoxy-1-methylethoxy)	$C_{10}H_{22}O_3$	190	N\A	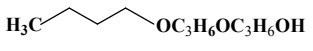
PG	57-55-6	Solvent	Propylene Glycol,1,2,-propanediol, 1,2-dihydroxypropane	$CH_3CHOHCH_2OH$	76.1	N\A	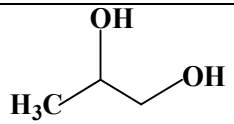

Distillates	64742-47-8	Solvent	Distillates (petroleum), hydrotreated light	N\A	N\A	N\A	N\A

[a]The above information is summarized based on several studies (Glover et al. 2014, Gong et al. 2014b, Kover et al. 2014).

Table 2-3. Salient physical and chemical properties of marine sediments used in this work.

Sample	Nitrogen[a] (%)	Carbon[a] (%)	Sulfur[a] (%)	SOM (%)	pH[b]	Cation Exchange Capacity (meq/100g)	Sand (%)	Silt (%)	Clay (%)	Textural Class[c]
Loamy Sand	0.07	0.43	0.210	0.7	7.00	21.21	85.0	5.0	10.0	Loamy Sand
Sandy Loam	0.15	1.58	0.682	2.7	7.38	37.38	56.3	31.3	12.5	Sandy Loam

Sample	Ca	K	Mg	P	Al	Cd	Cr	Cu	Fe	Mn	Na	Ni	Pb	Zn
							(mg/kg)							
Loamy Sand	301	177	536	11	60	0.1	0.1	5	241	35	3068	0.1	1	4
Sandy Loam	780	336	988	8	119	0.3	0.1	11	701	65	5057	0.4	2	9

[a] Total carbon, nitrogen and sulfur contents were determined following the combustion method (Kirsten 1979).

[b] Sediment pH was measured on a 1:1 sediment:water mixture via the Reference Soil Test Methods (UGA, 1983)

[c] Sediment texture was conducted following the hydrometer method (Bouyoucos 1962).

[d] Metal contents were measured per EPA method 3050B. Soil calcium, magnesium, potassium and sodium were first extracted per the Mehlich 1 procedure, filtered through a #1 qualitative filter paper, and then determined by a Varian Vista-MPX Radial Spectrometer.

2.2.2. Seawater and sediment samples

Seawater was collected at Grand Bay, AL, USA (N30.38/W88.31) as shown in Fig. A-1. Before use, the seawater was filtered through a membrane (0.45 μm) to remove suspended solids, and then sterilized through autoclaving at 121 °C for 35 minutes. The salient properties of the treated seawater include: pH = 8.88, dissolved organic carbon (DOC) = 0.43 mg/L, salinity = 3.2%, Cl^- = 18.55 g/L, NO^{3-} = 2.55 g/L and SO_4^{2-} = 4.25 g/L. To inhibit microbial activities during the experiments, 200 mg/L of sodium azide (an aerobic metabolic inhibitor) was added in the seawater.

Two marine sediments, a loamy sand and a sandy loam, were sampled at N30.37926/W88.30684 and N30.37873/W88.30679, respectively. The sediments were wet-sieved with seawater to obtain a fraction of 75-840 μm and then air-dried for 7 days. The dried aggregates were further oven-dried for 6 hours at 80 °C before use. Sediment analyses were performed by the Soil Testing Laboratory at Auburn University, and the method details have been described elsewhere (Gong et al. 2012). Table 2-3 gives salient properties of the sediments.

2.2.3. Dispersant-enhanced solubilization of PAHs

The apparent solubility of PAHs in seawater was measured in the presence various concentrations of the dispersant based on the procedure (Zhao et al. 2005). Individual solutions of a PAH were prepared by mixing 0.1 g of a PAH with 43 mL of seawater (greater than the apparent solubility of each PAHs) containing 0 to 200 mg/L of the dispersant. Upon mixing for 3 days, the vials were centrifuged at 3000 rpm (1509 g-force) for 10 minutes and 10 mL of the supernatants were carefully sampled and diluted with 1.0 mL of methanol. The PAH concentration was then quantified via HPLC (HP Series 1100, Hewlett Packard, CA, USA)

equipped with a UV detector and a Zorbax SB-C18 column (150×468 mm). The mobile phase consisted of 80% acetonitrile, 19.9% water, and 0.1% phosphoric acid. The operating flow rate was set at 1.0 mL/min at 40 °C with an optimal wavelength of 254 nm.

2.2.4. Sorption of Corexit EC9500A by sediment

Batch experiments were conducted to construct sorption/desorption isotherms of the dispersant with the sandy loam. Eight grams of the sediment were mixed with 42 mL seawater in the presence of 5 to 6000 mg/L of the dispersant. The mixtures were equilibrated under shaking for 3 days to reach equilibrium. The dispersant uptake was then determined by comparing the initial and equilibrium dispersant concentrations in the aqueous phase upon centrifugal separation of the sediment and seawater (3000 rpm for 10 minutes). The dispersant concentration was determined by measuring the surface tension using a CSC-DuNoüy Tensiometer (Central Scientific Company, Fairfax, VA, USA). The same tests were also carried out under deepwater conditions (Section 2.2.9).

2.2.5. Effects of dispersant on sorption kinetics of PAHs

Stock solutions for individual PAHs were prepared at 1 g/L in methanol. To facilitate PAH analysis, ^{14}C-radiolabeled PAHs were added into the stock solutions (1:50 v/v) before use. Sorption kinetic tests of PAHs with the two sediments were carried out in 44 mL glass vials fitted with Teflon-lined septa. PAH-laden seawater solutions were prepared by injecting 0.6 mL (for naphthalene or 1-methylnaphthalene) or 0.06 mL (for pyrene) of a PAH stock solution in 1000 mL of the seawater and then mixed for 12 hours in dark. To test the dispersant effects, Corexit EC9500A was added before mixing to give a dispersant concentration of 18 mg/L. The

methanol content was <0.1 vol.% to avoid co-solvent effect. The PAH sorption was initiated by mixing a PAH solution with a sediment of known masses. For naphthalene and 1-methylnaphthalene, 8 g of loamy sand was mixed with 40 mL of seawater, and 3 g of the sandy loam sediment was mixed with 42 mL of seawater. For pyrene, 0.6 g of the sediment was mixed with 43 mL seawater. The headspace for each vial was kept less than 0.5 mL to minimize volatilization loss. The vials were then sealed and mixed on an end-to-end rotator at 60 rpm in an incubator at 21 ± 1 °C. At predetermined times, vials were sacrificially sampled and centrifuged at 3000 rpm for 10 minutes and allowed to stand still for another 5 minutes. Then, 1 mL of each supernatant was pipetted to 10 mL of the scintillation cocktail, and then analyzed for the PAHs by liquid scintillation counting (Beckman LS-6500 Liquid Scintillation Counter, Fullerton, CA). To assure mass balance, PAHs in the sediment phase were extracted with hot methanol (70 °C) for 4 hours and analyzed, the results showed that the PAH recovery was >97%.

2.2.6. Effect of dispersant on sorption equilibrium and reversibility of PAHs

Following the same experimental procedure as in the kinetic tests, sorption isotherm tests were carried out at the same solid:solution ratio and in a broader range of initial PAH concentrations. The sorption equilibrium was reached in 3 days. The sorption isotherms were then obtained by measuring the equilibrium PAH distributions. To acquire the corresponding desorption isotherms, the vials were centrifuged at 3000 rpm for 10 minutes and then 96% to 99% of the supernatant was replaced with an equal volume of sediment-amended seawater to start the desorption tests. The sediment-amended seawater was prepared by mixing the sediment and seawater at the same solid:solution ratio as in the equilibrium tests to maintain the same background compositions. To test the dispersant effects, 18 or 180 mg/L of the dispersant was

added in the solutions. The vials were then re-equilibrated for 3 days under rotating to get the desorption isotherms.

2.2.7. Dual-mode modeling of sorption isotherms and kinetics

The dual-mode sorption model envisions SOM as a glassy polymeric sorbent, which sorbed a PAH through concurrent solid-phase dissolution and adsorption (hole-filling) (Xing and Pignatello, 1997; Zhao et al., 2002). In a sediment-dispersant system, the sorption of the dispersant components on sediment particles creates additional sink, which takes up PAHs through additional adsolubilization/partitioning. For a single solute system, the dual-mode isotherm model takes the form:

$$q_e = K_D C_e + \frac{bQC_e}{1+bC_e} \quad \textbf{(Eq. 1.1)}$$

where q_e (μg/g) is the equilibrium uptake of a PAH, C_e (μg/L) is the solute concentration in the aqueous phase, K_D (mL/g) is the partition coefficient between the aqueous phase and the dissolution domains including the dissolution domain of SOM and the sorbed surfactants, and b (mL/μg) and Q (μg/g) are the Langmuir affinity and capacity coefficients, respectively. The first term represents the linear partitioning, whereas the Langmuir term reflects the adsorption. While dissolution is considered linear and reversible, adsorption is generally non-linear and irreversible.

Following the dual-mode sorption concept, Zhao et al. (2002) formulated the following radial diffusion model to interpret the overall sorption kinetics:

$$\frac{\partial q_D}{\partial t} = D_a\left(\frac{\partial^2 q_D}{\partial r^2} + \frac{2}{R}\frac{\partial q_D}{\partial r}\right) \quad \textbf{(Eq. 1.2)}$$

where q_D is the uptake in the dissolution domain, r is the radial coordinate, t is time, and D_a is the apparent diffusivity defined by

$$D_a = D_D / \left(1 + \frac{bQ / K_D}{[1+(b / K_D) q_D]^2}\right) \quad \textbf{(Eq. 1.3)}$$

where D_D (m^2/h) is the diffusivity in the dissolution domain. The model assumes Fickian diffusion in the dissolution domain and immobilization in the holes, with microscopic local equilibrium between the two domains. The Crank-Nicolson finite difference method was employed to solve the equation under the experimental initial and boundary conditions (Zhao et al. 2002). The value of D_D/r_0^2 was obtained by fitting the solution to the experimental kinetic data, where r_0 is the mean effective radius of SOM particles.

2.2.8. Effects of dispersant dosage on PAH uptake

The effects of dispersant dosage on uptake of PAHs by the sediments weretested following the same protocol as in the sorption tests (Section 2.5) in a broad range of dispersant dosages (0-6000 mg/L for naphthalene and 1-methylnaphthalene, 0-280 mg/L for pyrene).

2.2.9. Sorption of PAHs under simulated deepwater conditions

To test the dispersant effects under deepwater conditions, equilibrium sorption experiments were conducted in 200 mL high-pressure stainless-steel reactors (Huihua Special Instruments, Tianjin, China) at the same solid:solution ratio as in the isotherm tests. NaCl was added to increase the salinity of seawater from 3.2% to 3.5%. The reactor pressure was kept at 16 ± 0.5 MPa and the reactors were then equilibrated for 3 days under rotating in an incubator set at 4 °C. The dispersant dosage was 0-5000 mg/L for naphthalene and 1-methylnaphthalene, and 0-350 mg/L for pyrene.

2.2.10. Effects of WAO and DWAO on sorption of PAHs

Water accommodated oil (WAO) and dispersed water accommodated oil (DWAO) were prepared following the protocol by (Singer et al. 2000). In brief, crude oil was gently mixed at the volume ratio of 1:200 (oil:seawater) in a 2000 mL glass vessel, and the mixture was sealed and magnetically stirred for 18 hours. After settling for 6 hours, WAO was obtained from the hose bib fitted with silicon tubing and clamp at the bottom of the vessel. DWAO was prepared following the same protocol except that the dispersant was added to the oil-seawater mixture at a dispersant:oil:seawater volume ratio of 1:20:4000. The equilibrium sorption tests were then carried out in the presence of WAO or DWAO following the same experimental procedure.

2.3.Results and discussions

2.3.1. Dispersant-facilitated solubilization of PAHs

Fig. 2-1 shows solubilization of the three model PAHs as a function of the dispersant dosage. The apparent solubility for each PAH nearly linearly increased with increasing dispersant concentration from 0 to 200 mg/L. The apparent critical micelle concentration (CMC) of Corexit EC9500A was determined to be 22.5 mg/L in seawater (Gong et al. 2014b). It is noteworthy that the dispersant enhanced the PAH solubility even at submicelle (<CMC) concentrations. At 18 mg/L, the dispersant increased the solubility by 5%, 11% and 44% for naphthalene, 1-methylnaphthalene and pyrene, respectively; at the point of CMC, the solubility enhancements were 7%, 12% and 71%, which were further increased to 27%, 59% and 660%, respectively, at 200 mg/L of the dispersant. Evidently, the formation of stable micelles turned the monomeric/solvent solubilization into the more effective micellar solubilization.

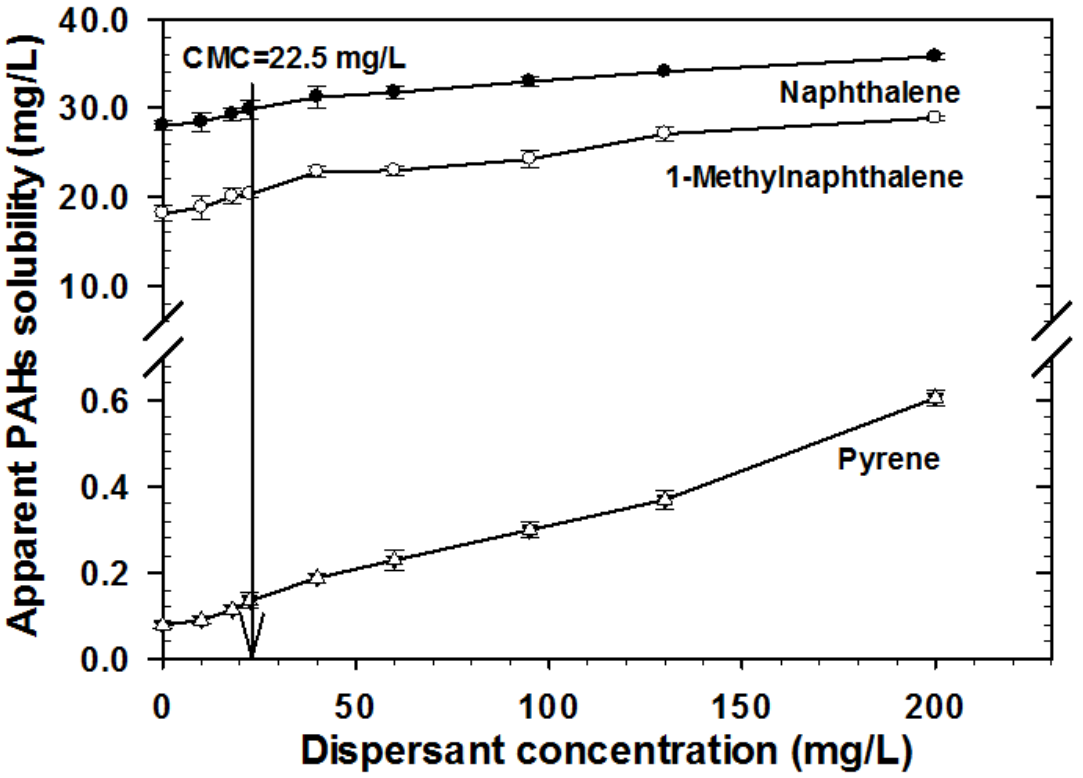

Fig. 2-1. Apparent solubility of three model PAHs as a function of Corexit EC9500A concentration.

The observed solubility enhancement in the submicelle concentrations of the dispersant contrasts those in pure surfactant systems. For example, Edwards et al. (1991) reported that individual pure surfactants had negligible effect on solubilization of the PAHs at <CMC, and they observed an abrupt solubility enhancement at CMC. Likewise, Mohamed and Mahfoodh (2006) reported the solubility of naphthalene remained constant when the concentration of an anionic surfactant (SDS) was <CMC;however, when SDS was mixed with a nonionic surfactant Tween 80, enhanced solubilization was evident for both naphthalene and pyrene. The researchers attributed the observation in part to the much lowered CMC of the mixed micelles than that of single SDS and to the synergistic surfactant–surfactant interaction occurring within the solubilization sites at submicellar concentrations. Lippold et al. (2008) reported a slight solubility

enhancement of pyrene at submicellar concentrations of SDS and attributed it to the formation of premicellar aggregates. Yet, the submicellar solubilization was overshadowed by the sharp solubility rise upon micellar solubilization at CMC.

Fig. 2-1 reveals the important roles of the solvents and synergistic effects of the solvent-surfactants mixture at both submicellar and micellar concentrations. Corexit 9500A contains one anionic, three nonionic surfactants and three solvents (Table 2-2). Indeed, the CMC value of Corexit 9500A is higher than that for Tween 80 (14 mg/L), and nearly the same as for Tween 85 (23 mg/L), but much lower than that for DOSS (578 mg/L), indicating that the Tween surfactants are the predominant ingredients in the dispersant (though it has not been disclosed by the manufacturer). In general, nonionic surfactants are more effective in solubilizing hydrophobic hydrocarbons than anionic surfactants (Mohamed and Mahfoodh, 2006) due to the lower CMC for the former. Nonionic surfactants are poorly soluble, which would confine the formation of micelles and dispersion of PAHs or oil. Mixing with anionic surfactants and solvents promotes solubilization of the nonionic surfactants, and the interactions between the nonionic and anionic surfactants decrease the repulsive forces among the ionic heads, facilitating formation more and denser micelles at an overall lower CMC (Zhao et al. 2005). Tokuoka et al. (1995) concluded that the effective solubilization area and the radius of mixed micelles are larger than those of pure surfactant micelles. Kamil and Siddiqui (2013) asserted that solubilization of PAHs commenced at the surfactant CMC and was proportional to the concentration of surfactant in micelles.

Indeed, the CMC value of Corexit 9500A is higher than that for Tween 80 (14 mg/L), and nearly the same as for Tween 85 (23 mg/L), but much lower than that for DOSS (578 mg/L), indicating that the Tween surfactants are the predominant ingredients in the dispersant (though it

has not been disclosed by the manufacturer). The unusual solubility enhancement at dispersant <CMC is attributed primarily to the solvent effects. The solvents not only increase the PAH solubility by lowering the solution dielectric constant, but may facilitate submicellar aggregation of the surfactant molecules. Martino and Kaler (1995) reported that propylene glycol decreases the value of the Hamaker constant by replacing the water molecules in the lamellar phase. As a result, the lamellar stability is lowered, and the inter-bilayer and intra-aggregate interactions between nonionic and anionic surfactants promote the formation of mixed micelles.

The data shown in Fig. 2-1 also demonstratesthat the dispersant was much more effective in solubilizing more hydrophobic PAHs. This is consistent with the results by Mohamed and Mahfoodh (2006), who studied solubilization of naphthalene and pyrene by SDS-Tween 80 mixed surfactants. For naphthalene, the solubilization occurs at the mixed micelle-water interface, and the synergistic effects of the mixed surfactants are virtually absent due to the very weak interactions between the hydrophilic groups of the two surfactants. In contrast, pyrene is most likely solubilized in the micellar cores, and thus, the solubilization of pyrene makes better use of the synergistic effect of the mixed surfactants/solvents. The statement agrees with that by Gao et al. (2002) who stated that SDS molecules in the SDS-Tween 80 binary micelles have more restricted motional freedom, and thus a more rigid microenvironment for pyrene, than in SDS self-aggregated micelles. Conventionally, theeffectiveness of a surfactant to solubilize a given solubilizate is quantified in terms of molar solubilization ratio (MSR), which reflects the slope of the solubility enhancement lines (Fig. 2-1) at surfactant > CMC (Srivastava and Ismail 2014). In this work, the lack of the exact molecular compositions of the dispersant prohibited from obtaining the MSR values. Consequently, we adopted an alternative approach by quantifying the PAH partitioning between micelles and water (Zhou and Zhu 2005). At

dispersant ≥CMC, the micelle-water partition coefficient, K_{mic} (L/g), is defined on a mass concentration basis as:

$$K_{mic} = \frac{S_{mic}}{S_w C_{mic}} = \frac{S - S_{CMC}}{S_w (C_{dis} - C_{CMC})} \quad \textbf{(Eq. 1.4)}$$

where S_{mic} (g/L) is the concentration of a PAH in the micelles, S_w (g/L) is the PAH solubility in seawater free of dispersant, C_{mic} (g/L) is the concentration of dispersant in micelle form, and S and S_{CMC} are the apparent solubility of the PAH at a dispersant concentration of C_{dis} (g/L) and at CMC (C_{CMC}), respectively.

In the submicellar range, we define a pseudo-partition parameter K_S (L/g) as:

$$K_S = \frac{S_S}{S_w C_{dis}} = \frac{S - S_w}{S_w C_{dis}} \quad \textbf{(Eq. 1.5)}$$

where S_S (g/L) is the concentration of a PAH solubilized through solvents and surfactant monomers/aggregates at <CMC.

Table 2-4 lists the K_{mic} and K_S values based on linear regression fittings. The more hydrophobic PAHs have larger K_S and K_{mic}values, implying the greater sensitivity to the dispersant at concentrations below and above the CMC. This trend agrees with the previous observations with pure anionic surfactants or nonionic surfactants (Ko et al., 1998; Mohamed and Mahfoodh, 2006; Zhou and Zhu, 2005).

Table 2-4. Parameters for the solubilization of three PAHs

	K_S (L/g) (R^2)	K_{mic}(L/g) (R^2)	log K_{ow}
Naphthalene	2.46 (0.93)	1.14 (0.97)	3.36
1-methylnaphthalene	5.81 (0.95)	2.54 (0.94)	3.87
Pyrene	24.18 (0.93)	32.24 (0.98)	5.18

With the three PAHs, we observed a good linear correlation between K_{mic} (and K_S) and K_{ow} as follows:

$$(g/L) \times K_{mic} = 0.0002 K_{ow} + 0.8272 \ (R^2=0.99) \quad \textbf{(Eq. 1.6)}$$

$$(g/L) \times K_S = 0.0001 K_{ow} + 3.4431 \ (R^2=0.99) \quad \textbf{(Eq. 1.7)}$$

2.3.2. Sorption of Corexit EC9500A by sediment

In Fig. 2-2, thesorption isotherms of the dispersant on the sandy loam under simulated surface water conditions and deepwater conditions is plotted. The S-shaped isotherms were observed for both cases, though the uptake was lower under deepwater conditions. For both cases, the low uptake (<4 mg/g) lingered until the dispersant concentration reached ~100 mg/L. Then, the uptake rose abruptly till ~280 mg/L, before reaching the maximum sorption capacity at >280 mg/L. Under deepwater conditions, the maximum uptake dropped by ~10%.

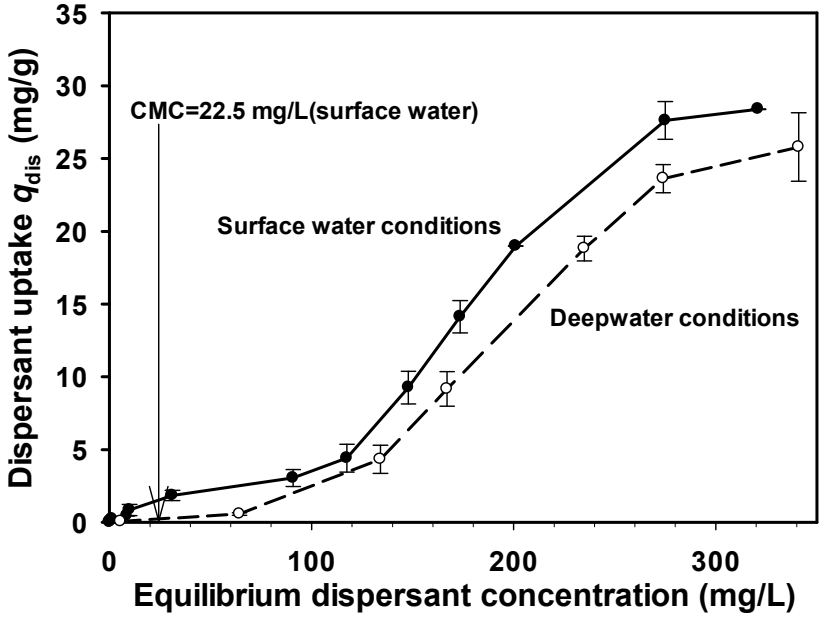

Fig. 2-2. Sorption isotherms of dispersant Corexit EC9500A on a loamy sand sediment under surface water conditions (21 ± 1 °C, 0.1 MPa, salinity = 3.2 wt.%) and deepwater conditions (4 °C, 16 MPa, salinity = 3.5 %).

The characteristic S-shaped isotherms are consistent with previous reports by Ko et al. (1998), who studied sorption of Tween 80 onto kaolinite and observed the sharp rise occurred at ~2 times CMC. Mechanistically, the isotherms may be broken down into three distinctive regions. In Region I (0-100 mg/L), the surfactants are adsorbed as monomeric molecules, resulting in the low uptake. DOSS molecules are typically sorbed on mineral surface through electrostatic interactions between the surfactant heads and the positively charged sediment surface sites, whereas the neutral surfactants are sorbed due to van der Waals interactions between the hydrophobic tails and the SOM. The characteristic steep rise in Region II (100-280 mg/L) reflects surface aggregation/accumulation of the surfactant molecules and formation of monolayered and/or bilayered hemimicelles and admicelles. It should be noted that the mixed solvents, anionic and nonionic surfactants may synergistically facilitate surface aggregation, resulting in larger and denser surfactant layers on the solid surface (Zhao et al. 2005). In Region III (>280 mg/L), a sorption plateau is reached/approached, which can be attributed to the electrostatic repulsion between anionic heads of DOSS, complete surface coverage, and competitive formation of aqueous-phase micelles.

The lower uptake at the deepwater temperature is counterintuitive given that sorption of organic compounds is typically exothermic. Karatepe (2003) examined Tween 80 sorption by lignite at 5 to 30 °C and observed similar effects. Increasing temperature gradually desolvates the head groups of the non-ionic surfactants, making them less hydrophilic and more compact (Paria and Khilar 2004). Thus, non-ionic molecules are less soluble at higher temperatures due to the dehydration of the polyoxyethylene chain, resulting in the higher uptake. In addition, lower temperature may condense the SOM, contributing to reduced sorption capacity.

2.3.3. Effects of dispersant on sorption kinetics of PAHs

Fig. 2-3 shows the sorption kinetics of the three PAHs on the two marine sediments with or without the dispersant. In all cases, rapid initial sorption rate was observed, and equilibrium was reached within 24 hours. The presence of 18 mg/L of the dispersant increased the equilibrium naphthalene uptake from 53.0% to 55.9% for sandy loam, and from 44.2% to 47.5% for loamy sand. Likewise, the dispersant increased the 1-methylnaphthalene uptake from 52.3% to 57.5% and pyrene uptake from 74.3% to 85.3% by loamy sand. In all cases, the *t*-test *p* values are <0.05 at the 0.05 level of significance. Evidently, the dispersant facilitated sorption of more PAHs to the sediments.

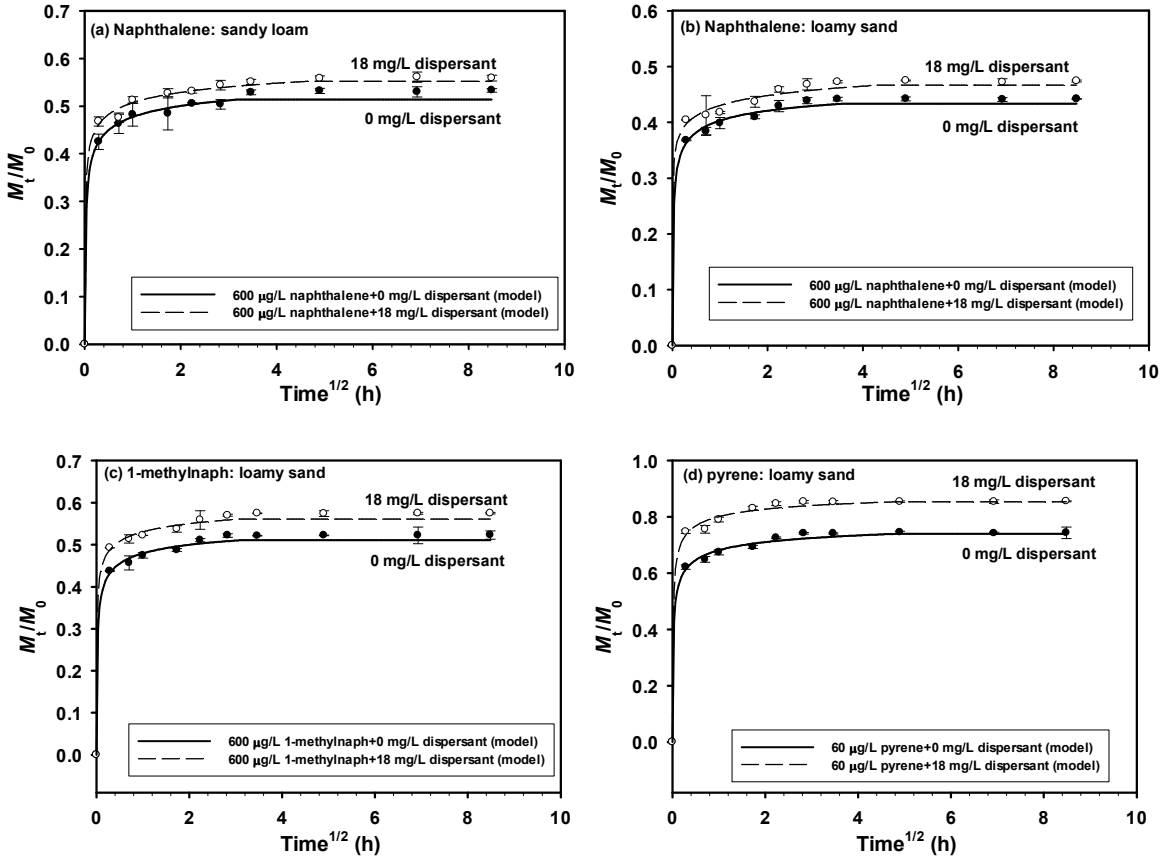

Fig. 2-3. Sorption kinetics of PAHs in the absence or presence of 18 mg/L of Corexit EC9500A onto **(a)** sandy loam and **(b, c, d)** loamy sand sediments. M_t: PAH mass uptake at time

t, and M_0: total mass in the system. Symbols: Experimental data; Lines: Dual-mode model simulations.

The dual-mode kinetic model was able to adequately interpret the sorption kinetic data (Fig. 2-3). And based on the sorption isotherm parameters (Section 2.3.4. and Table 2-5), the diffusion parameter (D_D/r_0^2) was obtained by fitting the model to the experimental data. In all cases, the presence the dispersant increased the diffusivity, indicating reduced mass transfer resistance, which can be attributed to the dispersant softening of SOM and the added sinks of sorbed hemimicelles and admicelles.

Table 2-5.Equilibrium sorption parameters for PAHs onto sediments in the absence and presence of dispersant Corexit EC9500A

PAHs	Soil	Initial dispersant concentration (mg/L)	K_D(mL/g)	b (mL/mg)	Q(μg/g)	K_d or K_d^o (mL/g)	D_D/r_0^2 (1/h)	K_{oc} (mL/g)	q_{dis} (mg/g)
Naphthalene	Sandy loam	0	10.8	3.6	3.0	18.5±1.8	0.8		
		18	12.4	3.6	3.0	20.3±1.8	1.0		
		180	28.9	3.6	3.0	34.0±1.2			
Naphthalene	Loamy sand	0	2.5	1.4	1.5	4.2±0.4	1.3	1032±98	0
		18	3.0	1.4	1.5	5.0±0.3	1.5		0.1
		180	8.0	1.4	1.5	9.8±0.3			0.9
1-methylnaph	Loamy sand	0	2.7	2.8	1.9	6.1±0.9	0.2	1498±221	0
		18	3.8	2.8	1.9	7.2±0.7	0.3		0.1
		180	11.6	2.8	1.9	16.1±0.6			0.9
Pyrene	Loamy sand	0	84.5	48.4	4.4	222.9±28.1	0.1	54769±6880	0
		18	285.6	48.4	4.4	450.0±22.5	0.1		0.6
		180	21.3	48.4	4.4	143.7±31.2			4.6

Note: K_d and K_d^o are calculated as mean ± standard deviation based on the experimental isotherm data (Fig. 2-4).

2.3.4. Effects of dispersant on sorption/desorption isotherms of PAHs

In a dispersant-free system, the PAH distribution coefficient (K_d, L/g) between the aqueous phase and the solid phase is expressed as:

$$K_d = \frac{q_e}{C_e} \quad \textbf{(Eq. 1.8)}$$

where q_e (mg/g) and Ce (mg/L) are PAH concentrations in the sediment and water phase, respectively. Accordingly, the sediment organic carbon-normalized distribution coefficient (K_{oc}, L/g) is given by:

$$K_{oc} = \frac{K_d}{f_{oc}} \quad \textbf{(Eq. 1.9)}$$

$$f_{om} = 1.72 \times f_{oc} \quad \textbf{(Eq. 1.10)}$$

where f_{oc} and f_{om} are fractions of organic carbon and organic matter in sediment. K_d and K_{oc} were obtained via linear fitting to the sorption isotherm curves and are given in Table 2-5.

Fig. 2-4 shows the PAH sorption isotherms at various concentrations of the dispersant. For all PAHs, sandy loam (SOM content = 2.7%) exhibited greater sorption capacity than loamy sand (SOM content = 0.7%). The dual-mode model nicely simulated the isotherms in call cases. Based on the model premises, the Langmuir term was set as constant at various dispersant concentrations, i.e., the dispersant effect on the PAH uptake is affected by the fitted K_D values (Table 2-5). The dispersant at 18 mg/L increased the uptake of all PAHs, e.g. it increased K_D for naphthalene by 22% with loamy sand and 238% for pyrene (Table 2-5). Further increasing the dispersant to 180 mg/L further increased K_D for naphthalene and 1-methylnaphthalene, but diminished sorption of pyrene, indicating that the dispersant effect is dependent on hydrophobicity of the PAHs. For more hydrophobic PAHs, the dispersant more profoundly enhance the PAH uptake at low dispersant dosages, but the solubilization effect of the dispersant surpasses the adsolubilization effect at elevated dispersant concentrations.

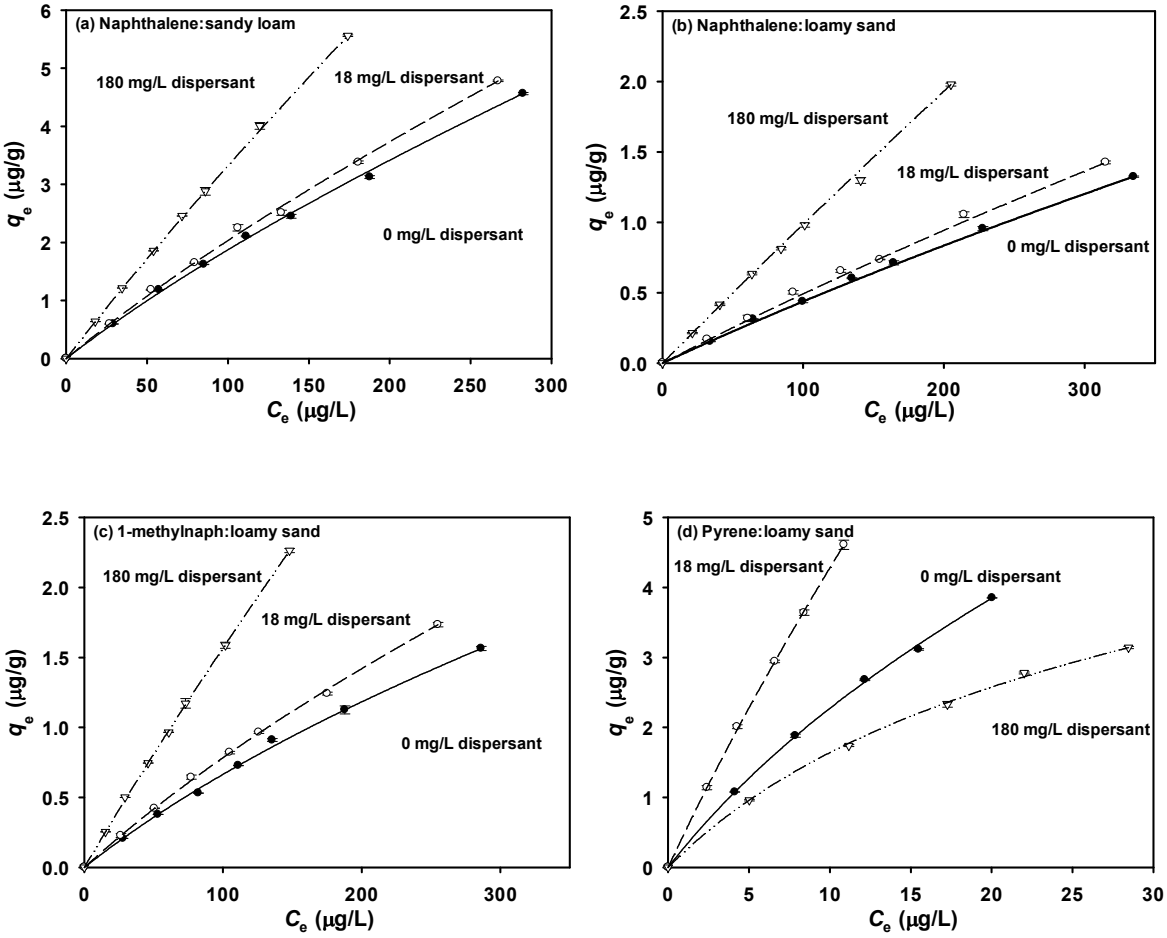

Fig. 2-4. Sorption isotherms of PAHs in the presence of 0, 18 and 180 mg/L of Corexit EC9500A with **(a)** sandy loam, and **(b, c, d)** loamy sand sediments. Symbols: Experimental data; Lines: Dual-mode model simulations.

Fig. 2-5 plots the sorption and desorption isotherms of each PAH at 0, 18 and 180 mg/L of the dispersant. In the absence of the dispersant, the sorption of naphthalene and 1-methylnaphthalene was fully reversible, while a modest but significant hysteresis was observed for pyrene. Notably, the presence of the dispersant induced a phenomenal sorption hysteresis for all cases, and the higher the dispersant concentration, the more the sorption irreversibility. The dispersant-facilitated hysteresis is attributed to the uptake of the dispersant (Fig. 2-2) and the

dispersant adsolubilization of the PAHs. Zhang and Zhu (2010) reported that Tween 80 inhibited desorption of PAHs from soil and they attributed it to elevated hydrophobicity of soil.

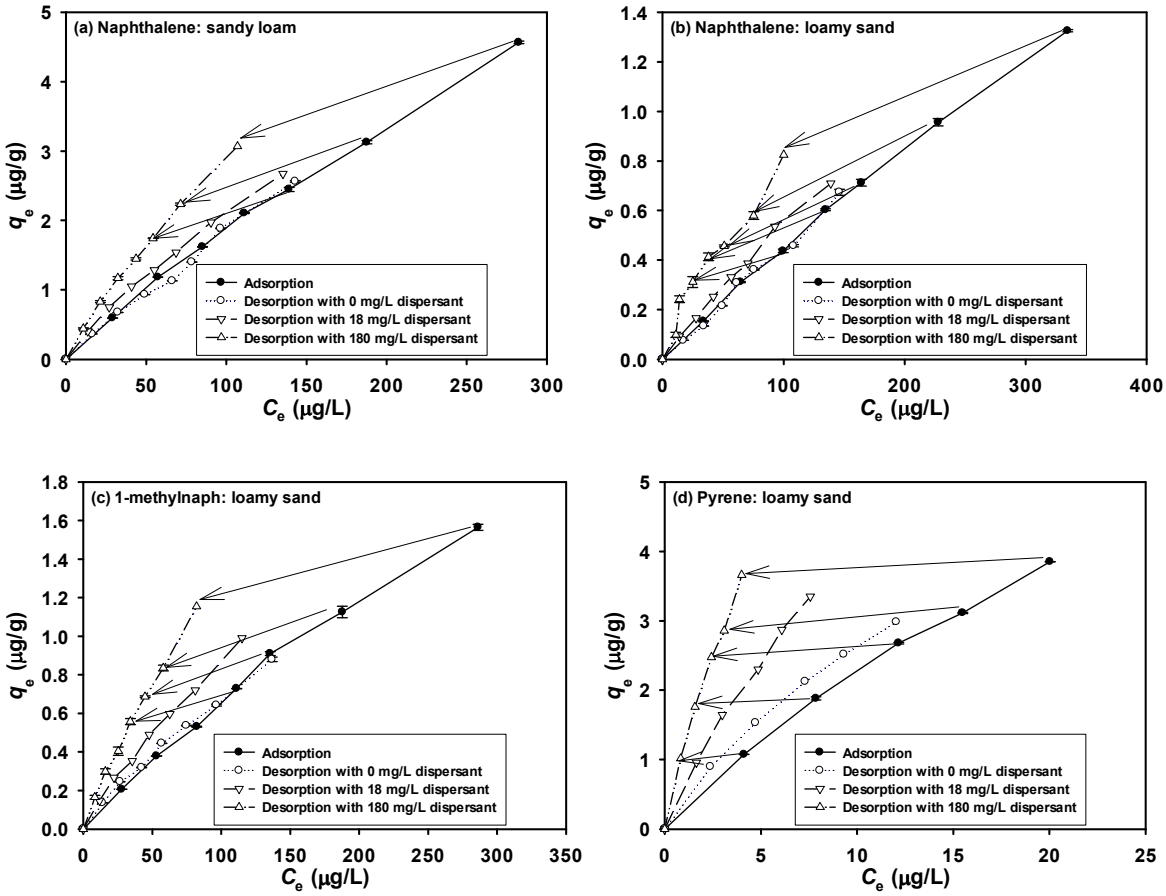

Fig. 2-5. Sorption and desorption isotherms of PAHs with **(a)** sandy loam and **(b, c, d)** loamy sand sediments in the presence of 0, 18 and 180 mg/L of the dispersant.

2.3.5. Effects of dispersant dosage on PAH uptake

The dispersant effect on the sediment sorption of PAHs was further investigated over a broad range of dispersant dosages. In a dispersant-sediment-seawater system and at dispersant >CMC, the overall distribution coefficient of a PAH between the sediment and seawater (K_{d}^{o}) is described by:

$$K_{\mathrm{d}}^{o}=\frac{q_{\mathrm{e}}}{C_{\mathrm{e}}}=\frac{K_{\mathrm{sdis}}q_{dis}+K_{\mathrm{d}}}{1+C_{\mathrm{mic}}K_{\mathrm{mic}}}=\frac{\mathrm{Adsolubilization}+\mathrm{SOM}}{1+\mathrm{Solubilization}} \qquad \textbf{(Eq. 1.11)}$$

where K_{sdis}(L/g) is the PAH partition coefficient to the sorbed dispersant, q_{dis} (g/g) and C_{mic} (g/L) are the equilibrium uptake and the aqueous micelle concentration of the dispersant, respectively. Conceptually, the magnitude of K_d^o and the corresponding equation terms reflect the relative level of the adsolubilization and solubilization effects of the dispersant, i.e., dispersant-facilitated solubilization decreases K_d^o, whereas partitioning into the soil-sorbed dispersant increases K_d^o. Accordingly, K_{sdis} in the submicelle concentration range is refined as:

$$K_d^o = \frac{q_e}{C_e} = \frac{K_{sdis} q_{dis} + K_d}{1 + C_{dis} K_s} = \frac{\text{Adsolubilization} + \text{SOM}}{1 + \text{Solubilization}} \qquad \textbf{(Eq. 1.12)}$$

where C_{dis} (g/L) is the equilibrium dispersant concentration.

Fig. 2-6 and Fig. A-2 show that K_d^o increases with increasing dispersant concentration in the low concentration range until it reaches a peak at elevated dispersant concentrations. For naphthalene (the most soluble PAH with logK_{ow} = 3.37), K_d^o is barely affected at C_{dis}<100 mg/L, but increased steadily with increasing dispersant thereafter, indicating that adsolubilization was predominant at C_{dis}>100 mg/L. For 1-methylnaphalene (K_{ow} = 3.87), a stronger adsolubilization was evident at C_{dis} > 100 mg/L (Fig. A-2), and K_d^o reached a peak of 0.32 at C_{dis} = 275 mg/L, with a peak K_d^o/K_d of 56.1. A comparison with the dispersant sorption isotherm (Fig. 2-2) revealed that the increase in K_d^o is positively correlated with the dispersant uptake, and the sharp rise in dispersant uptake at C_{dis}>100 mg/L facilitated the sharp rise in PAH sorption. K_d^o of pyrene (logK_{ow} = 5.18) increased much more sharply even in the low dispersant range and reached a distinct peak near CMC, with a peak K_d^o/K_d of 2.89 (Fig. 2-6d). The solubilization effect became predominant (K_d^o/K_d<1) at C_{dis}> 26 mg/L. Following the concept by Zhou and Zhu (2005) for surfactants, we define the total dispersant dosage at which the wash off

of the target solute starts (i.e., K_d^o/K_d=1) as the critical washing concentration (CWC). Our results indicate that for more soluble PAHs, the dispersant-enhanced adsolubilization outweighs the solubilization effect over a broad dispersant concentration range (>10x CMC), i.e., with a very high CWC. Conversely, for less soluble PAHs, it is characterized with a sharp rise in the dispersant-enhanced adsolubilization in a much narrow concentration range, with a much lower CWC.

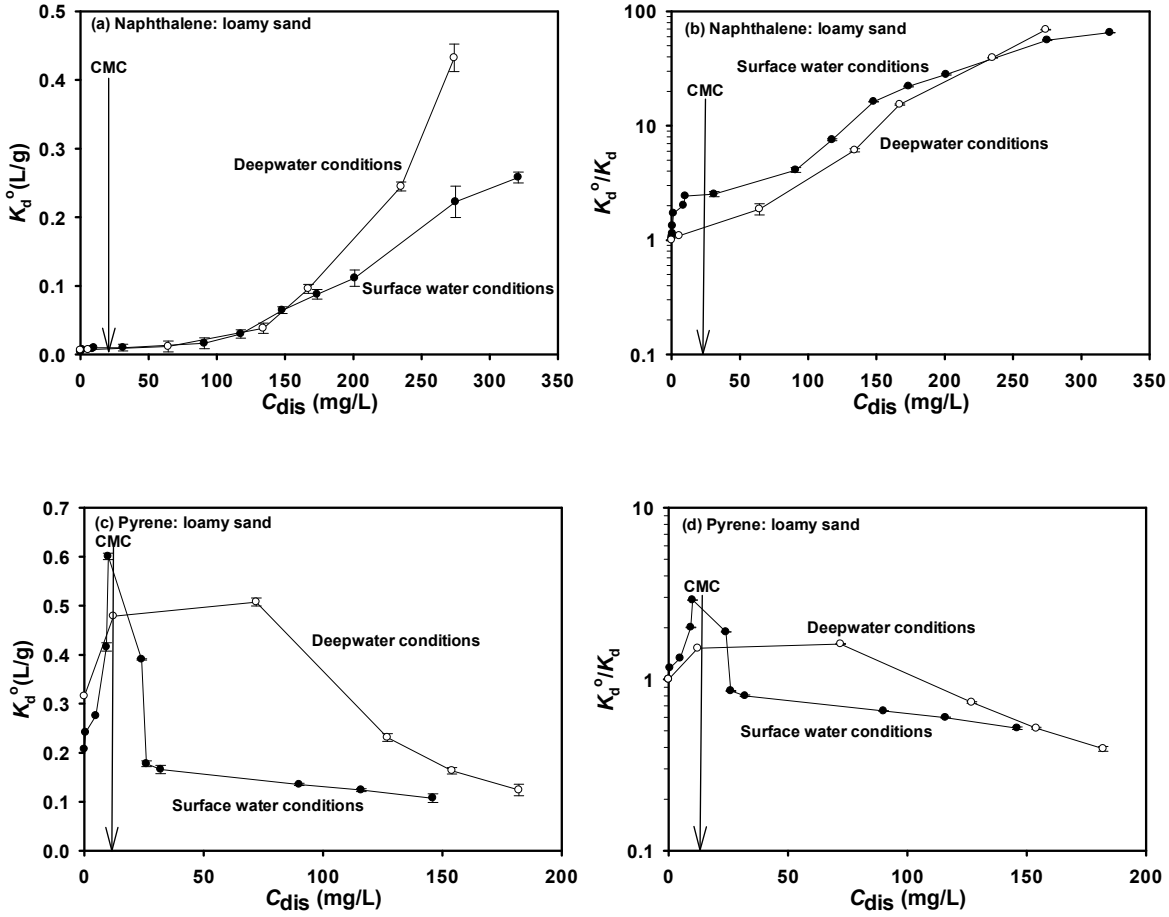

Fig. 2-6. (a, c) The apparent soil-water distribution coefficients (K_d^o) of naphthalene and pyrene. **(b, d)** K_d^o/K_d for naphthalene and pyrene as a function of equilibrium Corexit EC9500A concentration under surface water conditions and deepwater conditions.

To further examine the role of sorbed dispersant in the PAH sorption, Fig. 2-7 plots K_{sdis} (the PAH partition coefficient to sorbed dispersant) versus the aqueous dispersant concentration. K_{sdis} for both naphthalene and 1-methylnaphthalene kept increasing over a wide concentration range, confirming the important role of the sorbed dispersant. For pyrene, K_{sdis} increased with dispersant and reached a peak before CMC, and then dropped abruptly at ~CWC, indicating the formation of aqueous micelles sharply reduced pyrene uptake. Interestingly, K_{sdis} remained nearly constant thereafter until C_{dis}> 100 mg/L, suggesting the pyrene partitioning was proportional between the two phases. The results revealed that PAHs of higher K_{ow} tend to partition into sorbed hemimicelles/admicelles at C_{dis}< CMC, but are more prone to partitioning into the aqueous micelles once they are formed. The observation differs from that in surfactant-only systems. For instance, Ko et al. (1998) and Zhou and Zhu (2005) observed constant K_{sdis} in the above-CMC range for naphthalene and phenanthrene with SDS and TX 100, but a dropping K_{sdis} with increasing Tween 80. The important role of the dispersant in enhanced PAH sorption is further revealed by the fact that the K_{sdis} values are greater than the corresponding K_{oc} (Table 2-5) by a factor of 1.11 to 17.77.

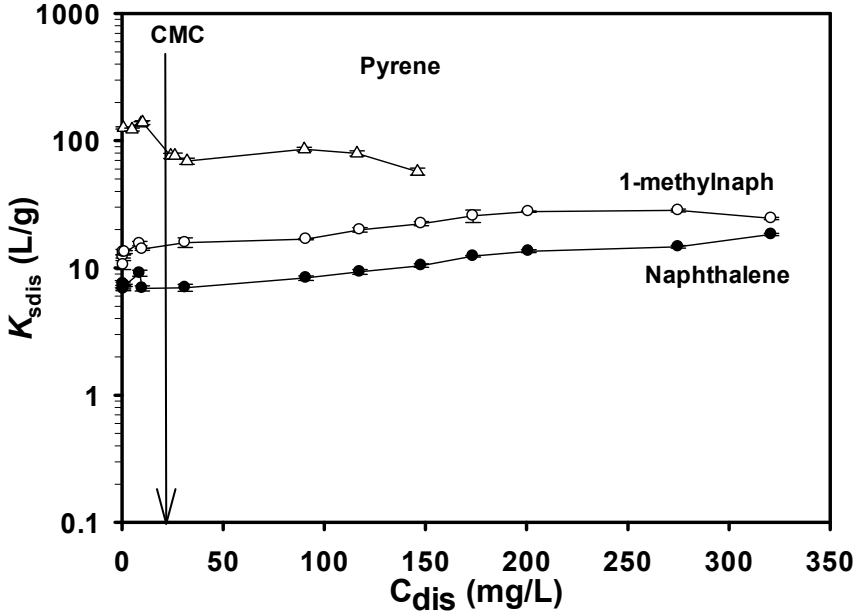

Fig. 2-7. The PAH partition coefficient to sediment-sorbed dispersant (K_{sdis}) as a function of equilibrium aqueous concentration of Corexit EC9500A (C_{dis})

2.3.6. Effects of dispersant on uptake of PAHs under deepwater conditions

Fig. 2-6 and Fig. A-2 compare the K_d^o and K_d^o/K_d vs. C_{dis} curves for the PAHs under the surface and deepwater conditions (16 MPa, 4 °C, salinity = 3.5 wt.%). For the less hydrophobic PAHs (naphthalene and 1-methylnaphthalen), the dispersant enhanced the PAH uptake to a lesser extent (i.e., a lower K_d^o/K_d) under the deepwater conditions, though K_d^o increased steadily with increasing dispersant uptake. For pyrene, a much broader peaking profile was evident under the deepwater conditions, where the CWC was extended from 50 to 180 mg/L.

Under the deepwater conditions the solubility of naphthalene, 1-methylnaphthalene and pyrene dropped by 44.2%, 45.3% and 63.3%, respectively. The deepwater conditions also diminished the dispersant solubilization effectiveness. For instance, in the presence of 200 mg/L of the dispersant, the dispersant-facilitated solubility for the three PAHs decreased by 50.7%, 56.9% and 72.8%, respectively. Such solvent-driven process resulted in higher overall PAH

uptake (i.e., higher K_d) at lower temperature (He et al. 1995, Zhang et al. 2009). Then, the diminished dispersant effect (lower K_d^o/K_d) under the deepwater conditions is attributed to the lowered dispersant uptake and heightened K_{oc}.

The salting-out effect plays an insignificant role in lessening the solubilization effect of the dispersant than temperature and pressure. Of the latter, temperature exerts more effects on the solubility than pressure (Oliveria et al. 2009). The surfactant CMC is remarkably heightened at the deepwater temperature, and the temperature effect is enlarged under saline conditions (Schick 1963). For instance, lowering temperature from 25 to 5 ^oC in a 0.6 M NaCl solution increased the CMC for n-dodecanol by 61% (Schick, 1963). Higher salt concentration lowers the CMC, but to a lesser extent. On the other hand, pressure was reported to be an important factor governing the formation and characteristics of surfactant micelles, and smaller micelles are formed under elevated pressure, which diminishes the dispersant solubilization effect on PAHs (Innocente et al. 2009).

2.3.7. Effects of WAO and DWAO on sorption of PAHs

Fig. 2-8 shows that the presence of WAO and DWAO increases the uptake for all three PAHs on the sediment. The equilibrium uptakes of naphthalene, 1-methylnaphthalene and pyrene were enhanced by 3.2%, 5.5% and 8.6%, respectively in the presence of WAO, and 14.1%, 19.2% and 15.3% by DWAO. Gong et al. (2014b) reported that the Corexit EC9500A greatly enhanced the solubility of various petroleum hydrocarbons, such as linear aliphatic hydrocarbons, branched aliphatic hydrocarbons, aromatic hydrocarbons, cyclic aliphatic hydrocarbons and alkenes. As a result, the sediment will take more of these dispersed hydrocarbons when exposed to DWAO than WAO, which in turn results in more hydrophobic sorption sites for PAHs. In addition, the petroleum components can act as a “plasticizer” for

SOM, which softens or swells SOM, facilitating accessibility of the sorption sites (Jonker et al. 2003). Moreover, the dispersant and the petroleum components may interact synergistically on the sediment surface, facilitating formation of more and larger hemimicelles/admicelles.

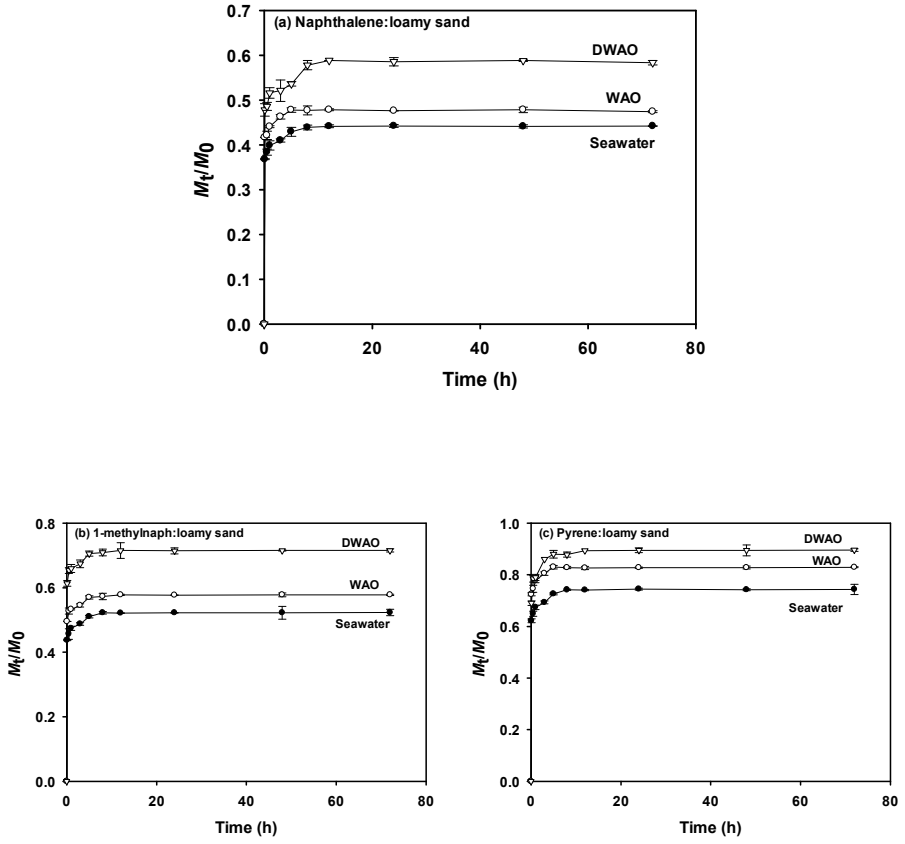

Fig. 2-8. Effects of WAO and DWAO on sorption kinetics of PAHs onto a loamy sand sediment.

2.4.Conclusions

This study investigated effects of a prototype oil dispersant on solubilization, sorption and desorption of three model PAHs with two representative Gulf Coast marine sediments under surface water and deepwater conditions. The primary findings are summarized as follows:

(1) The dispersant can linearly enhance the solubilities of PAHs. While pure surfactants enhance PAH solubilization primarily in the above-CMC concentration range, the dispersant effectively enhanced PAH solubilization in both sub- and above-micellar concentrations. Partitioning of PAHs to the dispersant micelles/aggregates correlates well with the K_{ow} values of the PAHs.

(2) The dispersant can be sorbed onto the sediment and the sorption isotherm displayed a characteristic S-shape, and the abrupt rise in dispersant uptake occurred at the dispersant concentration ~5 times higher than CMC. The dispersant uptake was ~10% lower under deepwater conditions.

(3) The dispersant enhanced both the sorption extent and rates of the PAHs for both sediments. The sorbed dispersant provides additional adsolubilization capacity for PAHs, and the presence of the dispersant during desorption of PAHs rendered remarkable hysteresis for the PAHs. The PAH partition to the sorbed dispersant exceeded that to SOM by a factor of1.11 to 17.77, indicating sorption to the sorbed dispersant was the key mechanism for enhanced PAH uptake and hysteresis.

(4) The dual-mode models were able to adequately simulate the sorption isotherms and kinetics in the presence of various concentrations of the dispersant, and the dispersant-enhanced PAH uptake can be quantified by the linear partition parameter K_D.

(5) For more soluble PAHs (naphthalene and 1-methylnaphthalen), the uptake increases linearly with increasing dispersant concentration over a broad dispersant concentration range (up to 270 mg/L), while for less soluble PAHs (e.g., pyrene), K_d^o/K_{d} peaked at the half CMC, and a "wash off" of the sorbed PAH ($K_d^o/K_{\mathrm{d}}< 1$) occurred at slightly above the CMC.

(6) The deepwater conditions diminished the dispersant effect on solubilization, resulting in much lowered PAH solubility, and enhanced uptake of the PAHs, despite the lowered dispersant uptake.

(7) The presence of WAO and DWAO markedly enhanced the uptake of the PAHs due to the elevated uptake of oil hydrocarbons and the dispersant.

The results may aid in understanding the roles of oil dispersants on environmental distribution, fate, and transport of oil dispersants, spilled oil and persistent oil components.

Chapter 3. Dispersion, sorption and photodegradation of petroleum hydrocarbons in seawater-sediment systems

This chapter summarizes the effects of dispersant on dispersion of crude oil *via* using varied dispersant oil ratios (DORs). Total petroleum hydrocarbons (TPHs), *n*-alkanes and both parent and alkylated PAHs were investigated to explore the distribution of these key petroleum hydrocarbons. The effectiveness of three model dispersants were compared. The sorption and photodegradation behaviors of these dispersed petroleum hydrocarbons were also studied under simulated marine conditions.

3.1.Introduction

The Deepwater Horizon (DwH) oil spill on April 20th, 2010 released 7.94×10^8–1.11×10^9 L of Louisiana Sweet Crude (LSC) oil into the Gulf of Mexico (Reddy et al. 2012, Sammarco et al. 2013). The spilled oil contains saturated *n*-alkanes, polycyclic aromatic hydrocarbons (PAHs), and their alkylated homologues with over 50% as low-molecular-weight petroleum hydrocarbons (methane and C2-C11 alkanes) (Ryerson et al. 2012). During the spill, elevated concentrations of oil components such as *n*-alkanes, PAHs (both parent PAHs and alkylated ones), benzene, toluene, ethylbenzene and xylene (BTEX) were detected in both surface and deepwater samples (Camilli et al. 2010, Diercks et al. 2010, Sammarco et al. 2013, Wade et al. 2011). To mitigate the environmental impact, approximately 8.21×10^6 L of chemical dispersants (Corexit EC9500A and Corexit 9527A) were applied to break surface oil slicks into fine droplets and disperse oil components into the water column (Kujawinski et al. 2011). Among the petroleum hydrocarbons, *n*-alkanes are not major health hazards since the C-C bonds linked chains are readily biodegraded, however, biological effects tests suggest that other persistent oil components, especially PAHs, are highly toxic, carcinogenic and mutagenic and

can pose long-term threat to the environmental and ecological health (Turner et al. 2014). Long chained *n*-alkanes, and PAHs were commonly detected in oil residuals near in shoreline areas including salts marshes, sediments, coastal wetlands, oil mousse/tar balls and submerged oil mats (Liu et al. 2012b, Turner et al. 2014, Yin et al. 2015a, Yin et al. 2015b). The coastal ecosystem were heavily damaged by spilled oil and oil residuals. Based on a field study tracking gill tissues of larval and adult fish in Louisiana area, aberrant protein expression, physiological and reproductive impairment remained significant (Whitehead et al. 2011). In addition, a study conducted at Pensacola Beach, FL, revealed that the spilled oil had a profound impact on both abundance and community composition of indigenous bacteria in marine system (Kostka et al. 2011). As the long-term effects of this environmental disaster continue to unfold, researchers have proposed a range of risk parameters and long-term monitoring strategies to determine the contaminant levels in the affected areas (Gohlke et al. 2011).

Now, five years after the spill,our knowledge on the fate and transformation of the spilled oil remains rudimentary, not only because of the unprecedented amounts of spilled oil and dispersants applied, but also owing to the fact that the spilled oil experienced a unique series of complex processes following their release at a depth of 1500 m (Reddy et al. 2012). While oil in the water column appears gone five years after the DwH spill, weathered or persistent oil remains in coastal sediment such as Bay Jimmy and the barrier islands near Grand Isle, LA (Turner et al. 2014). Typically, released oil undergoes a variety of weathering processes including evaporation, dissolution, dispersion, photochemical oxidation, water-oil emulsification, bio-degradation and adsorption onto suspended particulate materials (Wang and Fingas 1997). While limited field data have indicated the weathering trend of persistent oil components such as >C18 alkanes and PAHs (polycyclic aromatic hydrocarbons) in sediments (Turner et al. 2014),

the rate and extent of various weathering mechanisms have been lacking. Based on the oil budget calculator developed by Department of Interior (DOI) and National Oceanic and Atmospheric Administration (NOAA), the direct recovery from the wellhead, burning and skimming removed 17%, 5% and 3% of spilled oil, respectively (Lubchenco 2010); 25% of the oil was naturally evaporated or dissolved during the travel from wellhead to the gulf surface/shoreline; and chemical dispersion and natural dispersion accounted for 8% and 16% removal of total oil, respectively; and the residual amount (26%) included the oil on/below the surface in forms of light sheen or tar balls. Based on our prior work, significant amounts of oil components including linear aliphatic hydrocarbons, branched aliphatic hydrocarbons, cyclic aliphatic hydrocarbons, aromatic hydrocarbons, and alkenes have been sorbed by marine sediments, which may greatly extend the natural weathering processes (Gong et al. 2014b).

Both dissolution and dispersion are important processes governing the fate and distribution of released oil. Dissolution is the process by which oil hydrocarbons are dissolved into water forming a solution, whereas dispersion is the processes by which oil slicks are broken down into smaller droplets and dispersed in water column (Lubchenco 2010). Due to the low solubility of petroleum hydrocarbons, oil dispersants are often applied to enhance the apparent solubility of the hydrocarbons and to increase their bioavailability. The *n*-alkanes are extremely insoluble, the solubility gets lower for longer chained *n*-alkanes (Diallo et al. 1994). Low molecular weight PAHs such as naphthalene, phenanthrane are considered as a major soluble fraction of petroleum (Gong et al. 2014a, Zhao et al. 2015). Both *n*-alkanes and PAHs can be effectively solubilized via commonly used surfactants (Bruheim et al. 1999, Edwards et al. 1991). Dispersants are mainly composed of surfactants and have been used for oil spill mitigation for more than 50 years (Board 2005). Both surfactants and solvents in dispersants are responsible for dispersing

petroleum hydrocarbons. Typically, the solubilities of light crude and heavy crude are 10-50 and 5-30 mg/L, respectively (Fingas 2012). Based on studies on 8 EPA approved dispersants, researchers observed that at a dispersant-oil ratio (DOR) of 1:10, the total petroleum hydrocarbons (TPHs) in the water column ranged from 6.8 mg/L with the least effective dispersant (JD-2000) to 1800 mg/L with the most effective ZI-400. Using the dispersant Corexit 9500A at a DOR of 1:100, researchers observed the concentration of total *n*-alkanes increased from 73 to 5492 μg/L (Özhan et al. 2014). Corexit EC9500A can also effectively solubilize both parent PAHs and their alkylated homologous (Gong et al. 2014b, Zhao et al. 2015).Limited information is available on whether different petroleum hydrocarbons are dispersed equally or preferentially. Furthermore, information is lacking on how different dispersants behave in terms of dispersion of various petroleum components with various M.W. and molecular structures.

Sorption of petroleum hydrocarbons onto suspended particulate matter or sediments has been recognized as an important process for oil transport (Gong et al. 2014a). In sediment-water systems, the distribution of petroleum hydrocarbons between sediment and water is governed via soil organic matter (SOM) content and properties of hydrocarbons. The introduction of an oil dispersant poses two contrasting effects on the sorption behavior of oil components: on the one hand, the dispersant can enhance solubilization of petroleum hydrocarbons thereby favoring the desorption process, on the other hand, the surfactants molecules can also be sorbed on the sediment surface and then serve as an added sorption sink for petroleum hydrocarbons, resulting in more uptake of petroleum hydrocarbons. For instance, in the presence of 18 mg/L of Corexit 9500A, the uptake of phenanthrene by a loamy sand sediment was increased by 7% compared to that without dispersant (Gong et al. 2014b). Zhao et al. also found that such contrasting effects (solubilization versus adsolubilization) are dependent on the DOR (Zhao et al. 2015).

Photodegradation under solar irradiation is an important natural weathering process for petroleum hydrocarbons in marine systems, yet,the photodegradation rate and extent may vary for different types or portions of petroleum hydrocarbons. For example, petroleum *n*-alkanes are readily biodegraded but are recalcitrant to sunlight irradiation due to their lack of ability to absorb UV (Tjessem and Aaberg 1983). It was also reported the photodegradation of *n*-alkanes were enhanced with increasing amounts of a photosensitizer (e.g., quinones or PAH-alcohols, such as anthraquinone or 1-naphthol) (Boukir et al. 2001, Guiliano et al. 1997). Theoretically, PAHs are intrinsically stable considering the π electrons are delocalized over the aromatic rings. They are highly photo-reactive owing to the ability to absorb light in UV region and direct photolysis is the main mechanism associated with the degradation of linear PAHs (Plata et al. 2008). Interestingly, when various PAHs are mixed with *n*-alkanes (1:100 mole/mole) and irradiated under UV, photoalkylation occurred readily and significant amounts of alkylated PAHs were formed within 5h (Mahajan et al. 2003). Little has been reported on the details ofphotodegradation of petroleum hydrocarbons in the presence of oil dispersants (or dispersed petroleum hydrocarbons).

The overall goal of this work is to investigate the dispersant-facilitated dissolution, sorption/desorption and photodegradation of petroleum hydrocarbons in marine water-sediment systems. The specific objectives were to: (1) investigate the effects of three model dispersants on dispersion of various types and fractions of petroleum hydrocarbons, (2) determine the effects of dispersants on sediment sorption of dispersed petroleum hydrocarbons, and (3) explore the photodegradation patterns of dispersed petroleum hydrocarbons under simulated solar irradiation.

3.2.Materials and methods

3.2.1. Chemicals and materials

Chromatographic gradeacetone, hexane and dichloromethane (DCM) were purchased from Fisher Scientific (Fair lawn, NJ, USA). Silica gel (60-200 μm) was acquired from Sigma-Aldrich (St. Louis, MO, USA) and was activated prior to each use. Sodium azide (NaN_3) of analytical grade was obtained from Fisher Scientific. Dispersants Corexit EC9500A and Corexit 9527A were acquired per courtesy of Nalco Company (Naperville, IL, USA), whereas SPC 1000 was purchased from Polychemical Corporation (Chestnut Ridge, NY, USA). A standard reagent consisting of 16 EPA listed PAHs, a standard of *n*-alkanes mixtures (C9-C40), Pristane (Pr), Phytane (Ph), two internal standards (5α-androstane for *n*-alkanes and fluorene-d_{10} for PAHs), and a surrogate standard mixture of naphthalene-d_8, acenaphthene-d_{10}, phenanthrene-d_{10} and benzo(a)pyrene-d_{12} were purchased from Supelco (Bellefonte, PA, USA).

Activation of the silica gel was performed following an established protocol (Wang et al. 1994). The silica gel was rinsed three times with acetone, hexane and DCM sequentially. Following initial air-drying, the silica gel was heated in the oven at 50 °C for 8 hours and subsequently at 180 °C for 20 hours to obtain the activated silica gel.

A surrogate LSC oil was acquired through the courtesy of BP Company (Houston, TX, USA). Before use, 1 L of crude oil was artificially weathered by purging the oil with air in a flask in dark at a pressure of 18 psi for 4 weeks to eliminate the lighter compounds, simulating the loss of volatile compounds at sea surface shortly after the oil spill (Li et al. 2009). After the weathering process, the LSC lost 33% of its initial mass, and its density increased from 0.81 to 0.91 g/cm^3.

3.2.2. Seawater and sediment samples

Seawater was collected from the top water column (30 cm) at Grand Bay, AL, USA (N30.38/W88.18) in October 2012. Before use, the seawater was filtered through a membrane (0.45 μm) to remove suspended solids, and then sterilized through autoclaving at 121 °C for 35 min. The salient properties of the treated seawater include: pH = 7.86, dissolved organic carbon (DOC) = 0.82 mg/L, salinity = 3.5 wt. %, Cl^- = 13.45 g/L, NO_3^- = 2.85 g/L and SO_4^{2-} = 4.25 g/L. The analytical methods have been provided elsewhere (Zhao et al. 2015). The treated seawater was free of *n*-alkanes and PAHs.

A loamy sand sediment was sampled at N30.37926/W88.30684 of the same area. The sediments were wet-sieved with seawater to obtain a fraction of 75–840 μm and then air-dried for 7 days. The dried aggregates were further oven-dried for 6 h at 80 °C before use. Sediment analyses were performed by the Soil Testing Laboratory at Auburn University, and the method details have been described elsewhere (Zhao et al. 2015). Table 2-3gives salient properties of the sediments. The total *n*-alkanes and PAHs in the sediment were 0.139 μg/g and 0.037 μg/g, respectively.

3.2.3. Dispersion of various petroleum hydrocarbons at various DORs

Water accommodated oil (WAO) and dispersant-enhanced WAO (DWAO) were prepared following a standard method (Singer et al. 2000). In brief, WAO was prepared in 2200 mL glass aspirator bottles containing a hose bib fitted with silicon tubing and clamp at the bottom of the vessels. Each bottle was filled with 1760 mL of seawater, leaving a 20% headspace. About 8.8 mL of the weathered LSC was carefully added to the seawater using a glass syringe (oil:seawater volume ratio = 1:200, v/v), and then the mixture was sealed and magnetically stirred for 18 h in dark. The stirring plate was adjusted to obtain a vortex of ~30% of the total volume of seawater.

After quiescent settling for 6 h, the WAO fraction was collected in glass vials with Teflon-lined caps from the bottom without disturbance of the oil remaining at the surface. DWAO was prepared following the same protocol except that a dispersant was added. The DOR was varied at 1:300, 1:50, 1:20, 1:10 and 1:2 (v/v). To compare the effectiveness, three oil dispersants (Corexit 9500A, Corexit 9527A and SPC 1000) were applied while holding the same DOR (1:20).

The WAO or DWAO was sampled at 250 mL and then analyzed for various fractions of petroleum hydrocarbons (*n*-alkanes, PAHs and their alkylated counterparts) following the procedure described in Section 3.2.6. As a control, dispersant solutions without oil were prepared under identical conditions and then extracted and analyzed for the non-petroleum hydrocarbons from the dispersants (Major et al. 2012) (See Section 3.2.6 for the analytical methods). The chromatogram peak areas associated with some non-petroleum hydrocarbons were deducted in quantifying the petroleum hydrocarbons following the approach by Hemmer et al. (Hemmer et al. 2011). All tests were conducted at least in duplicate to ensure the data quality and the error bars are calculated based on the standard deviation.

3.2.4. Sorption of dispersed petroleum hydrocarbons by sediment

The DWAO solution with Corexit EC9500A at DOR of 1:20 was used as the working solution. To inhibit microbial activities during the experiments, 200 mg/L of sodium azide was added in the solution before the sorption tests. The sorption batch tests were conducted by mixing 42 mL of the DWAO solution with 2 g of the sediment in amber glass vials. The vials then were placed on an end-to-end rotator at 60 rpm in dark at room temperature (22 ± 1 ºC). The vials were sacrificially sampled at predetermined time intervals then centrifuged at 3000 rpm (1509 g-force) and a combined total of 300 mL of supernatants was collected from 9 of the vials and then analyzed for various alkanes and PAHs. To test the effects of the dispersant, the

additional Corexit EC9500A (18 and 180 mg/L) was added into the initial DWAO solution, and the sorption tests were carried out under otherwise identical conditions. To confirm the mass balance, the sediment phase was extracted using DCM following a solid extraction procedure (Liu et al. 2012b) and analyzed for the TPHs. The results showed that the maximum error was <6.5%. Control tests were conducted using corresponding dispersant solutions under identical conditions to deduct the non-petroleum hydrocarbons.

3.2.5. Photodegradation of dispersed petroleum hydrocarbons

To ensure the consistency, 14L of a DWAO solution was prepared with Corexit EC9500A at a DOR of 1:20 and stored in a refrigerator at 4 ºC. For each run, 300 mL of the DWAO solution was transferred into a glass photo-reactor (with almost zero headspace as shown in Fig. 3-1), which was then sealed with a quartz plate cover (surface area= 78 cm^2). An Oriel Sol 1A solar simulator (Newport Corporation, Irvine, CA, USA) was used as the sunlight source and the light intensity was determined to be 232 W/m^2 on the solution surface. This light dose is in accord with the reported solar energy (208 W/m^2) in the Grand Bay area(NREL 2009). The sunlight simulator was operated in an intermittent fashion (i.e., 12 h light on and then 12 h off). Solution samples were collected at predetermined time intervals for 14 days. The temperature was controlled at 17 ± 1 ºC with a circulating water bath system. Control tests were carried out in dark to quantify mass losses due to other mechanisms (e.g., sorption and volatilization). The experiments were conducted in duplicate.

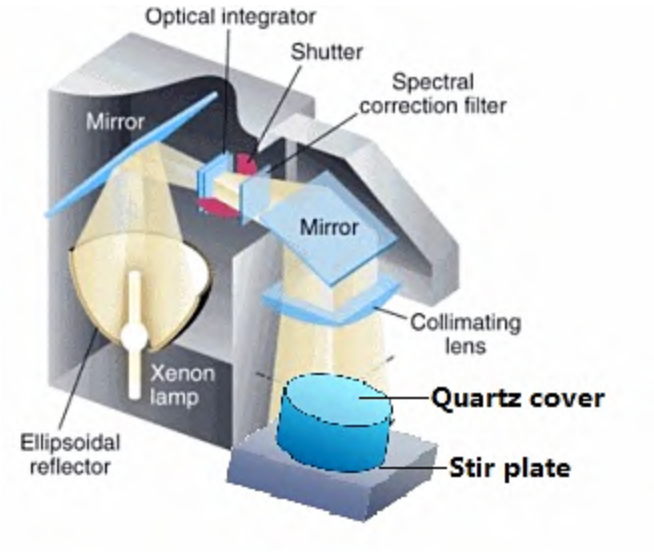

Fig. 3-1. Photoreactor and sunlight simulator

3.2.6. Sample preparation and analytical methods

For analysis of the crude oil, 15 μL of the weathered LSC was diluted with 1.5 mL of hexane and passed through 3 g of sodium sulfate drying column to remove moisture. The column was then rinsed by another 3 mL of hexane and the eluents were combined analyzed for TPHs *via* the GC-FID or GC-MS methods described below.

TPHs in water samples were extracted using DCM in three consecutive steps (250 mL solution with 30 mL DCM in each step). The extracts were combined and filtered through a glass column packed with 5 g of anhydrous sodium sulfate. The DCM extracts were then concentrated via a Rotovap evaporator (SENCO Technology Co. Ltd, Shanghai, China) and exchanged with hexane to a final volume of 10 mL. The clean-up and fractionation of the samples were carried out by modifying the procedure by Wang et al. (1997). Briefly, a chromatographic column was built by packing 3 g of anhydrous sodium sulfate on top of 3 g of the activated silica gel overlying 2 cm of glass wool at the bottom. The column was initially charged with 20 mL of

hexane and the sample was added before the top layer was exposed to the air. After loading the sample, 12 mL of hexane was added from the top to elute the saturated hydrocarbon fraction (*n*-alkanes) labeled as F1; then, 15 mL of hexane-DCM mixture (50% v/v) was introduced to elute the aromatic hydrocarbons referred to as F2. TPHs were then obtained by combining F1 and F2 at 1:1 (v/v), designated as F3. Before analysis, these fractions were further concentrated to 0.5 mL under a gentle nitrogen stream.

F1 samples were analyzed for *n*-alkanes (C9-C40) using a GC-FID (Agilent 6890 GC-FID system) equipped with a DB5 column (30 m × 0.25 mm, 0.25 μm film thickness). The injection volume was 1 μL with a split ratio of 20. The column temperature was programmed to ramp from 40 to 280 °C at a rate of 8 °C min^{-1} and then held at 280 °C for 60 min (Fu et al. 2014, Liu et al. 2012b). GC-MS was also used for reanalyzing the samples in total ion mode to identify the non-petroleum hydrocarbons based on the NIST library and the peaks in control batches of dispersant solution. The *n*-alkenes were quantified based on the internal standard of 5α-androstane and external standards of *n*-alkenes (C9-C40).

PAHs in F2 were analyzed using GC-MS (Agilent Gas Chromatography 7890A coupled with the 5975C Series Mass Spectrometry). The 16 parent PAHs (specified in EPA Method 610) and 17 alkylated homologues were targeted. The analytical method was optimized and the selected ion monitoring (SIM) mode was set up based on the previous reports and the NIST library in GC-MS (Liu et al. 2012b, Wang et al. 2007). A DB-EUPAH column (30 m × 0.18 mm, 0.14 μm film thickness) was used to separate the analytes. The inlet temperature was set at 250 °C. The GC oven temperature was programmed as follows: 40 °C (1 min hold) ramped to 280 °C at 8 °C/min and held for 40 min. The sample injection volume was 2 μL. Standard curves were developed for each PAH following EPA Method 610 and the alkylated homologues were

estimated according to a semi-quantitative method using relative response approach described somewhere else (Wang et al. 2007, Yin et al. 2015b). The recoveries of the surrogate standards naphthalene-d_8, acenaphthene-d_{10}, phenanthrene-d_{10} and benzo(a)pyrene-d_{12} were 75-81%, 81-89%, 92-101% and 91-103%, respectively. Table 3-1 and A-4list the selected characteristic ions used for determining each PAH and reference standards for alkylated homologs.

For the TPH measurement in F3, we adopted the definition that TPHs refer to the sum of all GC-resolved and unresolved hydrocarbons (Wang and Fingas 1997). The resolvable TPHs appear as peaks and the unresolved complex mixture (UCM) appears as a "hump" in the chromatograms. The total TPHs, which include both peaks and humps on the chromatograms of GC-FID (programmed in the same was as for *n*-alkanes analysis), was quantified using the baseline corrected total area and calculated based on the average response of *n*-alkenes standards (Faksness et al. 2008).

Table 3-1. Target compounds and quantification ions (QIs)

Abbr	Compounds	QIs	Abbr	Compounds	QIs
	Parent PAHs			**Alkylated PAHs**	
	2-Ring			**2-Ring**	
Naph	Naphthalene	128	C1-Naph	C1-Naphthalenes	142
			C2-Naph	C2-Naphthalenes	156
	3-Ring		C3-Naph	C3-Naphthalenes	170
Acl	Acenaphthylene	152	C4-Naph	C4-Naphthalenes	184
Ace	Acenaphthene	154			
Fluo	Fluorene	166		**3-Ring**	
Phen	Phenanthrene	178	C1-Fluo	C1-Fluorenes	180
An	Anthracene	178	C2-Fluo	C2-Fluorenes	194
			C3-Fluo	C3-Fluorenes	208
	4-Ring		C1-PhenAn	C1-Phenanthrenes/anthracenes	192
Fl	Fluoranthene	202	C2-PhenAn	C2-Phenanthrenes/anthracenes	206
Py	Pyrene	202	C3-PhenAn	C3-Phenanthrenes/anthracenes	220
BaA	Benz(a)anthracene	228	C4-PhenAn	C4-Phenanthrenes/anthracenes	234
Chry	Chrysene	228			
				4-Ring	
	5 or 6-Ring		C1-FlPy	C1-Fluoranthrenes/pyrenes	216
BbF	Benzo(b)fluoranthene	252	C2-FlPy	C2-Fluoranthrenes/pyrenes	230
BkF	Benzo(k)fluoranthene	252	C3-FlPy	C3-Fluoranthrenes/pyrenes	244
BaP	Benzo(a)pyrene	252	C1-ChryBa	C1-Chrysenes/benz(a)anthracene	242
IP	Indeno(1,2,3-cd)pyrene	276	C2-ChryBa	C2-Chrysenes/benz(a)anthracene	256
DA	Dibenz(a,h)anthracene	278	C3-ChryBa	C3-Chrysenes/benz(a)anthracene	270
BgP	Benzo(ghi)perylene	276			

3.3.Results and discussion

3.3.1. Oil characterization

Fig. A-3 gives the GC-FID chromatograms of the crude oil used in this work. Fig. 3-2a shows the surrogate crude oil had resolved *n*-alkanes ranging from C9 to C40. The sum of all the *n*-alkanes amounted to 120.1 mg/mL, with C13 being most abundant accounting for 9.1% of the total *n*-alkanes. The C11-C20 was the most abundant group accounting for 67% of total

n-alkanes. The fraction of higher M.W. (C30-C40) *n*-alkanes represented 3% of total *n*-alkanes. Pr and Ph are commonly detected isoprenoids in crude oil, and the Pr/Ph ratio for the surrogate oil was 0.95, which is comparable to the reported value of 0.90 for the Macondo Crude oil (MC252) (Table 3-2).The carbon preference index (CPI) represents the relative abundance of odd-numbered *n*-alkanes to that of even-numbered ones (Ehrhardt and Petrick 1993). The CPI of the oil in this work was measured to be 0.99, which is nearly the same as the reported value of 1.00 for the MC252 oil (Liu et al. 2012b). UCM are mainly composed of branched alkanes, cycloalkanes, aromatics and slightly polar compounds (Faksness et al. 2008, Frysinger et al. 2003, Volkman et al. 1992). The UCM of LSC as shown in Fig. A-3 was quite small and only accounted for 47.1% of TPH. In addition, the n-C17/Pr and n-C18/Ph ratios are also quite comparable, confirming that the surrogate oil used in this work is indeed representative of key characteristics of the MC252 oil.

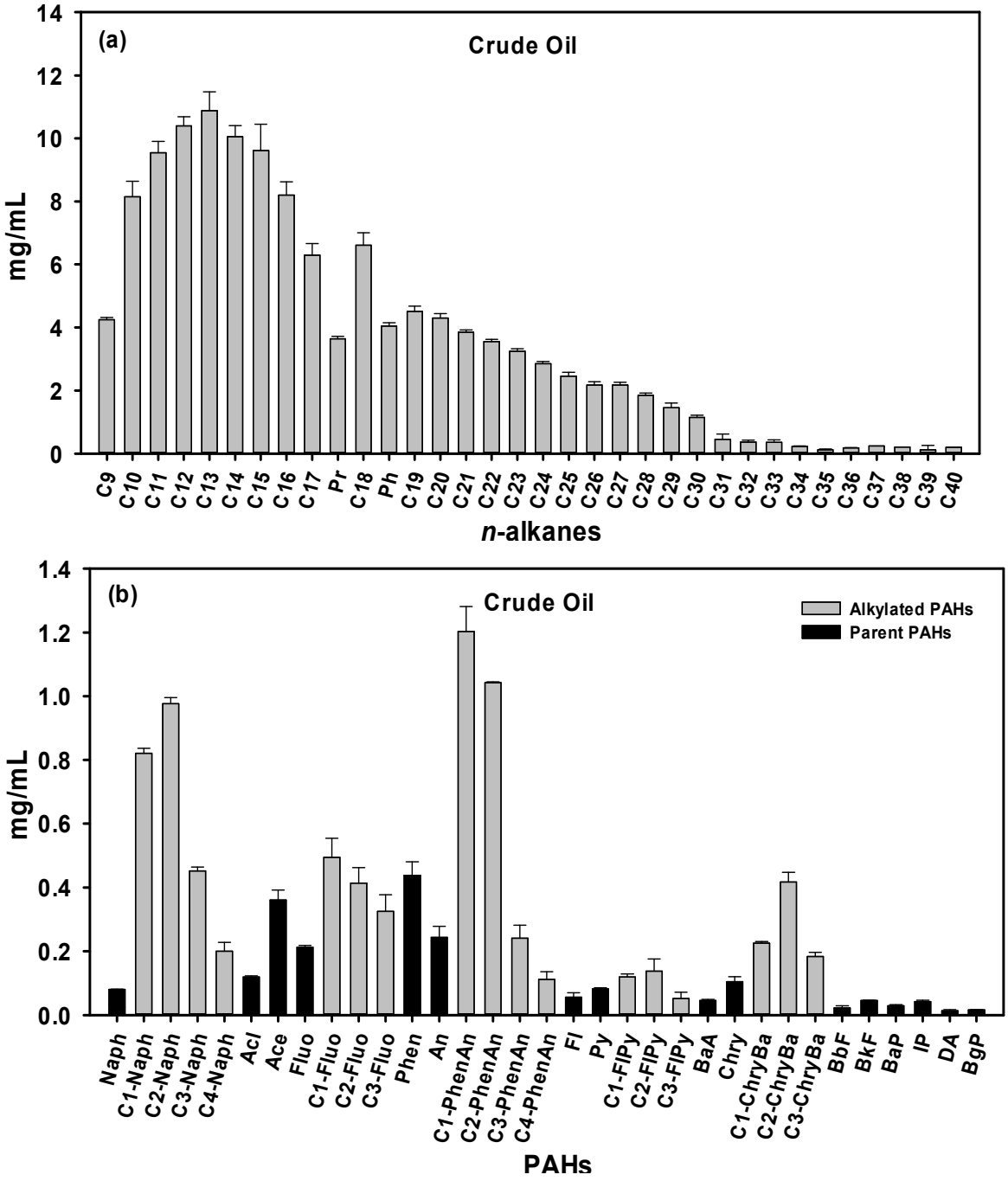

Fig. 3-2. Concentrations of *n*-alkanes (C9-C40), Pristane (Pr), Phytane (Ph) **(a)** and PAHs **(b)** in crude oil

Fig. 3-2b shows the concentrations of 16 parent PAHs and 17 alkylated PAH homologues in the oil sample. The total concentration of the parent PAHs was 1.91 mg/mL Evidently, phenanthrene (Phen) was the most abundant PAH in the oil, accounting for 22.9% of the total PAHs, followed by acenaphthene (Ace), anthracene (An) and fluorene (Fluo), making up 18.9 %, 12.8%, and 11.1%, respectively. Naphthalene (Naph) was reported to constitute 64% of total PAHs in fresh MC252 (Liu et al. 2012b), but represented only 4.2% in the weathered sample, indicating that naphthalene is subject to substantial volatilization loss during the weathering (air-purging) process. The 3-ring PAHs (Acl, Ace, Fluo, Phen and An) constituted 71.9% of the total parent PAHs. Chrysene (Chry) was the most predominant 4-ring PAH and the 4-ring parent PAHs accounted for 15.1% of the total parent PAHs. PAHs with 5 or more rings accounted only for 8.8% of the total parent PAHs.

The combined concentration of alkylated PAHs was 7.41 mg/mL, which is 3.88 times higher than that of the parent PAHs, and the concentrations of individual alkylated PAH homologues all exceeded the corresponding parent PAHs, in consistency with other studies (Liu et al. 2012b, Yin et al. 2015b). For example, concentrations of alkylated naphthalenes (C1 to C4-Naph) and fluorenes (C1 to C3-Fluo) were 30.6 and 5.8 times higher than those of naphthalene and fluorine, respectively. Lastly, alkylated PAHs with 2, 3 and 4 rings accounted for 33.0%, 51.7% and 13.3% of the total alkylated PAHs, respectively, indicating that the 3-ring PAHs are the predominant components for both parent or alkylated PAHs.

3.3.2. Distribution various fractions of petroleum hydrocarbons in DWAO of various DORs

Fig.3-3a shows the distribution of *n*-alkanes in the DWAO prepared with Corexit 9500A at DORs ranging from 1:300 to 1:2. This range covered the suggested surface application DOR (1:20) and the deepsea DOR of Corexit 9500A (1:250) used during the DwH accident (Coolbaugh et al.). In addition, the reported critical micelle concentration (CMC) was 22.5 mg/L (Gong et al. 2014b), and in this work, the applied dispersant amount was ~15.7 mg/L and 2.37 g/L for DOR of 1:300 and 1:2 respectively. Without the dispersant, the WAO contained only 0.11 mg/L of *n*-alkanes, while in the presence of the dispersant at a DOR of 1:300, the total dispersed amount of *n*-alkanes increased by nearly 4.5 fold indicating the dose of Corexit 9500A under CMC also effectively dispersed the *n*-alkanes. At DOR of 1:50 (~90 mg/L of dispersant), the total *n*-alkanes was increased by 85 fold compared to the WAO. And the total *n*-alkanes in the water column were increased further with increasing DOR and it was seemingly there was no fractional changes for *n*-alkanes at various DORs. And the concentrations of *n*-alkanes was observed to be proportionally increased while DOR increased from 1:100 to 1:20 (Özhan et al. 2014). However, if the C9-C40 was divided into four groups as shown in Fig. A-8 and A-9, it was evident that the concentration of group C9-C10 and C11-C20 was linearly related to the DORs ranging from 1:300 to 1:2. While for the group of C21-C30 and C31-C40, the concentration was only linearly increased at DORs ranging from 1:300 to 1:10. When DOR increased from 1:10 to 1:2, the C21-C30 only increased 29% and C31-C40 remained unaltered. And in all cased, C13 was the most abundant species and group of C11-C20 was the most abundant group, which were in accord with the profile of *n*-alkanes LSC oil.

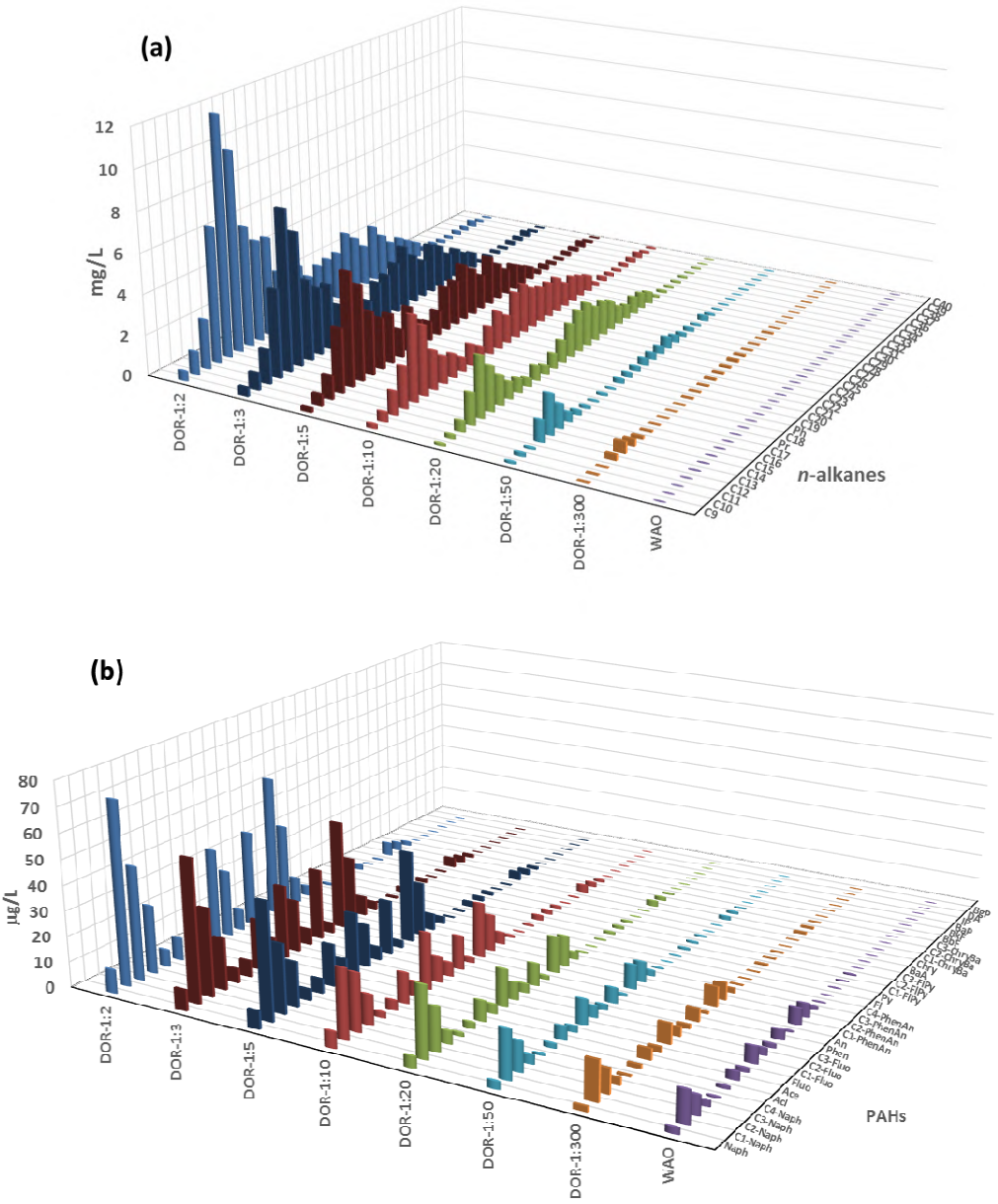

Fig. 3-3. Distributions of *n*-alkanes **(a)** and PAHs **(b)** in WAO and DWAOs prepared at DORs from 0 to 1:2.

The CPIs of all DWAOs were observed in the range of 0.98-1.07, which are comparable to the values for WAO (0.93) or the crude oil (0.99), suggesting the dispersion process did not alter

the CPI. And the n-C17/Pr and n-C18/Ph ratios remained almost same (Table 3-2), indicating there was no significant biodegradation of the dispersed oil in the DWAOs. The overall dispersed TPH ranged from 1.56 to 155.06 mg/L when DORs were increased from 1:300 to 1:2, and the documented TPH ranged from 0 to 11400 mg/L with an average of 202 mg/L in surface seawater sampled from Gulf of Mexico during and after the DwH accident (Sammarco et al. 2013), this high concentration of TPH might due to both chemical dispersion and natural dispersion via biosurfactants in marine systems.

Fig. 3-3b shows the distribution of various parent and alkylated PAHs in the DWAOs. Again, more PAHs were dispersed at elevated dispersant concentrations. In WAO, no 5, 6-ringed PAHs were dispersed and total parent PAHs and alkylated PAHs were 13.8 and 49.4 μg/L. And based on the Fig. A-10 and A-11, when sorted out by the ring numbers, 1-ringed to 4-ringed parent and alkylated PAHs were almost linearly dispersed into water column at all DORs rang. It is also noteworthy that the concentrations of alkylated PAHs decreased with the increasing level of alkylation in the DWAOs. For example, the concentration of alkylated naphthalene follows the order of: C1-Naph> C2-Naph> C3-Naph> C4-Naph, which is consistent with the trend without the dispersant. The dispersion of 5, 6-ringed PAHs were linearly correlated to the DORs ranging from 1:300 to 1:10, and the concentration of such PAHs groups reached a plateau at higher DORs, suggesting that solubilization was saturated or the limitation of dispersant on solubilizing these PAHs. The presence of the dispersant at a DOR of 1:50 elevated the total PAHs by only 1.51 times compared with that in the WAO, which is much less than for *n*-alkanes.

Table 3-2. Characteristics of LSC oil, WAO and DWAOs with three oil dispersants.

	LSC[a]	MC252[b]	WAO	Dispersant 9500A at various DORs					9527A	SPC1000
				1:300	1:50	1:20	1:10	1:2	DOR=1:20	DOR=1:20
TPH(mg/L)	226.90		0.20	1.56	17.83	54.03	75.20	155.06	34.02	80.95
UCM(mg/L)	106.85		0.10	1.06	8.40	25.44	35.41	73.02	16.02	38.12
Total Alkanes(mg/L)	120.05		0.11	0.50	9.43	28.59	39.79	82.04	18.00	48.83
Total parent PAHs(μg/L)	1.91		13.76	16.72	20.76	30.83	45.63	103.04	24.08	36.76
Total alky-PAHs(μg/L)	7.41		49.44	63.38	77.73	114.11	156.32	347.86	97.21	149.03
Alky-PAHs/Parent PAHs	3.88		3.59	3.79	3.74	3.70	3.43	3.38	4.04	4.05
n-C17/Pr	1.64	1.60	1.71	1.67	1.67	1.69	1.70	1.67	1.63	1.84
n-C18/Ph	1.63	1.60	1.62	1.65	1.65	1.63	1.63	1.60	1.56	1.64
Pr/Ph	0.95	0.90	1.05	1.13	1.11	0.95	1.06	1.07	0.88	0.95
CPI	0.99	1.00	0.93	0.98	0.98	1.07	1.04	0.98	0.82	1.06

[a] Concentration unit for crude oil is mg/mL.
[b] Data from Liu et al. (2012).

The seemingly lower dissolution of PAHs than *n*-alkanes by the dispersant can be attributed to the lower abundance of PAHs in the oil and the different solubilization mechanisms for alkanes and PAHs. Hydrophobic organic compounds (HOCs) can be solubilized via two sites of surfactant: micellar core and polyxyethylene shell.Nonpolar and polar HOCs favor to be incorporated into the micellar core and polyxyethylene shell respectively (Diallo et al. 1994). The *n*-alkanes are nonpolar HOCs and their molar solubilization ratios (MSRs) are found to decrease sharply with the increasing of hydrophile-lipophile balance (HLB) of surfactants. While the MSRs for PAHs are found to increase to a maximum as HLB increases then decreases (Diallo et al. 1994). The surfactants in the dispersant with various HLB may pose different solubilization effects on the *n*-alkanes and PAHs. For PAHs, the solubilization sites are also dependanton their hydrophobicity. For example, naphthalene and pyrene are solubilized at the polyxyethylene shell and in the inner core of the micelle, respectively (Mohamed and Mahfoodh 2006), and the estimated MSRs of Corexit 9500A are also different for these two PAHs (Zhao et al. 2015). Thus, some *n*-alkanes may compete with highly hydrophobic PAHs for the solubilization sites in the micelle cores. In addition, with the presence of an oil phase, the PAHs with higher hydrophobicity are more favorable to incorporate into the oil phase (Walter et al. 2000).

3.3.3. Effects of three dispersants on distribution of dispersed petroleum hydrocarbons

The three model dispersants, Corexit 9500A, Corexit 9527A and SPC 1000 were compared for their effectiveness for dispersing the petroleum hydrocarbons. Figs. 3-4a and 3-4b show the distributions of *n*-alkanes and PAHs in the DWAO solutions prepared with the three dispersants. Notably, the distributions of different fractions of *n*-alkanes differed remarkably for the three dispersants. Corexit 9527A appeared more selective for the lower M.W. *n*-alkanes (C10-C16)

with an unusually high dissolution capacity for C10 and C11, and the group of C10-C20 accounted for 70.0% of total *n*-alkanes. Corexit 9500A favorably dispersed both groups of C11-18 and C19-C28, accounting for 47% and 42%, respectively, of the total *n*-alkanes. In contrast, SPC 1000 appeared much more effective over a broad range of *n*-alkanes (C12-C28). The total dispersed TPHs were 31.0, 54.0 and 85.0 mg/L for Corexit 9527A, Corexit 9500A and SPC1000, respectively. The results agree with the observation by Hemmer et al. (Hemmer et al. 2011). Blondina et al. (1999) also observed that Corexit 9500A is 20-40% more effective than Corexit 9527A in a seawater with salinity of 3.5% and they claimed that the performance of Corexit 9527A is heavily affected by salinity (Blondina et al. 1999). The high salinity (3.5%) of seawater in this work could be a main reason for the limited performance of Corexit 9527A.

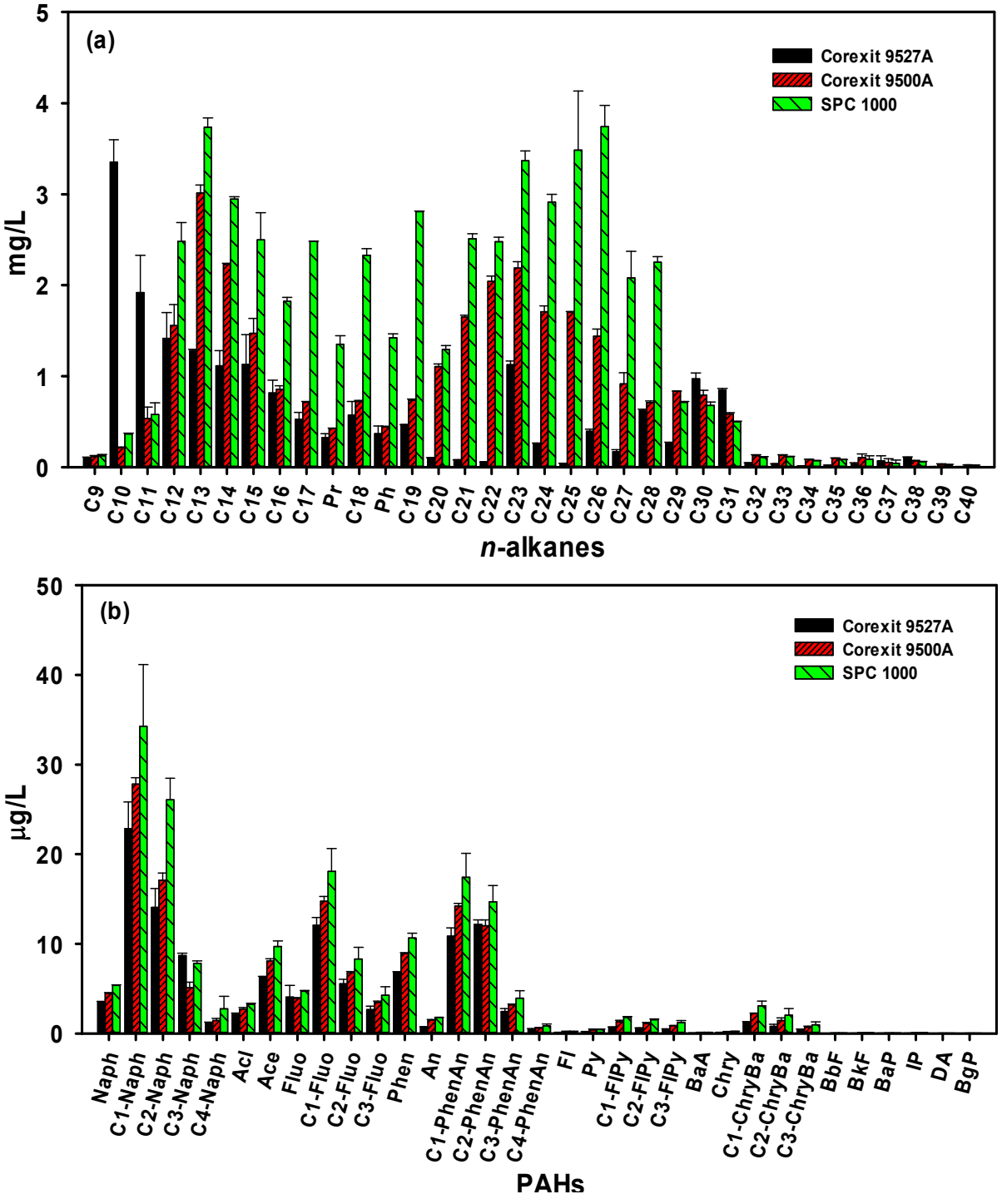

Fig. 3-4. Distributions of *n*-alkanes**(a)** and PAHs **(b)** in DWAOs prepared with Corexit 9527A, Corexit 9500A, and SPC 1000 respectively at DOR (1:20).

Unlike *n*-alkanes, the distribution of dispersed PAHs displayed a quite similar trend for the three dispersants. The total amount of PAHs (combined parent and alkylated PAHs) dispersed was 121.3, 144.9, and 185.8 μg/L, respectively, for Corexit 9527A, 9500A and SPC1000, which again indicates that SPC1000 is the most effective dispersant.

The GC-MS total ion chromatograms in Fig. A-4, A-5 and A-6 confirm the remarkably different distributions of petroleum hydrocarbons for the three dispersants. The reported components of three dispersants were summarized in Table 3-3 and 3-4. For the two Corexit dispersants, 9500A is usually considered as a better formula and it shares the same surfactants as 9527A, but it does not include 2-butoxy ethanol as a solvent (George-Ares and Clark 2000, Scelfo and Tjeerdema 1991). The difference of the GC resolvable solvents in two dispersants were evidenced in Fig. A-4 and A-5. These two dispersants shared the same peaks of 1-hexanol, 2-ehyl-, DPnB and fumaric acid and the results in accord with the previous studies (Major et al. 2012). The solvent, ethanol, 2-butoxy- was identified only in DWAO of 9527A with a significant huge peak suggesting the main role of this solvent in dispersing the TPHs. While for the 9500A, the peak of solvent DPnB was much larger than that in 9527, indicating the predominant role of this solven in 9500A. While for the SPC dispersant, no similar components from Corexit dispersant were identified, instead, only di(propylene glycol) methyl ether was observed in DWAO. Thus, the discrepancy betweenthe solvents in the three dispersants might cause the different dispersion effects. In addition, as discussed in previous section, the solubilization of both *n*-alkanes and PAHs are highly related to HLB of the surfactants,andthe different components and their weight percentages could be another reason.

Table 3-3. Chemical constituents of dispersant Corexit EC9500A and Corexit 9527A[a]

Name	CAS number	Ionic property	Synonym	Molecular formula	Average MW (g/mol)	CMC (mg/L)	Chemical structure
Span 80	1338-43-8	Neutral surfactant	Sorbitan, mono-(9Z)-9-octadecenoate	$C_{24}H_{44}O_6$	428.61	N\A	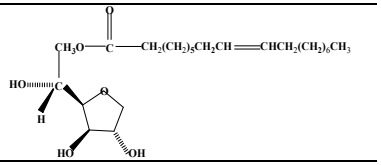
Tween 80	9005-65-6	Neutral surfactant	Sorbitan, mono-(9Z)-9-octadecenoate, poly(oxy-1,2-ethanediyl) derivs.	$C_{64}H_{124}O_{26}$	1310	14	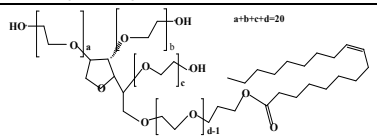
Tween 85	9005-70-3	Neutral surfactant	Sorbitan, tri-(9Z)-9-octadecenoate, poly(oxy-1,2-ethanediyl) derivs	$C_{60}H_{108}O_8 \cdot (C_2H_4O)n$	1838.57	23	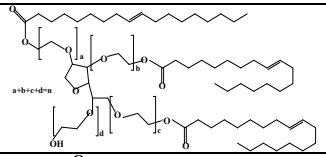
DOSS	577-11-7	Anionic surfactant	Butanedioic acid, 2-sulfo-, 1,4-bis(2-ethylhexyl) ester, sodium salt (1:1)	$C_{20}H_{37}SO_7Na$	444.57	578	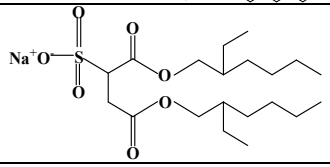
DPnB	29911-28-2	Solvent	Propanol, 1-(2-butoxy-1-methylethoxy)	$C_{10}H_{22}O_3$	190	N\A	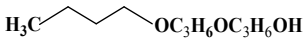
PG	57-55-6	Solvent	Propylene Glycol,1,2,-propanediol, 1,2-dihydroxypropane	$CH_3CHOHCH_2OH$	76.1	N\A	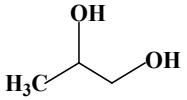
Distillates	64742-47-8	Solvent	Distillates (petroleum), hydrotreated light	N\A	N\A	N\A	N\A

Ethanol, 2-butoxy[b]	111-76-2	Solvent	2-Butoxyethanol	$C_6H_{14}O_2$	118.17	N\A	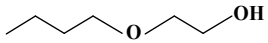

[a]The above information is summarized based on several studies (Glover et al. 2014, Gong et al. 2014b, Kover et al. 2014).

[b]This chemical component is not included in the composition of Corexit 9500A

Table 3-4. Chemical constituents of dispersant SPC 1000[a]

Name	CAS number	Ionic property	Molecular formula	Average MW (g/mol)	CMC (mg/L)	Chemical structure
Poly(ethylene glycol) monooleate	9004-96-0	Neutral surfactant	$C_{20}H_{40}O_4$	344	215	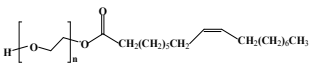
Amines, tallow alkyl, ethoxylated	61791-26-2	Neutral surfactant	N\A	N\A	N\A	N\A
Cocamide DEA	68603-42-9	Neutral surfactant	$CH_3(CH_2)_nC(=O)N(CH_2CH_2OH)_2$, n ~ 8-18	N\A	120	N\A
alkyloxy polyethylene oxyethanol	84133-50-6	Neutral surfactant	$C_{12\text{-}14}H_{25\text{-}29}[CH_2CH_2O]xH$	N\A	56	N\A
Di(propylene glycol) methyl ether	34590-94-8	Solvent	$C_7H_{16}O_3$	148	N\A	N\A

a The above information is summarized based on several studies (Corazza et al. 2010, Kanagalasara et al. 2012)Carbide, U. (2015) Tergitol Surfatants, Product description.

3.3.4. Sorption of petroleum hydrocarbons in DWAOs

Fig. 3-5 shows theuptake of *n*-alkanes and the PAHs onto the loamy sand sediment (Fig. A-12 indicated that the sorption equilibrium reached after two days). After two days of equilibration, the sediment sorbed 52.2% of total *n*-alkanes. The distribution of *n*-alkanes in the solid phase resembled the distribution profiles of the hydrocarbons in DWAOs. This observation indicates that the dispersant played important roles in sorption of the hydrocarbons, i.e., the dispersant molecules facilitated adsolubilization of the oil components on the sediment (Gong et al. 2014b, Zhao et al. 2015). When 18 mg/L of the dispersant was added into the as-prepared DWAO, the uptake of shorter-chained alkanes (C10-C13) increased slightly (3.2%) while total *n*-alkanes uptake remained almost unaffected; further increasing the dispersant to 10 times higher, of the sorbed *n*-alkanes decreased from 310 to 169 mg/L (45%), and much greater desorption effect was observed for higher M.W. alkanes (C>20).

At equilibrium, the sediment sorbed 0.56 μg/g or 86.0% of the parent PAHs and 1.93 μg/g or 80.3% of alkylated PAHs. Interestingly, the ratio of alkylated PAHs to parent PAHs remained same as the ratio in the initial DWAO solution, indicating all PAHs were sorbed proportionally, which again suggesting the sorption was facilitated by or coupled with the dispersant sorption. In addition, the uptake of alkylated PAHs was negatively correlated with the alkylation level, for example the uptake of alkylated naphthalene were found follow the order of: C1-Naph>C2-Naph>C3-Naph>C4-Naph. When additional dispersant was added, 18 mg/L of Corexit 9500A increased the uptake of 2-ring and 3-ring PAHs 18.5 and 10% respectively. The addition of 180 mg/L of dispersant can enhance the solubilization of PAHs resulting in a reduced uptake.

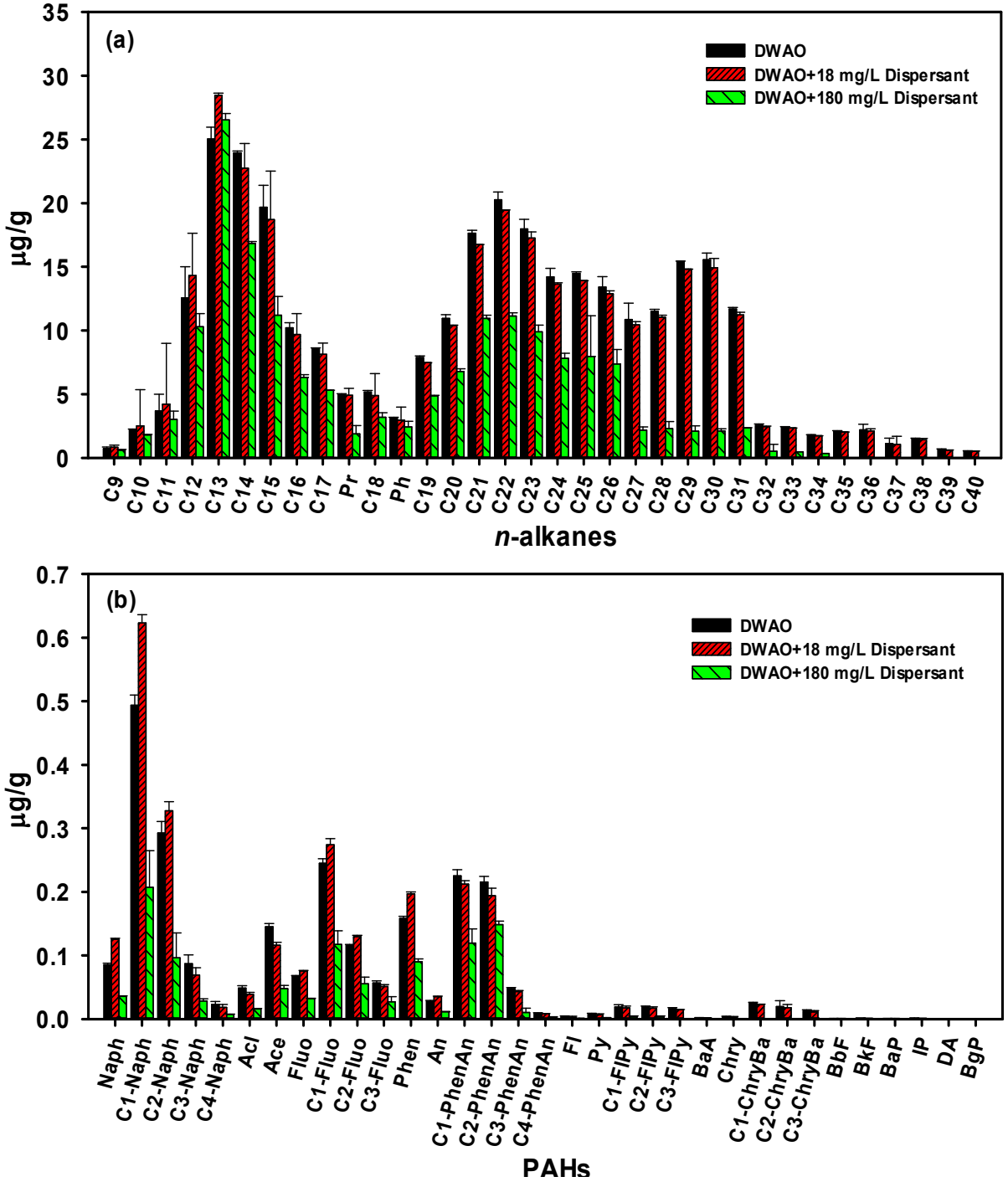

Fig. 3-5. Uptakes and distributions of *n*-alkanes **(a)**, and PAHs **(b)** adsorbed in a sandy loam marine sediment. The DWAO was prepared with Corexit 9500A at DOR=1:20.

The sorption mechanism of PAHs and *n*-alkanes onto sediments are quite different in the water-sediment systems. The *n*-alkanes, unlike PAHs, undergo only nonspecific van der Waals interactions with sorbing sites on sediment (Endo et al. 2008). While for PAHs, the sorption mechanisms are far more complicated and include
"absorption into amorphous" or "soft" natural organic matter or non-aquous phase liquid", "absorption into condensed or "hard" organic polymeric matter", "adsorption onto water-wet organic surfaces", "adsorption to exposed water−wet mineral surfaces" and adsorption into microvoids or microporous minerals" (Luthy et al. 1997). While the introduction of dispersants/surfactants can change the distribution of HOCs via posing two contradicting effects: solubilization and adsolubilization. At lower concentrations, the adsorbed dispersant monomers or aggregates serve as addition sink for taking up more hydrocarbons; on the other hand, at elevated concentrations, the resultant surfactant micelles tend to retain more hydrophobic oil hydrocarbons in the solution phase (Zhao et al. 2015). In surfactant enhanced remediation strategies, the soil-sorbed surfactants molecules usually has weaker retardation capacity for HOCs with higher hydrophobicity and a lower critical washing concentration (CWC) (or lower dose) of surfactant is needed to wash off these HOCs (Zhou and Zhu 2005).

3.3.5. Photodegradation of dispersed petroleum hydrocarbons under simulated sunlight

Fig. 3-6 shows the evolution of*n*-alkanes during the solar irradiation, and Fig. A-7 exhibits the GC chromatograms at Day 2 and Day 4 (One day = 12 h irradiation and 12 h off time). Separate control tests indicated that a total of 22% of *n*-alkanes was lost in 14 days due to volatilization or possible bio-degradation. At Day 2, no significant photodegradation was observed; at Day 7, about 42% of the total *n*-alkanes were lost, and at Day 14, 58.7% was depleted. The CPIs remained unaffected after 14 days of irradiation. Based on the GC

chromatogram in Fig. A-5, not only the alkane peaks were decayed, but the UCM area also decreased. An increase of C17/Pr and C18/Ph wre observed confirming the higher photochemical reactivity of branched alkanes than the linear alkanes.

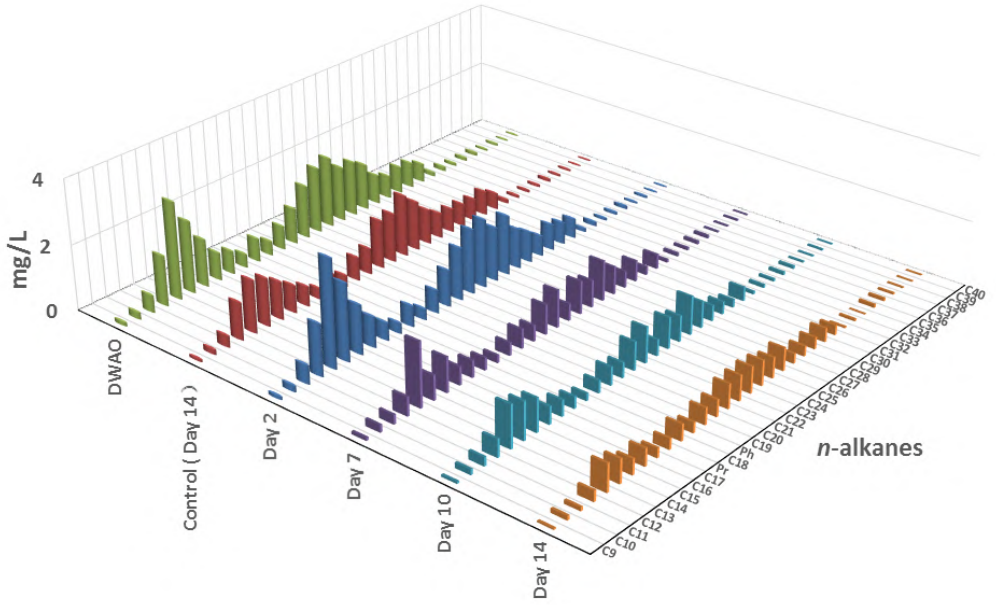

Fig. 3-6. Distributions of *n*-alkanes during photodegradation of DWAO. Experimental conditions: solar energy=232 W/m^2, the simulator was operated in an intermittent fashion (i.e., 12 h light on and then 12 h off), temperature= 17 ± 1 ºC

Fig. 3-7 presents the photodegradation kinetics of three prototype PAHs, i.e., parent and alkylated naphthalene, phenanthrene and fluorene. In all cases, the PAHs were photodegrade rather rapidly and nearly complete degradation was observed in 14 days though the trends appeared different. The parent Naph and Phe were decayed gradually during the two weeks, while the alkylated homologs all peaked at Day 3 then decayed, and the homologs with higher alkylation levels showed higher peaks, i.e., C4-Naph>C3-Naph>C2-Naph>C1-Naph. The fact

that the alkylated PAHs all exceeded the initial levels indicates that the sunlight was facilitating the alkylation of parent or lower level alkylated PAHs whilst photodegradation of the PAHs was also taking place; and the photo-facilitated alkylation rate outweighed the degradation rate in the early stage of the reaction and reached a peak at Day 3. It is noteworthy that for the Fluo group, not only alkylated homologs, but also the parent fluorine peaked at Day 3. The possible reason could be that Fluo is one of the product of Phe photo-degradation (Kou et al. 2008).

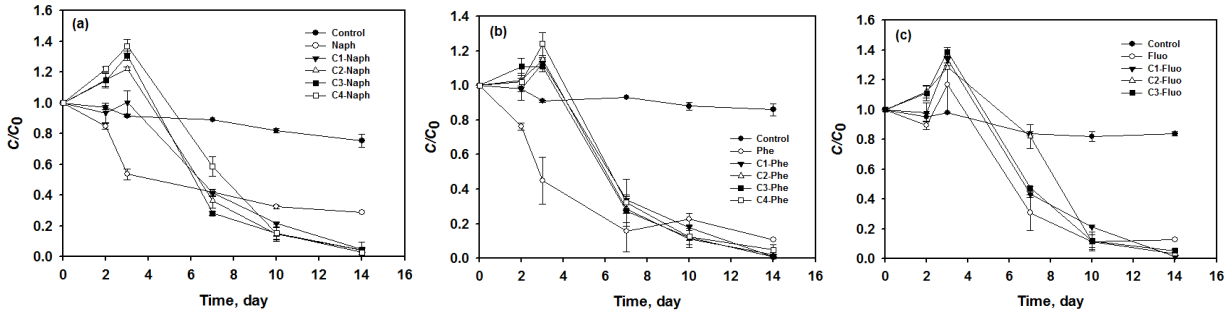

Fig. 3-7. Photodegradation kinetics of dispersed Naph **(a)**, Phe **(b)** and Fluo **(c)** homologs in DWAO under sunlight irradiation. Experimental conditions: solar energy=232 W/m^2, the simulator was operated in an intermittent fashion (i.e., 12 h light on and then 12 h off), temperature= 17 ± 1 ºC

The overall general photo-oxidation pathways of *n*-alkanes following: 1) As the mechanisms proposed, when an alkane C_nH_{2n+2} is photodegraded, the formation of 1-alkane $C_{n'}H_{2n'}$, with n'≤n-3 and methyl ketones $C_{n''}H_{2n''}O$, with n''≤n-2 can be produced (Ehrhardt and Petrick 1985, Guiliano et al. 1997); 2) degradation rate of *n*-alkanes under same conditions decreases with the length of the carbon chain; 3) the presence of photosensitizer is required for *n*-alkanes irradiation, while in the dispersed petroleum solution, PAHs can be easily photo-degraded and produce effective photosensitizers, for example alkynaphthalenes can produce quinones, antracene and phenanthrane can also produce anthraquinone, which is

considered as the best photosensitizer (Guiliano et al. 1997); 4) the branched alkanes have higher photo reactivity than linear alkanes (Rontani and Giral 1990).

The PAHs can be photodegraded via: 1) direct photolysis; 2) energy transfer from an excited PAH triplet state to molecular oxygen and 3) electron transfer from an excited singlet or triplet PAH state to molecular oxygen (Fasnacht and Blough 2002, 2003). The direct photolysis activity is closelyrelated to the quantitative structure of PAHs (Chen et al. 2000).In the present work, theoretically, the photo activity for the abundant PAHs in DWAO was found to follow the order of Fluoranthene ≥Pyrene>C1-Anth(1, Anth)>Anthracene>Phenanthrene>C1-Naphthalene (1, Naph)>Naphthalene (Chen et al. 2000); however, the degradation rate did not adhere to this order, the main reason likely the readily occurring PAH alkylation.

In addition, the components of Corexit 9500A can also be involved into the photolysis of DWAO. Solvent PG can be effectively degraded via indirect photolysis in the presence of high HO· concentrations (Kover et al. 2014). In addition, direct photolysis didn't contribute the overall degradation of surfactant DOSS and solvent DPnB (<30%), but the sensitized photolysis might occur with the presence of HO· (Glover et al. 2014). The presence of surfactants and solvent molecules can consume or compete the HO· with the petroleum hydrocarbons. It is also evidenced via the GC chromatogram in Fig. A-7. The peak area of fumaric acid in solvent was reduced about 89.3% suggesting the photolysis of such solvents. While the peak area of DPnB was only reduced by 8.2%, indicating the insignificant photolysis of this solvent.

3.4.Conclusions

This study investigated the dissolution, sorption and photodegradation of dispersed petroleum hydrocarbons in seawater-sediment systems. The primary findings are summarized as follows:

(1) Higher dose of dispersant Corexit 9500A could disperse more *n*-alkanes and PAHs into water column, the dispersant is more selective for lower M.W. *n*-alkanes (C11-C30), while the dispersant was least effective toward the longer chained alkanes (C30-C40) or PAHs with 5-6 rings even at a high DOR of 1:20. The dispersant was much more effective for *n*-alkanes than PAHs.

(2) Corexit 9500A, Corexit 9527A and SPC 1000 dispersed the petroleum hydrocarbons differently in terms of total dispersed TPHs and fractions of petroleum hydrocarbons. For *n*-alkanes, Corexit 9500A dispersed C11-C18 and C19-C28 effectively, whereas Corexit 9527A more favored short chained alkanes (C10-C16). SPC 1000 was the most effective dispersant which can disperse a broader range of alkanes (C12-C28), and 1.02 times 2.7 more TPHs than Corext 9500A and 9527A, respectively. The three dispersants showed comparable effectiveness for dispersing petroleum PAHs.

(3) The petroleum hydrocarbons sorbed in a sandy loam sediment resembled the profile of those in the DWAO solutions. The addition of 18 mg/L of the dispersant didn't significantly affect the uptake profiles. When the dispersant was increased to 180 mg/L, the overall uptake of *n*-alkanes and PAHs was reduced by 47% and 42%, respectively, due to formation of micelles and the micelle-enhanced solubilization effects.

(4) Both dispersed*n*-alkanes and PAHs in the DWAOs were readily photodegraded under simulated sunlight, though both photodegradation and photo-facilitated alkylation of the PAHs were concurrently taking place.

Chapter 4. A New Type of Cobalt-Doped Titanate Nanotubes for Enhanced Photocatalytic Degradation of Phenanthrene

In this chapter, we summarize the development and characterization of a new type of Co-doped TNTs and test their photocatalytic activity under solar irradiationusing phenanthrene as a model PAH. An optimized hydrothermal-calcination method was developed for preparing the desired catalyst. Thepreparedphotocatalysts were tested for the efficacy inphenanthrene photodegradation. Typical characterization methods including morphology, crystal phases, and composition of Co-TNTs were studied to further elucidate the mechanism ofenhanced photocatalytic activity.

4.1.Introduction

With increased incidents of water pollution and ever growing energy demands, low-energy water treatment technologies become more and more appealing(Shannon et al. 2008). As such, catalytic photodegradation of various pollutants using solar irradiation has elicited great interest in recent years(Schneider et al. 2014). Traditionally, TiO_2-based materials have been the most widely used photocatalysts, and have been found effective in a variety of environmentally related uses, such as solar-driven hydrogen production, and photocatalytic decomposition and adsorption of organic contaminants(Chen and Burda 2008, Chen and Mao 2007, Liu et al. 2013c, Pelaez et al. 2012, Tan et al. 2014).

TiO_2 is a typical *n*-type semiconductor with relatively large band gaps. The band gaps for the three main crystal phases, i.e., anatase, rutile and brookite, are 3.2, 3.0 and 3.2 eV, respectively(Pelaez et al. 2012). Although TiO_2 can effectively utilize UV light, its large band gaps limit its optical absorption in the solar spectrum, which consists of UV, visible and infrared (IR) radiations with a relative energy distribution of ~5%, 43% and 55%, respectively(Chen et

al. 2015, Shankar et al. 2015). As a result, a great deal of effort has been devoted to improving the visible light absorption of TiO_2. While nanoscale TiO_2 has shown to offer improved catalytic activity, the sedimentation characteristics limit the separation from water and reuse of the spent catalyst(Liu et al. 2013a).

Of various modifications, one-dimensional titanate nanotubes (TNTs) synthesized by hydrothermal treatment of TiO_2 have gained significant attention in recent years(Liu et al. 2013a, Liu et al. 2013b, Wang et al. 2013a, Xiong et al. 2011b). TNTs can serve as excellent adsorbents for heavy metals owing to their high specific area, great ion-exchange properties, easy solid-liquid separation and abundant functional groups (Liu et al. 2013a and 2013b). TNTs have been found to be poor photocatalysts despite their high surface area and crystalline structure due to the rapid electron-hole recombination rate upon excitation under illumination(Kim et al. 2012, Lee et al. 2007, Yu et al. 2006a). Therefore, researchers have studied various approaches to inhibit the electron-hole recombination, including calcination(Lin et al. 2008, Yu et al. 2006b), H_2O_2 treatment(Khan et al. 2006), acid treatment(Chen et al. 2015), and surface modification using non-metals such as C, F and P(Kim et al. 2012, Liu et al. 2012a) or metals such as Cu, Pd, and W(Chen et al. 2013, Grandcolas et al. 2013). Of these approaches, metal doping appears very promising. An appropriate metal dopant can not only inhibit the recombination of electron-hole pairs, but also facilitate absorption of visible light by narrowing the absorption band gaps. Cobalt is one of the commonly used dopant for modifying TiO_2, and cobalt oxides have narrower band gaps (e.g., ~2.4 eV for CoO and 2.19 eV for Co_3O_4) (Dahl et al. 2014, Marin et al. 2013). For instance, cobalt oxide/TiO_2 composite showed much improved photo-activity for organic compounds and H_2 production rate than plain TiO_2(Dai et al. 2013, Wang et al. 2013b, Zhang et al. 2012);however, cobalt as a potential dopant for TNTs has not been studied.

Polycyclic aromatic hydrocarbons (PAHs) are produced during incomplete combustion of fossil fuels, and important components of crude oil(Gong et al. 2014a, Zhao et al. 2015). Due to their toxic, mutagenic and carcinogenic properties, PAHs represent a major environmental concern associated with oil spill, discharge and seepage, and thus, have been classified as the priority pollutants by US EPA(Nam et al. 2008). In addition, PAHs (e.g. phenanthrene, anthracene, and pyrene) are rather persistent to photodegradation under solar light(Wen et al. 2002). PAHs can absorb light in the UV regions, and then be transformed into excited PAH molecules and photo-oxidized(Kou et al. 2008). Phenanthrene is one of the most commonly detected PAHs, consisting of three fused benzene rings, it is fairly resistant to natural photodegradation, and thus, has been often used as a prototype PAH for photolysis study(Jia et al. 2012, Sirisaksoontorn et al. 2009, Wangl et al. 1995).

The overall goal of this work was to develop and test a new type of cobalt-doped TNTs (Co-TNTs) for efficient photodegradation of PAHs under solar light. The specific objectives were to: (1) develop an optimized hydrothermal-calcination method for preparing the desired catalyst, (2) test the effectiveness of the catalyst for phenanthrene photodegradation, and (3) elucidate the mechanisms for enhanced photocatalytic activity by characterizing the morphology, crystal phases and compositions of Co-TNTs.

4.2.Experimental

4.2.1. Chemicals

All chemicals used in this study were of analytical grade or higher. TiO_2 nanoparticles (P25, 80% anatase and 20% rutile) were purchased from Degussa Corporation (Germany) and were used as the precursor for TNTs. $CoCl_2 \cdot 6H_2O$, NaOH, methanol (HPLC grade) and absolute ethanol were obtained from Acros Organics (Fair Lawn, NJ, USA). Terephthalic acid was

purchased from Alfa Aesar (Ward Hill, MA, USA) for hydroxyl radical detection. Deionized (DI) water (Millipore Co., 18.2 MΩ·cm) was used to prepare all solutions. Phenanthrene (the model PAH) was purchased from Alfa Aesar (Ward Hill, MA, USA), and was dissolved in methanol to form a stock solution of 2 g L^{-1}.

4.2.2. Synthesis of Co-doped TNTs

First, Co-TNTs were synthesized through a one-step hydrothermal method. In brief, 0.1, 0.2, 0.4 or 0.6 g $CoCl_2 \cdot 6H_2O$ was mixed with 1.2 g of the TiO_2 nanoparticles in a beaker with 20 mL DI water. The mixtures were magnetically stirred for 30 min and sonicated for another 30 min. Then, a NaOH solution (prepared with 29 g NaOH in 47 mL DI water) was added dropwise into each mixture in ca. 5 min, and then sonicated for another 60 min. Afterwards, each mixture was transferred into a Teflon reactor with stainless steel coating, and then purged with pure N_2 for 10 min to remove dissolved oxygen. Then, the reactors were heated at 150 °C for 48 h to complete the hydrothermal reaction. The resulting blue precipitates were separated and washed with DI water to neutral and then oven-dried at 80 °C for 4 h. The as-prepared materials are denoted as Co-TNTs for typographical convenience.

The Co loadings on Co-TNTs were determined according to EPA Method 3050B(Agency. 1996). Briefly, 0.2 g each of the materials was dispersed into 20 mL of concentrated nitric acid (65%) and shaken for 24 h, and the resulting solution was diluted 10 times and then analyzed for Co on an inductively coupled plasma-optical emission spectroscopy (ICP-OES, 710-ES, Varian, USA). Subsequently, the Co-TNTs were calcined at 400, 600 or 800 °C in a muffle furnace for 3 h, and the resultant catalysts are denoted as Co-TNTs-xxx (xxx indicates the calcination temperature). The photocatalytic activities of the materials prepared with different Co loadings and calcination temperatures were then tested to optimize the recipe. For comparison, neat TNTs

were also synthesized following the traditional hydrothermal method without Co loading(Chen et al. 2002, Xiong et al. 2010), where 1.2 g TiO_2 (P25) and 10 M NaOH were mixed and heated at 130 °C for 72 h. In selected cases, the TNTs were calcined at 600 °C for 3 h, and the calcined TNTs are designated as TNTs-600.

4.2.3. Material characterizations

The morphology of material was analyzed using Tecnai30 FEG transmission electron microscopy (TEM, FEI, USA) operated at 300 kV. The crystal phase of the sample was obtained by means of a Bruker D2 phaser X-ray diffractometer (XRD, Bruker AXS, Germany) using Cu Kα radiation (λ = 1.5418 Å) at a scan rate (2θ) of 4o/min. AXIS-Ultra X-ray photoelectron spectroscopy (XPS, Kratos, England) analysis was performed to determine the elemental composition and oxidation sate of materials using Al Kα X-ray at 15 kV and 15 mA. The standard C 1s peak (Binding energy, Eb = 284.80 eV) was used to eliminate the static charge effects. The Brunauer-Emmett-Teller (BET) surface area was measured on an ASAP 2010 BET surface area analyzer (Micromeritics, USA) in the relative pressure range of 0.06–0.20. Pore size distribution was obtained following the Barret-Joyner-Halender method. Nitrogen adsorption volumes at the relative pressure of 0.99 were used to determine the pore volumes and the average pore diameters. Diffuse reflectance UV-visible absorption spectra (UV-DRS) of the materials were obtained using a UV-2400 spectrophotometer (Shimadzu, Japan). BaSO4 powder was used as the reference at all energies (100% reflectance) and the reflectance measurements were converted to absorption spectra using the Kubelka-Munk function. The sedimentation rate tests of the materials were evaluated following the UV absorbance of the particle suspensions using a UV-vis spectrophotometer (UV1800, Shimadzu, Japan) (the particles were first dispersed in DI water with sonication) (Liu et al. 2013a).

4.2.4. Photocatalytic degradation

Fig. 4-1 shows the experimental setup for the photodegradation of phenanthrene, which includes a sealed glass photo-reactor (volume = 250 mL) with a quartz cover, an Oriel Sol 1A solar simulator (Newport, USA) with a 450 W xenon lamp, a water circulating system and a magnetic stirrer. The solar irradiation was set at of 85±0.5 mW/cm^2 (AM 1.5G). The reactor temperature was maintained at 25±0.2 °C through the circulating water.

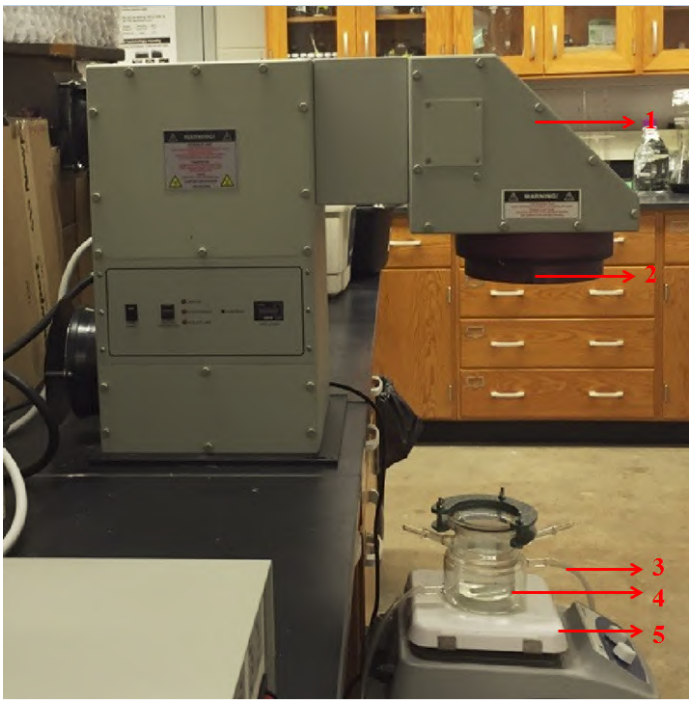

Fig. 4-1. Photocatalytic reaction set-up. (1) Simulated solar light system; (2) Xenon lamp; (3) Circulating water; (4) Glass reactor; (5) Magnetic stirrer.

Photocatalytic degradation kinetic tests were carried out with various materials under the simulated solar light. Specifically, 200 µg/L of phenanthrene and 1.0 g/L of a given material were loaded in the photo-reactor. The mixture was stirred for 2 h in dark to reach the phenanthrene adsorption equilibrium. Afterwards, the reactor was subjected to the solar irradiation. Water samples (1 mL each) were taken at predetermined times and immediately

centrifuged at 8000 rpm (6400 g-force) for 10 min. The supernatant was then mixed with methanol at 1:1 (v/v) ratio, and then analyzed for phenanthrene using an Agilent 1260 Infinity high performance liquid chromatography (HPLC) system equipped with a Poroshell 120 EC-C18 column (50 × 4.6 mm, 2.7 μm). The column temperature was held constant at 30 °C, and the mobile phase was comprised of acetonitrile and water at 70:30 (v/v) and at a flow rate of 1 mL min^{-1} in the isocratic mode. The eluate was analyzed with a UV diode array detector at 254 nm. The detection limit for phenanthrene was ~1 μg/L. Control tests were conducted in the absence of any catalysts but under otherwise identical conditions.

Based on the screening tests, Co-TNTs-600, the most active catalyst prepared with 2.26 wt.% of Co loading and at a calcination temperature of 600 ^{o}C, was further tested for reusability. After an adsorption-photocatalysis cycle, the catalyst was recovered by filtering the suspension using a 0.22 μm Polytetrafluoroethylene (PTFE) membrane, and then reused by repeating the same adsorption-photodegradation cycle. Separate tests indicate that air-drying the catalyst had no effect on its catalytic activity.

The zero-order and first-order kinetic models are tested to interpret the kinetic data(Al-Ekabi and Serpone 1988, Liu et al. 2014):

$$C_0 - C_t = k_0 t \quad \textbf{(Eq. 4.1)}$$

$$\ln(C_0 / C_t) = k_1 t \quad \textbf{(Eq. 4.2)}$$

where C_0 and C_t (μg/L) are the phenanthrene concentrations at time zero and t (min), respectively, and k_0(μg/(L·h)) and k_1 (h^{-1}) are respective rate constants.

4.2.5. Measurement of hydroxyl radicals (•OH)

The production of hydroxyl radicals (•OH) by various Ti-based materials was measured following the photoluminescence (PL) technique using terephthalic acid as the probe molecule. As terephthalic acid reacts with •OH, 2-hydroxyterephthalic acid will form with a high fluorescent, and the fluorescence intensity is proportional to the amount of •OH. In each test, 0.2 g of a material was dispersed in a mixture of 0.5 mmol terephthalic acid and 2 mmol NaOH with a total volume of 200 mL in the photo-reactor. After 2-h illumination under the solar light, samples were taken and micro-filtered. The PL spectra were then obtained on a fluorescence spectrophotometer (SpectraMax M2, Molecular Devices, CA, USA) at an excitation wavelength of 425 nm.

4.3.Results and discussion

4.3.1. Photocatalytic activity of Co-doped TNTs under different synthesis conditions

Fig. 4-2 shows photocatalytic degradation of phenanthrene by Co-doped TNTs prepared with various cobalt loadings and/or at different calcination temperatures. Table 4-1 lists the best fitted parameters for photocatalytic kinetic models. In all cases, the first-order model is able to adequately interpret the kinetic data ($R^2 > 0.98$), with much better fittings than the zero-order model. Fig. 4-2a shows that increasing the initial $CoCl_2 \cdot 6H_2O$ dosage from 0.1 to 0.2 g in the hydrothermal reaction enhanced the apparent rate constant (k_1) from 0.24 to 0.39 h^{-1}. Further increasing the cobalt dosage from 0.2 to 0.6 g only modestly affected the k_1 value (0.39 to 0.43 h^{-1}), with nearly the same finial phenanthrene removal of >98%. At the initial $CoCl_2 \cdot 6H_2O$ concentrations of 0.1, 0.2, 0.4 and 0.6 g, the Co loadings were (wt%): 1.13, 2.26, 2.68 and 2.81, respectively. Further characterizations (Section 3.2) confirmed that cobalt is immobilized as adsorbed ions. Doubling the initial $CoCl_2 \cdot 6H_2O$ from 0.1 to 0.2 g also doubled the Co loading,

resulting in 62.5% increase in k_1. Further increasing $CoCl_2 \cdot 6H_2O$ from 0.2 to 0.6 g resulted in only 0.55 wt% increase in Co loading, and thus, only modest enchantment in the photocatalytic activity. The much less further gain in photo-activity can also be due to lowered accessibility of the Co sites upon calcination (see Section 3.2). Based on Fig. 4-2a, the optimal initial $CoCl_2 \cdot 6H_2O$ dosage was set at 0.2 g.

Table 4-1. Parameters of zero-order and first-order kinetic models for photocatalytic degradation of phenanthrene by Co-doped TNTs synthesized under different conditions.

Kinetic model	Parameters	Initial $CoCl_2 \cdot 6H_2O$ mass (g)				Calcination temperature (°C)		
		0.1	**0.2**	**0.4**	**0.6**	**400**	**600**	**800**
Zero-order	k_0(μg/(L·h))	19.93	22.91	23.38	23.69	11.63	22.91	16.25
	R^2	0.8441	0.6335	0.5318	0.5326	0.9192	0.6335	0.8540
First-order	$k_1(h^{-1})$	0.24	0.39	0.43	0.41	0.083	0.39	0.16
	R^2	0.9949	0.9927	0.9970	0.9947	0.9841	0.9927	0.9950
12-h Removal efficiency (%)		90.8	98.6	98.9	98.8	58.4	98.6	82.5

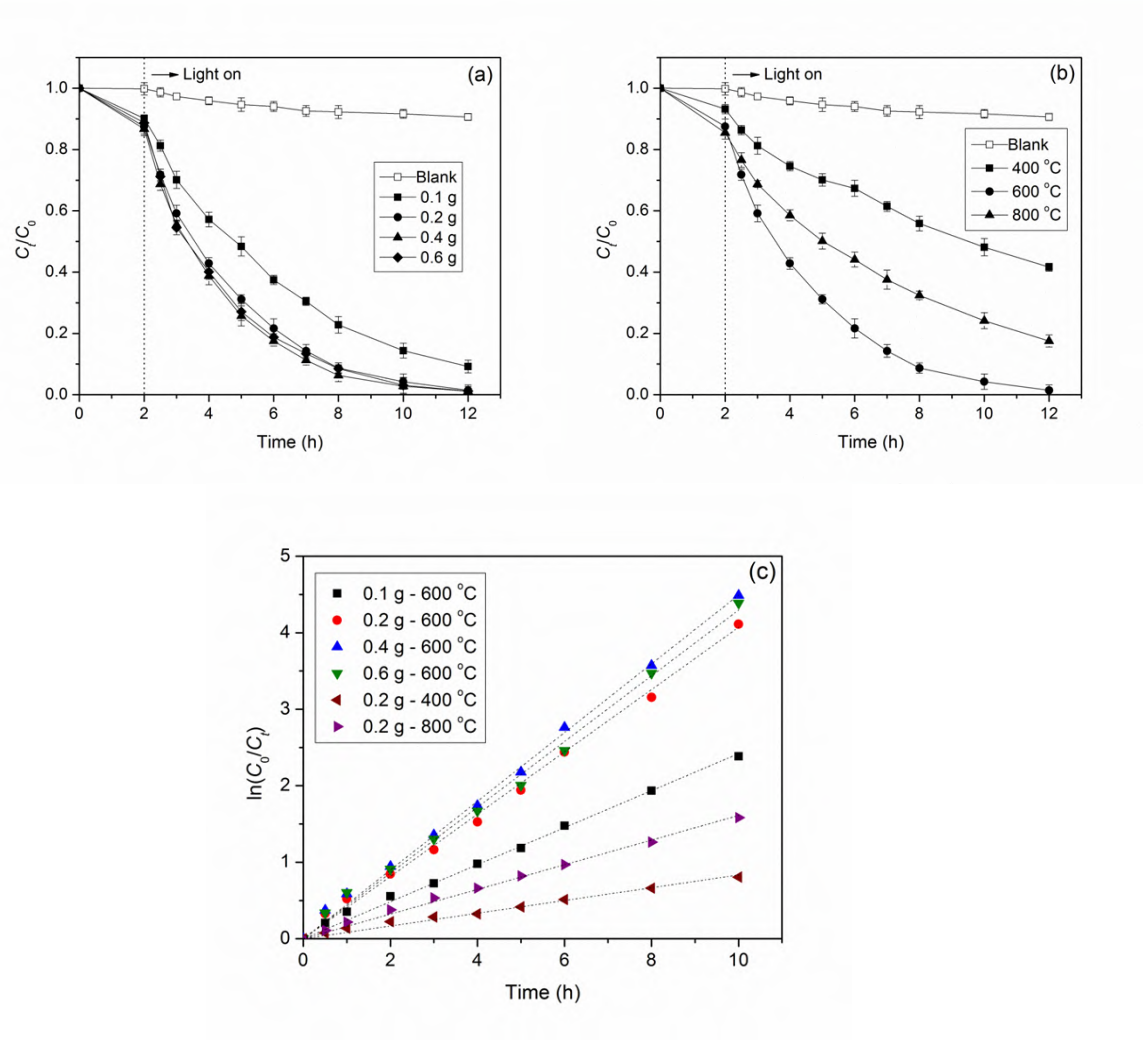

Fig. 4-2. Photocatalytic degradation of phenanthrene by Co-doped TNTs synthesized at **(a)** different Co loadings (but fixed calcination temperature of 600 oC) and **(b)** various calcination temperatures (but identical Co loading of 2.26%). Lines in **(c)** are linear first-order model fittings for all the materials. (Initial phenanthrene = 200 μg/L, material dosage = 1.0 g/L, pH = 7.0 ± 0.2, temperature = 25 ± 0.2 oC).

Increasing the calcination temperature from 400 to 600 °C dramatically increased the k_1 value from 0.083 to 0.39 h^{-1} (by a factor of 4.7);however,the rate was lowered to 0.16 h^{-1} when it

was calcined at 800 °C. Calcination temperature is highly related to the crystallinity of materials. Previous studies indicated that increasing the calcination temperature from 400 to 600 °C enhances the crystalline phase of anatase, yet higher temperatures (> 700 °C) would cause the formation of rutile, a much weaker photocatalyst than anatase(Lee et al. 2007, Yu et al. 2006c). Considering both photocatalytic activity and cost effectiveness, Co-TNTs-600 synthesized with a Co loading 2.26 wt%) and a calcination temperature of 600 °C was chosen as the optimal photocatalyst, which was then fully characterized and studied to elucidate the underlying mechanisms for the enhanced photocatalytic activity.

4.3.2. Morphology, crystal phases and compositions of Co-doped TNTs

Fig. 4-3 shows TEM images of TiO_2, TNTs and Co-TNTs-600. The precursor TiO_2 is present as aggregated particles with a primary particle size range of 20−50 nm (Fig. 4-3a). Upon the hydrothermal treatment, TiO_2 was transformed into TNTs, which appear as multilayer (4−5 layers) nanotubes, with an inner diameter of ~4.5 nm and outer diameter of ~9 nm (Fig. 4-3b) (Xiong et al. 2010). The interlayer distance of the nanotubes is 0.75 nm, which is assigned to the crystal plane of titanate (200) (Chen et al. 2002). When Co-TNTs were calcinated at 600 °C, the TNTs were broken into shorter nanotubes with an interlayer distance of 0.68 nm (200) (Fig. 4-3c), indicating the high-temperature calcination partly damaged the tubular structure and shrank the interlayer distance. In addition, nanoparticles (10−30 nm) with a crystal distance of 0.35 nm were formed, which is in accordance with the crystal plane of anatase (101) (Zhang et al. 2011). Furthermore, the calcination resulted in some 2-5 nm nanoparticles (nano-dots), which were further confirmed to be CoO (Fig. 4-3c).

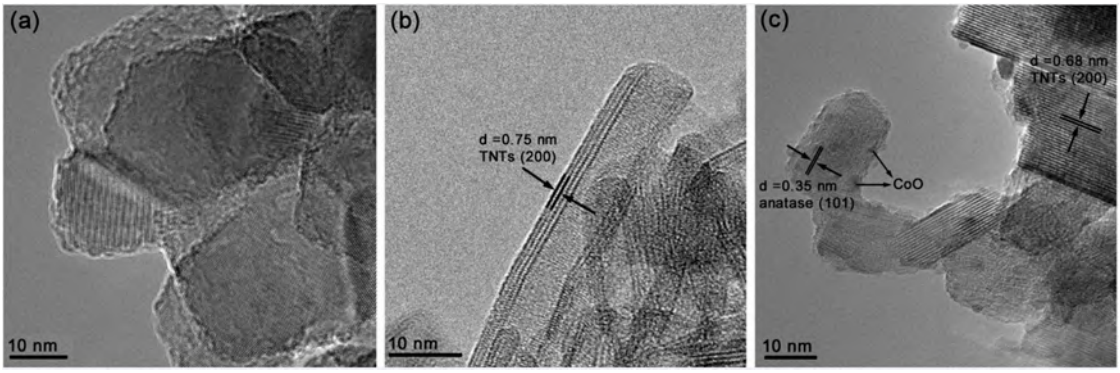

Fig. 4-3. TEM images of **(a)** TiO2 (P25), **(b)** TNTs, and **(c)** Co-TNTs-600.

Fig. 4-4 presents the XRD patterns for the materials. The pristine TiO_2 is a mixture of anatase and rutile, which was completely transformed to titanate upon the hydrothermal treatment. The peaks at 10°, 24°, 28° and 48° are all ascribed to sodium titanate(Liu et al. 2013c, Sun and Li 2003). The resulting titanate nanotubes are a kind of tri-titanate with a chemical formula of $Na_xH_{2-x}Ti_3O_7$ (x depends on the sodium content) and a skeletal structure of layered corrugated ribbons formed through edge-sharing of triple [TiO_6] octahedrons with H^+ and Na^+ located in interlayers(Liu et al. 2013a, Liu et al. 2013c, Xiong et al. 2011a). The peak at 10° represents the interlayer distance of TNTs (0.75 nm as shown in Fig. 4-3b) (Liu et al. 2013c, Sun and Li 2003). The XRD patterns for TNTs nearly resemble those of Co-TNTs, indicating that cobalt is loaded as Co(II) ions without formation of crystalline Co oxides in the hydrothermal process. When TNTs are calcinated at 600 °C (TNTs-600), titanate is partially transformed into anatase (peaks at ~25°, 47°, 55°, 58° and 67° JCPDS 21-1272) (Choi and Yong 2014), whereas part of the titanate phase remains as evidenced by the peaks at 10° and 28°. However, the interlayer peak at 10° is greatly weakened due to the damage of the tubular structure. For Co-TNTs-600, besides the crystal phases of titanate and anatase, a CoO crystal phase arises, as

reflected by the peaks at 36.5°, 42.4° and 61.5°(JCPDS 75-0393)(Qiao et al. 2009, Zheng et al. 2013). The interlayer peak was also observed, though significantly weakened and shifted from 9.5° to 11.3°, which is attributed to the breakage of the tubular and layered structure in the calcination process (Fig. 4-3c).

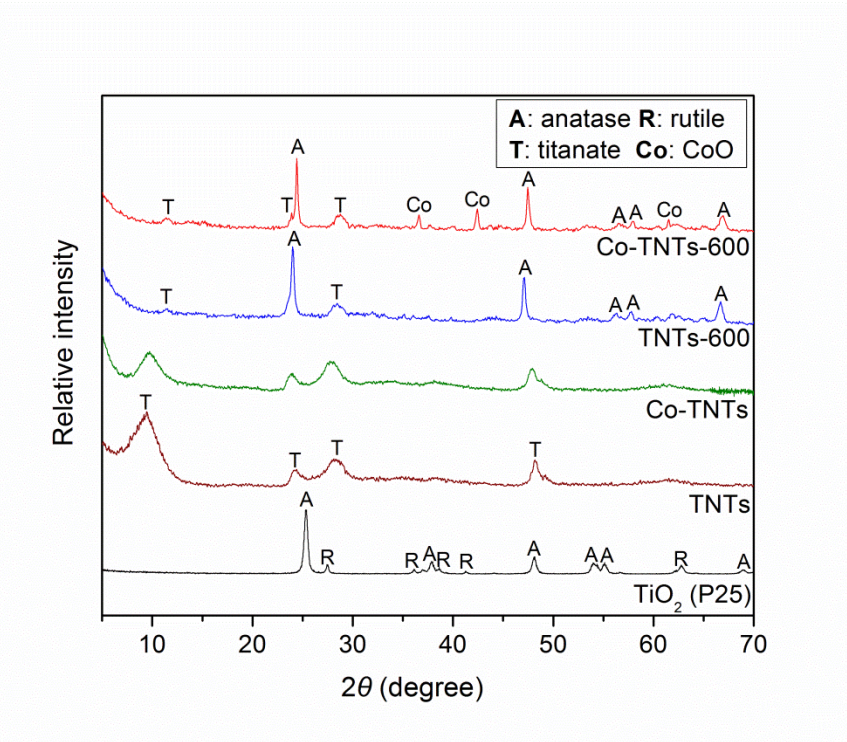

Fig. 4-4.XRD patterns of various Ti-based materials.(TNTs: Titanate nanotubes obtained via hydrothermally treatment of commercial TiO_2; Co-TNTs: Co(II) loaded TNTs; TNTs-600: TNTs calcinated at 600 ^oC; Co-TNTs-600: Co-doped TNTs calcinated at 600 ^oC).

Fig. 4-5 compares the FTIR spectra for the typical Ti-based materials. For TiO_2, the absorption bands at 662, 1633, and 3462 cm^{-1} are attributed to O−H, H−O−H, and Ti−O bonding vibrations(Park and Kang 2005). Upon the hydrothermal reaction, two new bands at 480 and 904 cm^{-1} are observed, which are assigned to the [TiO_6] octahedron and the four-coordinated Ti−O stretching vibrations, respectively(Liu et al. 2013a, Liu et al. 2013c, Xiong et al. 2011a). Like the

XRD data, the FTIR spectra for TNTs and Co-TNTs are rather alike though the Ti−O band is shifted from 904 to 894 cm^{-1}, which reflects the formation of Ti−O−Co. The FTIR data for TNTs and Co-TNTs confirm the incorporation of Co(II) ions, and the basic skeleton of the [TiO_6] octahedron remains intact during the hydrothermal treatment of TNTs. However, when calcined at 600 °C (TNTs-600), the [TiO_6] octahedron band shifted to 545 cm^{-1}, indicating the transition of titanate to TiO_2(anatase). For Co-TNTs-600, the new band at 747 cm^{-1}indicates the vibration of Co(II) in the tetrahedral hole (i.e. Co−O) (Lin et al. 2003), indicating conversion of Co(II) ions into CoO.

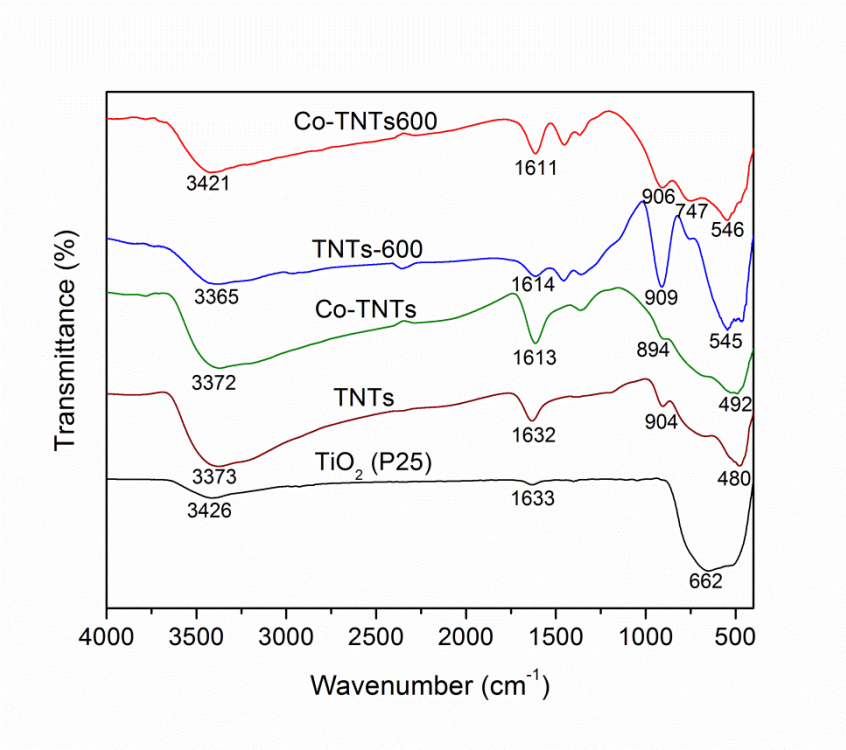

Fig. 4-5. FTIR spectra of various Ti-based materials.

Table 4-2 presents the BET surface area, total pore volume and average pore diameter of P25, TNTs and Co-TNTs-600. Compared to TNTs(Liu et al. 2014, Liu et al. 2013a, Xiong et al. 2011a), the BET surface area and total pore volume of Co-TNTs-600 are decreased from 272.3

$m^2 g^{-1}$ and 1.26 $cm^3 g^{-1}$ for TNTs to 72.5 $m^2 g^{-1}$ and 0.26 $cm^3 g^{-1}$, respectively, which is due to the collapse of layered tubular structure of TNTs at the calcination temperature. The BET surface area and total pore volume of Co-TNTs-600 are still larger than those of P25. The nitrogen adsorption-desorption isotherms with Co-TNTs-600 is aligned with the type IV isotherm with an H3 hysteresis loop according to the BDDT classification (Fig.A-13), indicating mesopores (2−50 nm) are dominant in Co-TNTs-600(Brunauer et al. 1940), which was further confirmed by the pore size distribution (Fig. A-14).

Table 4-2. Salient physical parameters of TiO_2, TNTs and Co-TNTs-600.

Material	BET surface area ($m^2 g^{-1}$)	Single point total pore volume($cm^3 g^{-1}$)	Average pore diameter (nm)
TiO_2 (P25)	46.9	0.18	15.5
TNTs	272.3	1.26	18.5
Co-TNTs-600	72.5	0.26	8.3

4.3.3. Photocatalytic degradation of phenanthrene by Co-doped TNTs

Fig. 4-6 compares photocatalytic degradation kinetics of phenanthrene by Co-TNTs-600 and other Ti-based materials. Again, the first-order kinetic model is able to better and adequately interpret the photocatalytic reaction kinetics (Table 4-3). Table 4-3 gives the resulting parameters of the zero- and first-order kinetic models. In the absence of photodegradation (initial 2 h), Co-TNTs-600 adsorbed 12.5% of phenanthrene (the maximum Langmuir capacity = 25.8 μg/g, Fig. A-15 and Table A-1),whereas the other materials adsorbed <6%. Generally, adsorption of

phenanthrene is attributed to hydrophobic effects and π-π interactions(Chen et al. 2007). Co-TNTs-600 is rather hydrophilic due to the abundant surface −OH groups and inorganic skeleton; hence, it cannot favorably adsorb hydrophobic compounds.

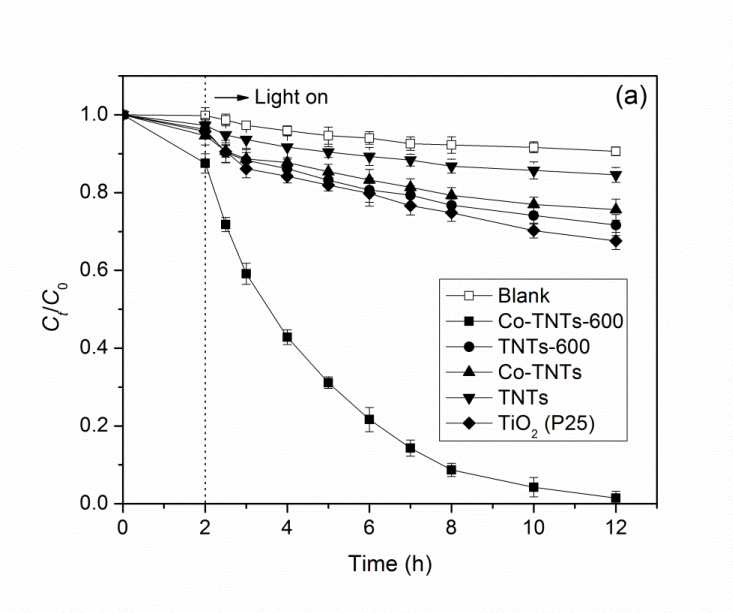

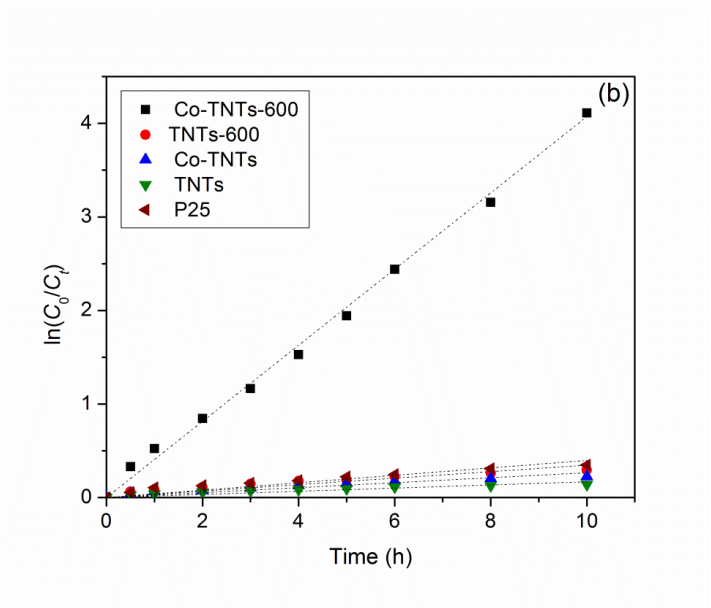

Fig. 4-6. (a) Photocatalytic degradation of phenanthrene by various Ti-based materials and **(b)** linear first-order model fitting for the different materials. (Initial phenanthrene = 200 μg/L, material dosage = 1.0 g/L, pH = 7.0 ± 0.2, temperature = 25 ± 0.2 ^{o}C).

Table 4-3. Parameters of zero-order and first-order kinetic models for photocatalytic degradation of phenanthrene by different Ti-based materials.

Material	Zero-order model		First-order model	
	k_0 (μg/(L·h))	R^2	k_1 (h^{-1})	R^2
Co-TNTs-600	22.91	0.6335	0.39	0.9927
TNTs-600	5.93	0.7581	0.035	0.8266
Co-TNTs	4.58	0.8226	0.027	0.8683
TNTs	3.11	0.7884	0.017	0.8181
TiO_2 (P25)	6.63	0.8149	0.040	0.8815

Fig. 4-7 compares the k_1 values and removal efficiencies (R). TNTs showed extremely low photocatalytic activity, with a low k_1 of 0.017 h^{-1} and with a phenanthrene removal of 15.5% at 12 h, which is even lower than that of the precursor TiO_2 (28.4%). The calcinated TNTs (TNTs-600) increased the removal to 32.5%, whereas doping Co on TNTs (without calcination) increased the removal to 24.4%. When Co-doping and calcination were combined (Co-TNTs-600), the k_1 value was dramatically increased to 0.39 h^{-1} and the removal to 98.6%. The rate constant is ~23 times that of TNTs and ~10 times of P25.

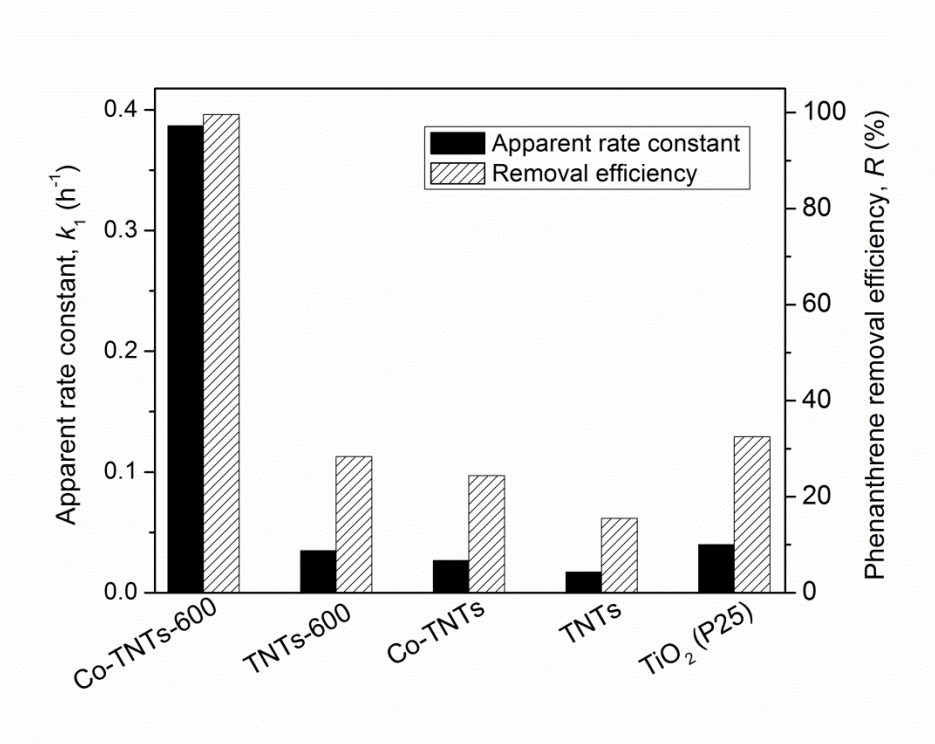

Fig. 4-7. Apparent rate constants (k_1) and removal efficiencies (R) for photocatalytic degradation of phenanthrene by variousTi-based materials.

Despite the highest specific surface area (Table 4-2), TNTs showed the lowest photocatalytic activity, which can be attributed to crushing of the TiO_2 crystalline, resulting in a high recombination rate of electron-hole pairs after excitation(Kim et al. 2012, Lee et al. 2007, Yu et al. 2006a). Upon incorporation of Co^{2+} (Co-TNTs), the recombination rate of electron-hole pairs is modestly curbed, resulting in the modest activity increase. The calcination of TNTs (TNTs-600) recovered some of the anatase crystalline (Fig. 4-4), resulting in a reactivity close to the precursor TiO_2. TiO_2 and TNTs-600 mainly absorb the UV fraction of the solar light, whereas Co-doped TNTs facilitate absorption of visible light. Therefore, the combination of Co-doping and calcination/crystallization resulted in the dramatic synergistic effect of Co-TNTs-600. Upon calcination, the Co(II) ions in TNTs are transformed to Co oxides, which

act as electron transfer mediator, inhibiting the hole-electron recombination in the photocatalytic process. In addition, the conversion of titanate anatase crystalline in the calcination process further impedes the electron-hole recombination. Section 3.4 presents more detailed mechanisms on the enhanced photocatalytic activity of Co-TNTs-600.

4.3.4. Mechanisms for enhanced photocatalytic activity of Co-TNTs-600

Fig. 4-8 displays the DRS UV-vis spectra of TNTs and Co-TNTs-600. Based on the data, the optical energy gaps for the materials are calculated using Eq. (4.3) (Feng et al. 2015):

$$\alpha h\nu = A\left(h\nu - E_g\right)^{n/2} \quad \textbf{(Eq. 4.3)}$$

in which α, h, ν, A and Eg represent the absorption coefficient, Planck constant, photon frequency, proportionality constant and band gap, respectively; and n is a constant depending on the optical transition type of a semiconductor (n = 1 for direct absorption; n = 4 for indirect absorption), and n = 4 for the titanate materials in this study.

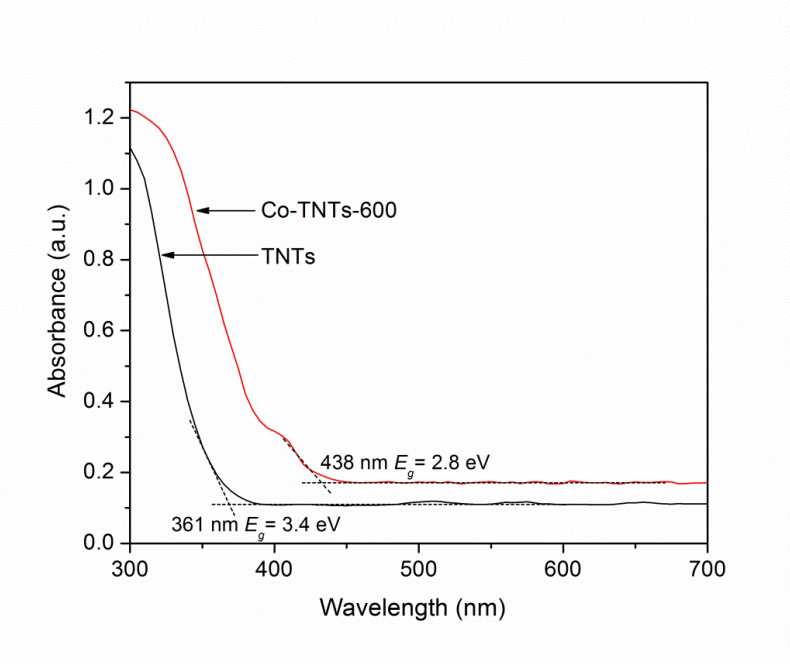

Fig. 4-8. DRSUV-vis spectra of TNTs and Co-TNTs-600.

Compared to TNTs, the absorption edge of Co-TNTs-600 shifts to visible region (from 361 to 438 nm), indicating the photo-effect under visible light is enhanced for Co-TNTs-600. The absorbance peak at ca. 430 nm for Co-TNTs can be attributed to the attachment of CoO(Zheng et al. 2013). The resulting Eg for Co-TNTs-600 is 2.8 eV, compared to 3.4 eV for TNTs and 3.2 eV for P25(Chen and Burda 2008). Therefore, a new e-donor level is formed in Co-TNTs-600, and this facilitates the transfer of the photo-generated electrons, thereby inhibiting the recombination of the electron-hole pairs.

The Fig. 4-9 shows PL spectra of terephthalic acid, this reflects the production of •OHfrom water under solar irradiation. The fluorescence intensity at 425 nm for the materials follows the sequence of: Co-TNTs-600 >> P25 > TNTs-600 > Co-TNTs > TNTs, which is consistent with that of the apparent rate constant (k_1) for phenanthrene degradation (Fig. 4-6 and Table 4-3). Enhanced production of the •OH radicals likely accounts for the enhanced photodegradation of phenanthrene by Co-TNTs-600.

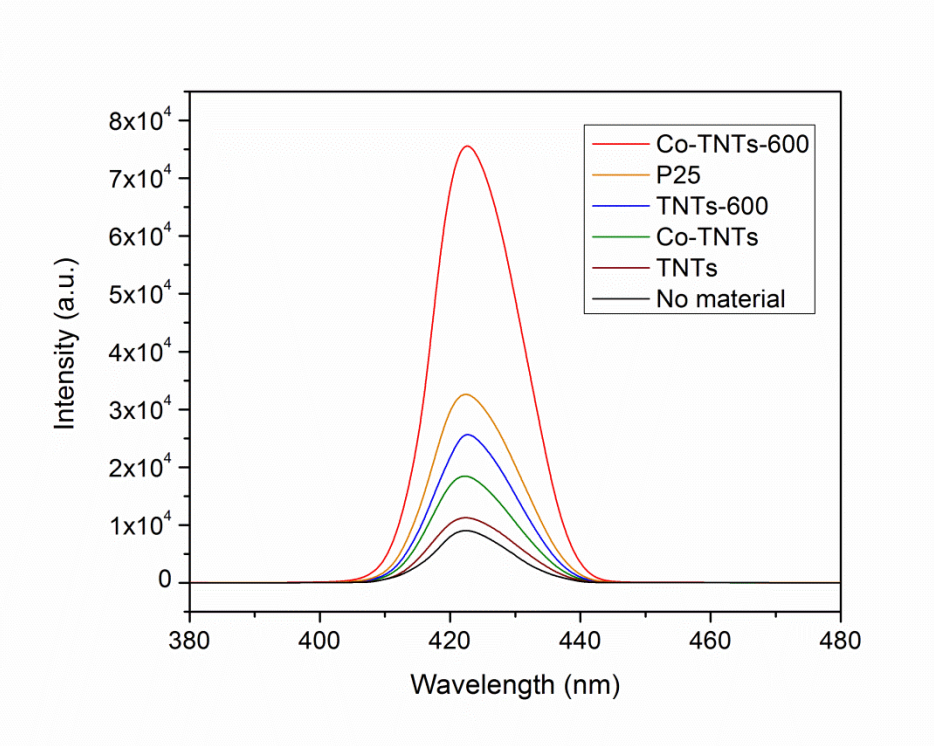

Fig. 4-9. PL spectra of various Ti-based materials under solar irradiation.

XPS analysis further demonstrates the role of Co in the photocatalysis. As shown in Fig. 4-10 and Table 4-4, the main elements for TNTs are Na (12.3%), Ti (23.4%) and O (64.3%), with a chemical formula of $Na_{1.58}H_{0.42}Ti_3O_7 \cdot 1.24H_2O$ based on the basic structure of tri-titanate and interlayered H^+/Na^+. For Co-TNTs-600, a Co 2p peak emerges in the XPS survey spectra (Fig. 8a). The Na content decreases from 12.3% for TNTs to 10.6% for Co-TNTs-600, which is due to the ion exchange of Co^{2+} with Na^+ in the hydrothermal process. The atomic percentage of Co is determined as 1.7% (2.66 wt%) by XPS, which is consistent with the Co loading dosage obtained from the EPA method (2.26 wt%), indicating a relatively low Co-doping can greatly enhance the photocatalytic activity of TNTs. For the high resolution of O 1s (Fig. 4-10b), the peaks at ca. 532 eV and 530 eV are assigned to the oxygen from the surface hydroxyl groups and the material lattice, respectively(Ou et al. 2008). For TNTs, the oxygen compositions can include

O from the surface Ti−OH ($E_b \approx 532$ eV) and the crystal lattice [Ti−O_6] ($E_b \approx 530$ eV) (Liu et al. 2013c). The lattice O in Co-TNTs-600 is 95.9%, compared to 94.4% for TNTs, indicating transition of titanate to TiO_2 (also see Fig. 4-4), as the content of hydroxyl groups in TNTs is higher than that in TiO_2 due to the hydrothermal treatment(Chen et al. 2002, Liu et al. 2013c, Xiong et al. 2010). In addition, the formation of CoO also leads to the increase of lattice O. For high resolution of Co 2p (Fig. 8c), the peaks at ca. 796 and 780 eV represent the Co $2p_{1/2}$ and $2p_{2/3}$ orbits, respectively(Konova et al. 2006, Wang et al. 2010). Specifically, the peak at 780 eV is assigned to Co^{2+}, indicating the formation of CoO after calcination(Konova et al. 2006). Moreover, there is a satellite Co^{2+} peak at ca. 786 eV, which belongs to Co-O-Ti (Co^{2+} in the interlayers of TNTs) (de la Pena O'Shea et al. 2011). The resulting CoO accepts the electrons excited by titanate and TiO_2 under visible light, thus inhibiting the recombination of electron-hole pairs.

Table 4-4. Atomic percentage contentin Co-TNTs-600.

Material	Element			
	Na	O	Ti	Co
TNTs	12.3	64.3	23.4	0.0
Co-TNTs-600	10.6	63.2	24.5	1.7

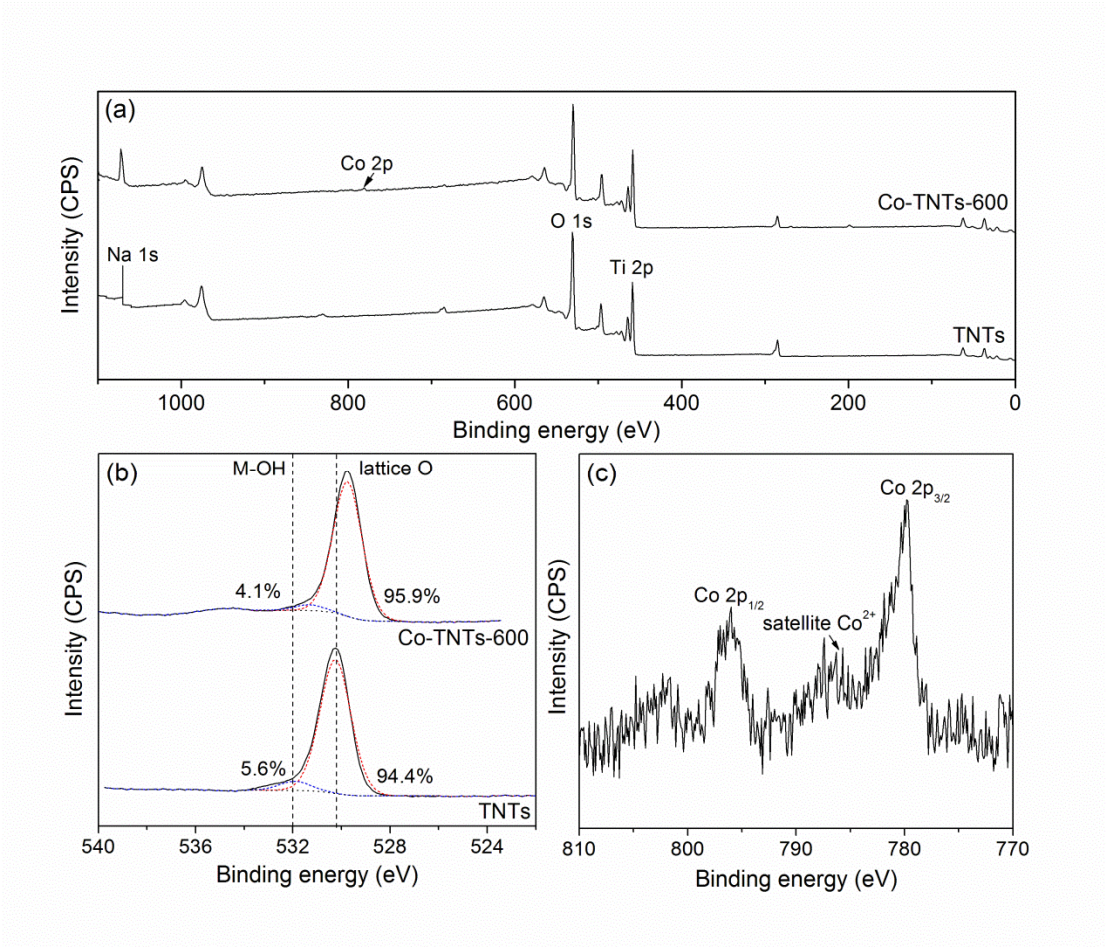

Fig. 4-10.XPS spectra of TNTs and Co-TNTs-600:**(a)** Survey, **(b)** high resolution of O 1s, and **(c)** Co 2p.

Fig. 4-11 illustrates the key mechanisms for the enhanced photocatalytic activity of Co-TNTs-600. Under illumination of solar light, anatase (the main one), TNTs and CoO all can generate a conduction band (e^-, electrons) and a valence band (h^+, holes). Because the pristine TNTs and TiO_2 are weakly responsive to visible light, the production of the reactive oxygen species (ROS), e.g. •OH, $•O_2^-$, $HO_2•$, H_2O_2, will be limited. In addition, the excited electron-hole pairs are prone to recombination for TNTs due to the loss of the crystalline phases. For Co-TNTs-600, however, photo-generated electrons are transferred by CoO coupled with a

reduction of Co^{2+} to Co^{+}, thus inhibiting the recombination of electron-hole pairs. The cobalt doping also shifts the light absorption edge to the visible light range and narrows down the energy gap to 2.8 eV, which means there is a new electron acceptor formed (in CoO) acting as photo-generated electrons transfer medium, and therefore, more visible light is absorbed by the new catalyst for photodegradation. Moreover, the rise in anatase crystalline promotes production of more electron-hole pairs under visible light and further impedes the electron-hole recombination. The holes can oxidize water molecules into the reactive oxygen species (ROS) (mainly ·OH), which are responsible for phenanthrene degradation.

Equations 4-14 depict the photocatalytic reactions during photodegradation of phenanthrene by Co-TNTs-600:

$$TiO_2/TNTs + h\nu \rightarrow TiO_2\ (e_{Ti}^{-}-h_{Ti}^{+}) \quad \textbf{(Eq. 4.4)}$$

$$CoO + h\nu \rightarrow CoO\ (e_{Co}^{-}-h_{Co}^{+}) \quad \textbf{(Eq. 4.5)}$$

$$Co(II) + e_{Ti}^{-} \rightarrow Co(I) \quad \textbf{(Eq. 4.6)}$$

$$Co(I) + O_2 \rightarrow Co(II) + \cdot O_2^{-} \quad \textbf{(Eq. 4.7)}$$

$$O_2 + e^{-} \rightarrow \cdot O_2^{-} \quad \textbf{(Eq. 4.8)}$$

$$\cdot O_2^{-} + H^{+} \rightarrow HO_2\cdot \quad \textbf{(Eq. 4.9)}$$

$$H_2O + h^{+} \rightarrow \cdot OH + H^{+} \quad \textbf{(Eq. 4.10)}$$

$$\cdot O_2^{-} + e^{-} + 2H^{+} \rightarrow H_2O_2 \quad \textbf{(Eq. 4.11)}$$

$$H_2O_2 + \cdot O_2^{-} \rightarrow \cdot OH + OH^{-} + O_2 \quad \textbf{(Eq. 4.12)}$$

$$\text{phenanthrene} + h^{+} \rightarrow \text{intermediates} \rightarrow \text{products} + CO_2 \quad \textbf{(Eq. 4.13)}$$

$$\text{phenanthrene} + \cdot OH\ (\text{or } \cdot O_2^{-}, HO_2\cdot, H_2O_2) \rightarrow \text{intermediates} \rightarrow \text{products} + CO_2 \quad \textbf{(Eq. 4.14)}$$

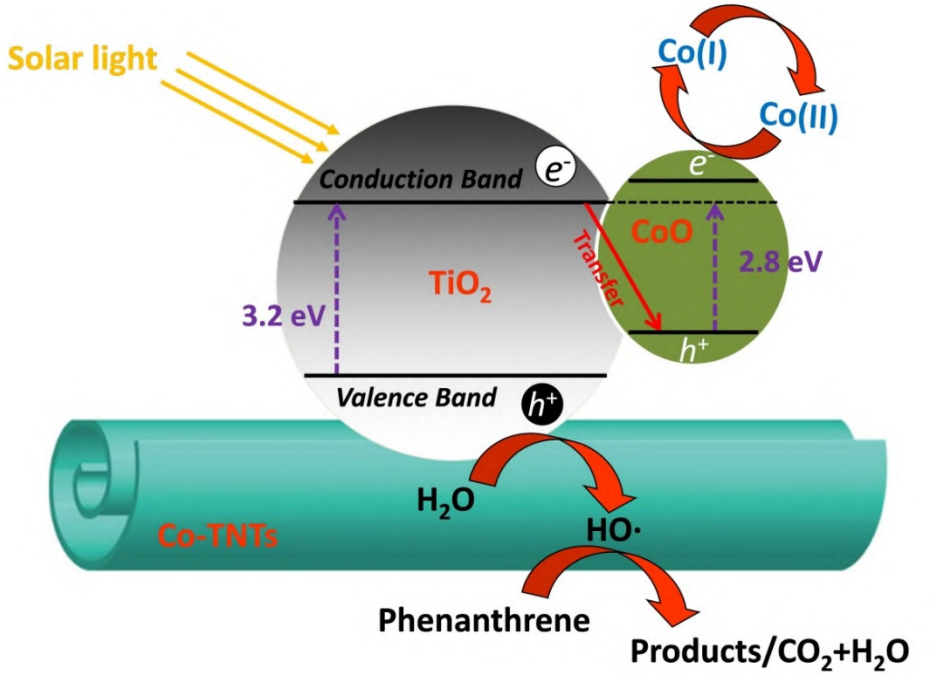

Fig. 4-11. Schematic illustration ofenhancedphotocatalytic activity of Co-TNTs-600.

4.3.5. Separation and reuse of Co-doped TNTs

One of the downsides for conventional TiO_2 (especially nano-TiO_2) has been related to poor separation from solutions, which not only limits its use in water treatment, but also prevents from effective recovery of the catalyst. Fig. 4-12 compares the sedimentation behaviors of Co-TNTs-600 versus P25and TNTs. In the 180 min of gravity sedimentation, 77.1% of Co-TNTs-600 settled, compared to 64.1% for TNTs and only 0.5% for P25. Over 94% removal of Co-TNTs-600 was achieved in 357 min of sedimentation.

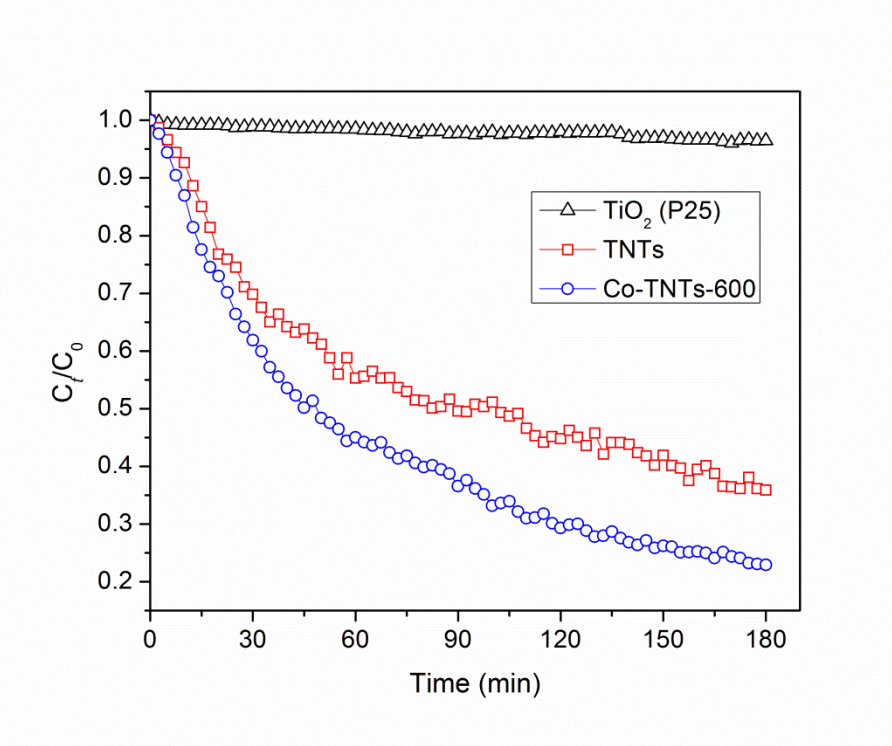

Fig. 4-12. Comparison on sedimentation kinetics of TiO_2, TNTs and Co-TNTs-600. (Material concentration = 0.5 g/L, pH = 5.0, temperature = 25 °C)

Fig. 4-13 shows photocatalytic degradation kinetics of phenanthrene by Co-TNTs-600 over 6 cycles of repeated uses, and Table A-2 lists the apparent rate constants, and the 12-h phenanthrene removal efficiency in each cycle. Evidently, the 12-h phenanthrene removal drops gradually and remains at 87.2% after 6 cycles of operations. In addition, the bleeding of Co from the catalyst totaled at only 4.20% in the 6 runs (2.87% in the first 2 runs) (Table A-3), which could be lowered to <0.3% had Co-TNTs-600 been pre-rinsed.

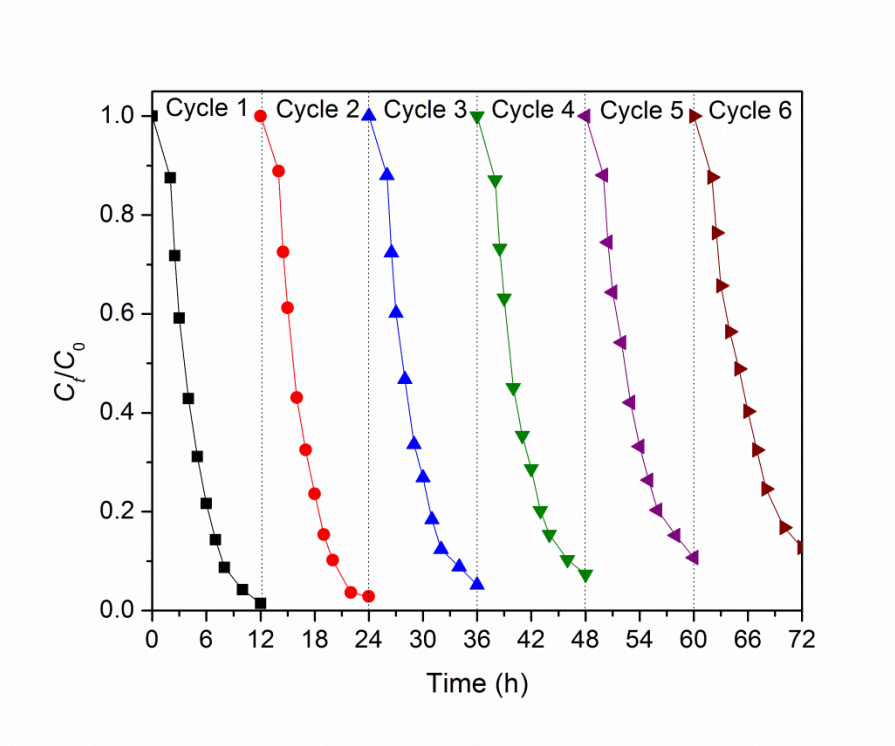

Fig. 4-13. Reusing the same Co-TNTs-600 in 6 consecutive runs of photocatalytic degradationof phenanthrene. (Initial phenanthrene = 200 μg/L, material dosage = 1.0 g/L, pH = 7.0 ± 0.2, temperature = 25 ± 0.2 ^{o}C).

4.4.Conclusions

This study developed and tested a new class of cobalt-doped TNTs for enhanced photocatalytic degradation of phenanthrene under solar light. The primary findings are summarized as follows:

Co-doped TNTs were successfully synthesized through a two-step process, i.e., hydrothermal treatment of commercial P25 as the Ti precursor followed by calcination at 600 ^{o}C. Co(II) ions are incorporated in TNTs in the hydrothermal reaction, which are further transformed into CoO in the calcination process. The optimized catalyst (Co-TNTs-600) was prepared at

2.26% Co loading and a calcination temperature of 600 ^{o}C. TEM, XRD, FTIR and XPS characterizations indicate that Co-TNTs-600 is a nano-composite consisting of titanate, anatase and CoO.

Co-TNTs-600 exhibited high photocatalytic activity for degradation of phenanthrene under solar light, with a 98.6% removal rate in 12 h at dosage of 1 g /L. The first-order kinetic model is able to adequately interpret the kinetic data, and the apparent rate constant was determined to be 0.39 h^{-1}, which is ~23 times higher than that of TNTs and ~10 times that of P25.

UV-vis DRS spectra of Co-TNTs-600 suggest that the absorption edge of Co-TNTs-600 shifts to the visible light region compared to P25 and un-calcined TNTs, and Co-TNTs-600 gives a much narrower optical energy gap of 2.8 eV, compared to 3.4 eV for TNTs and 3.2 eV for P25, indicating much improved sensitivity to visible light.

The CoO nanoparticles in Co-TNTs-600 can not only facilitate effective utilization of visible light for production of electron-hole pairs, but also serve as an electron transfer mediator that inhibits recombination of the pairs. Likewise, the anatase crystalline resulting from the calcination process promotes production of more electron-hole pairs and further impedes the electron-hole recombination.

Co-TNTs-600 can be efficiently separated via gravity-settling and then reused in multiple runs.

Overall, Co-TNTs-600 appears to be an efficient photocatalyst for degradation of persistent PAHs under solar light.

Chapter 5. Conclusions and Suggestions for Future Research

5.1.Summary and conclusions

During the Deepwater Horizon oil spill, more than 2 million gallons of dispersants were applied to break up oil slicks by lowering the interfacial tension between oil and seawater, and yet, the impacts of the dispersants on sorption, desorption, physical-chemical availability and the environmental fate of oil components are not well characterized. This work investigated effects of a prototype oil dispersant (Corexit EC9500A) on sorption/desorption of three model PAHs (naphthalene, 1-methylnaphthalene and pyrene) in sediment-seawater systems. Increasing the dispersant dosage from 0 to 200 mg/L linearly enhanced the solubility for all PAHs. Batch sorption tests showed that the dispersant at 18 mg/L enhanced naphthalene, 1-methylnaphthalene and pyrene uptake by ~3%, 5% and 11%, respectively. The dual-mode sorption model adequately simulated the sorption kinetics. The dispersant hindered desorption of the PAHs and resulted in desorption hysteresis. Different dosages of dispersant were applied to investigate the overall effect of dispersant on the distribution coefficients (K_d) of PAHs. The overall K_d is the balance of two competing mechanisms: adsolubilization and solubilization effect of dispersant. A strong dependence of dispersant isotherms was observed for naphthalene, 1-methylnaphthalen and phenanthrene demonstrating the predominant effect was adsolubilization. Thus, the addition of dispersant overall can enhance the uptake of these two PAHs. On the other handfor pyrene, since the solubilization effect outweighed the adsolubilization, the K_d peaked then decreased near CMC value of dispersant, and when more than 50 mg/L of dispersant added, the sorbed pyrene started to be remobilized. The deepwater conditions altered the PAHs solubility, decrease the dispersant uptake and lead to a right shift for the K_d values. This information is useful for

understanding roles of dispersants on the fate and transport of petroleum PAHs in marine systems and deepwater conditions.

Corexit 9500A was used to prepare dispersed water accommodated oil (DWAO) under varied dispersant-oil-ratios (DORs). Higher dose of dispersant can disperse more typical petroleum hydrocarbons including *n*-alkanes, PAHs into water column. While the profiles of distribution of petroleum hydrocarbons indicating the dispersion effectiveness differed with varied hydrocarbons. Especially the petroleum hydrocarbons with higher M.W. were more difficult to be dispersed even with an elevated concentration of dispersant. Three dispersants (Corexit 9500A, Corexit 9527A and SPC 1000) were compared for dispersing petroleum hydrocarbons. For *n*-alkanes, the Corexit 9500A disperse both C11-C18 and C19-C28 effectively. Corexit 9527A favored dispersion of short chained alkanes (C10-C16). SPC 1000 was the most effective dispersant which can disperse a broader range of alkanes (C12-C28). Additional dispersant of 180 mg/L introduced into the DWAO can enhance the solubilization effect thereby lowered the uptake of both PAHs and *n*-alkanes onto a loamy sand. In the DWAO, both *n*-alkanes and PAHs were readily photo-degraded under typical marine surface sunlight. Intensive alkylation of PAHs were observed in Day 3 and the concentrations of alkylated PAHs reached maxim values in Day 3 then followed by a fast decay in Day 4-Day 14.

Titanium related materials are promising photocatalysts for removal of persistent organic pollutants in environmental area. In this study, cobalt doped titanate nanotubes (Co-TNTs-600) were synthesized using TiO_2 (P25) through a first hydrothermal reaction and subsequentcalcination at 600 °C. The prepared material could efficiently photo-degrade phenanthrene under solar light with a high apparent rate constant of 0.3867 h^{-1}, which was ca. 23 times that of TNTs and 10 times of TiO_2 P25. Both the Co doping in the hydrothermal reaction

and subsequentcalcination are necessary for enhancement of the photocatalytic activity. TEM, XRD and XPS analysis indicates that TNTs-Co600 is a composite nanomaterial with phase of titanate, anatase and CoO. Titanate forms in the hydrothermal process, while in the calcination process, titanate partly transforms into anatase and Co(II) located in the interlayers of TNTs are oxidated into CoO. Moreover, DRS UV-vis spectra suggests that the adsorption edge of Co-TNTs-600 shifts to visible light region compared to TNTs and P25, with a narrower energy band of 2.8 eV compared to TNTs (3.4 eV) and P25 (3.2 eV). Therefore, the formation of CoO can act as the electron transfer mediatorin the photocatalytic reaction, which inhibited the recombination of hole-electron pairs mainly created by anatase under solar irradiation. In addition, TNTs-Co600 exhibited good reusability as the phenanthrene removal efficiency could also reach up to 87.2% even after 5 photocatalysis cycles.TheCo-TNTs-600 can be applied as an efficient photocatalyst for persistent polycyclic aromatic hydrocarbons (PAHs) remediation under solar light.

5.2.Suggestions for future research

The specific recommendations for future work were made as follows:

(1) Since dispersant is a mixture of both solvents and surfactants, the exact role of each component on the solubilization, sorption and desorption can be further explored *via* using the individual surfactant or solvent to conduct the aforementioned experiments under designed conditions. Even for the photodegradation process, each component may behavior differently under solar irradiation. Thereby the role of each component of dispersant on petroleum weathering, at least the key surfactants are of interest;

(2) For the further study with the deepwater conditions, other than temperature and pressure, some more bio-related materials, such as marine snow aggregates, should be considered to better simulate the real sub-sea conditions;

(3) Parent PAHs are intensively studied while the alkylated PAHs are less explored despite the fact they are more toxic and abundant than the parent ones in spilled oil. Thus, more investigations are requiredto characterize the alkylated PAHs. A series of study on photo-degradation of both parent and alkylated PAHs are of interest to compare their degradation pathways;

(4) The long-term fate of petroleum hydrocarbons are important and their toxicity are highly related withtheir transformation. Thus, more comprehensive monitoring systemsconsidering not only the abundance of contaminant, but also their toxicity should be developed.

(5) New materials should not only be developed and tested for their efficacy, but also studied for toxicity effects before practical applications. Photo-catalysts may be a promising materials for environmental remediation *only* when the materials are low-cost and non-toxic;

(6) Natural minerals are also photo-catalytic for degrading certain organic contaminants and simple modification may create some natural photocatalyst. Thus, the development of highly effective natural photocatalyst with simple and cheap modification is of interest.

Appendix

Appendix 1. Location of the sampling site for the sediments and seawater samples.

Fig. A-1. An overview of the sampling location of two marine sediments and seawater samples

Appendix 2. Additional data for Chapter 2: results of apparent soil-water distribution coefficients of 1-methylnaphthalene

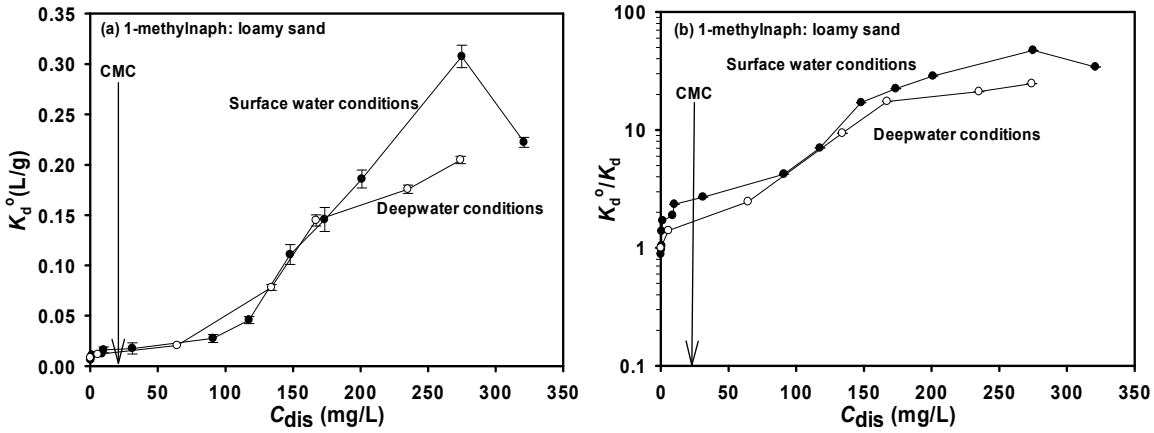

Fig. A-2. (a) The apparent soil-water distribution coefficients (K_d^o) of 1-methylnaphthalene and **(b)** K_d^o/K_d as a function of equilibrium Corexit EC9500A concentration under surface and deepwater conditions.

Appendix 3. Additional data for Chapter 3: GC chromatograms

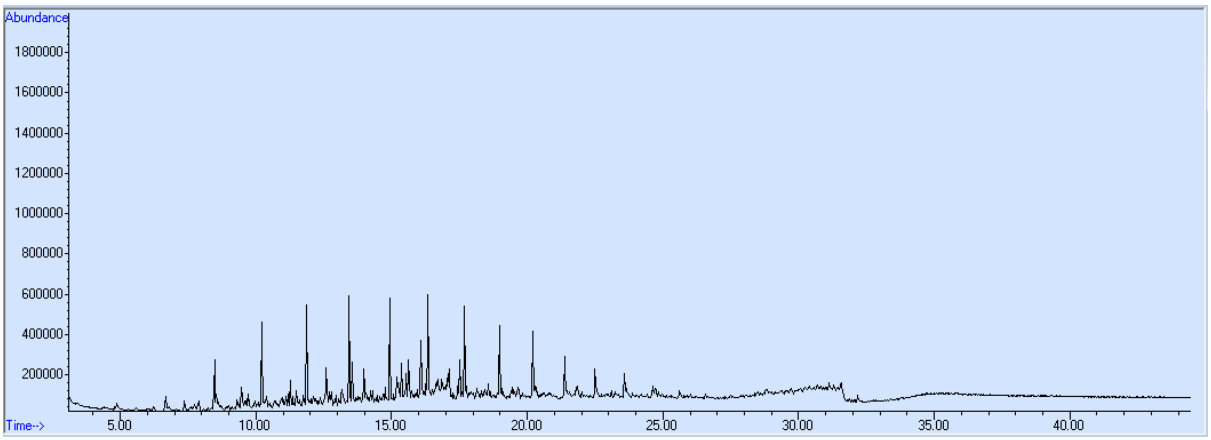

Fig. A-3. GC-FID chromatograms of the surrogate crude oil used in Chapter 3.

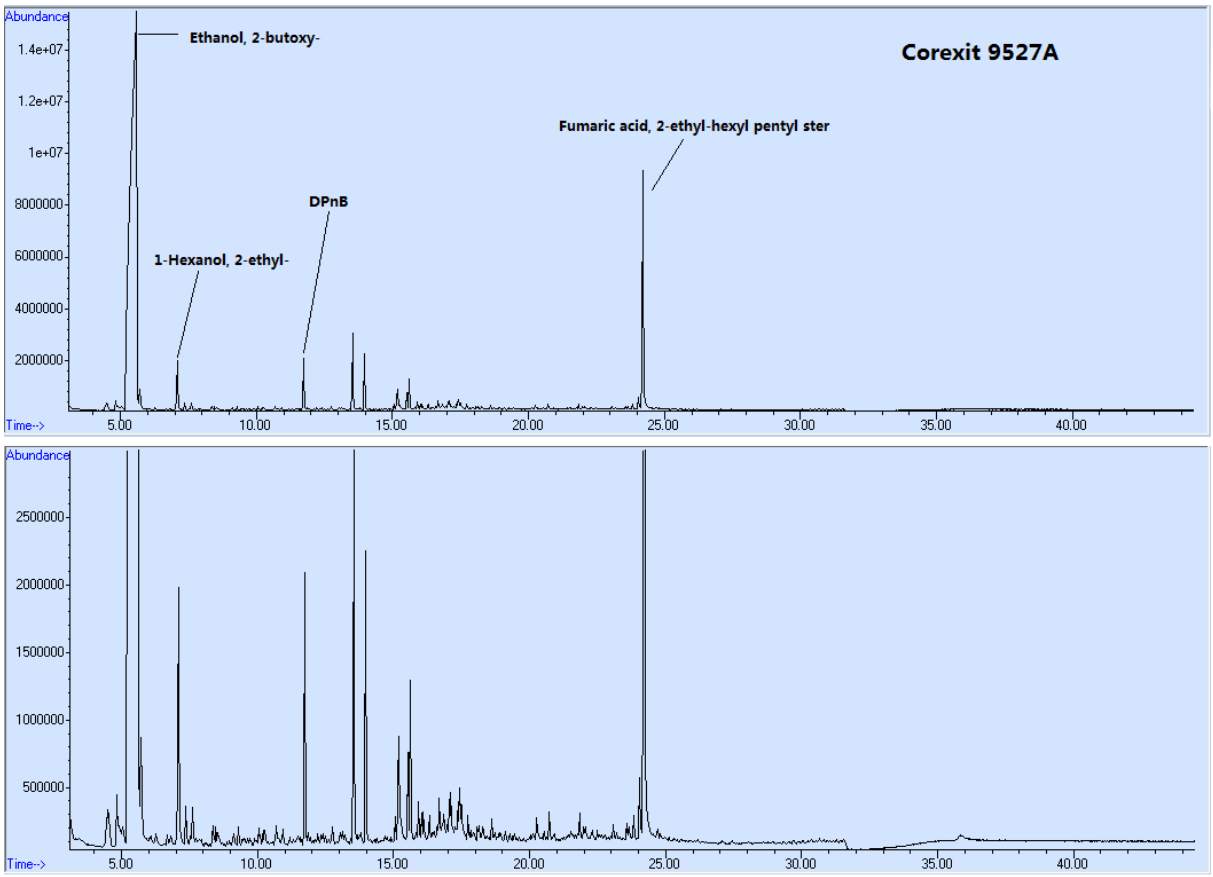

Fig. A-4. Total ion chromatogram of DWAO prepared using Corexit 9527A at DOR of 1:20.

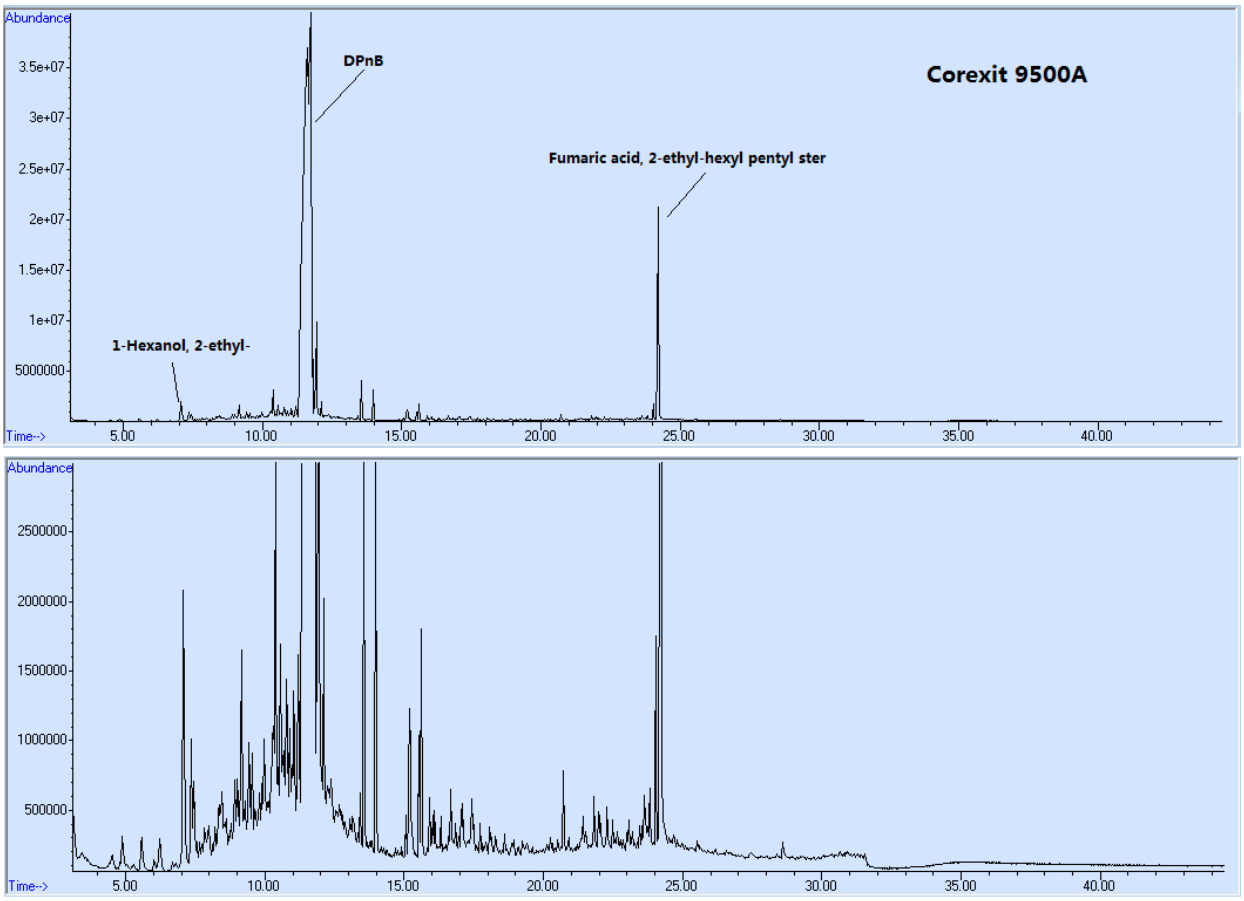

Fig. A-5. Total ion chromatogram of DWAO prepared using Corexit 9500A at DOR of 1:20.

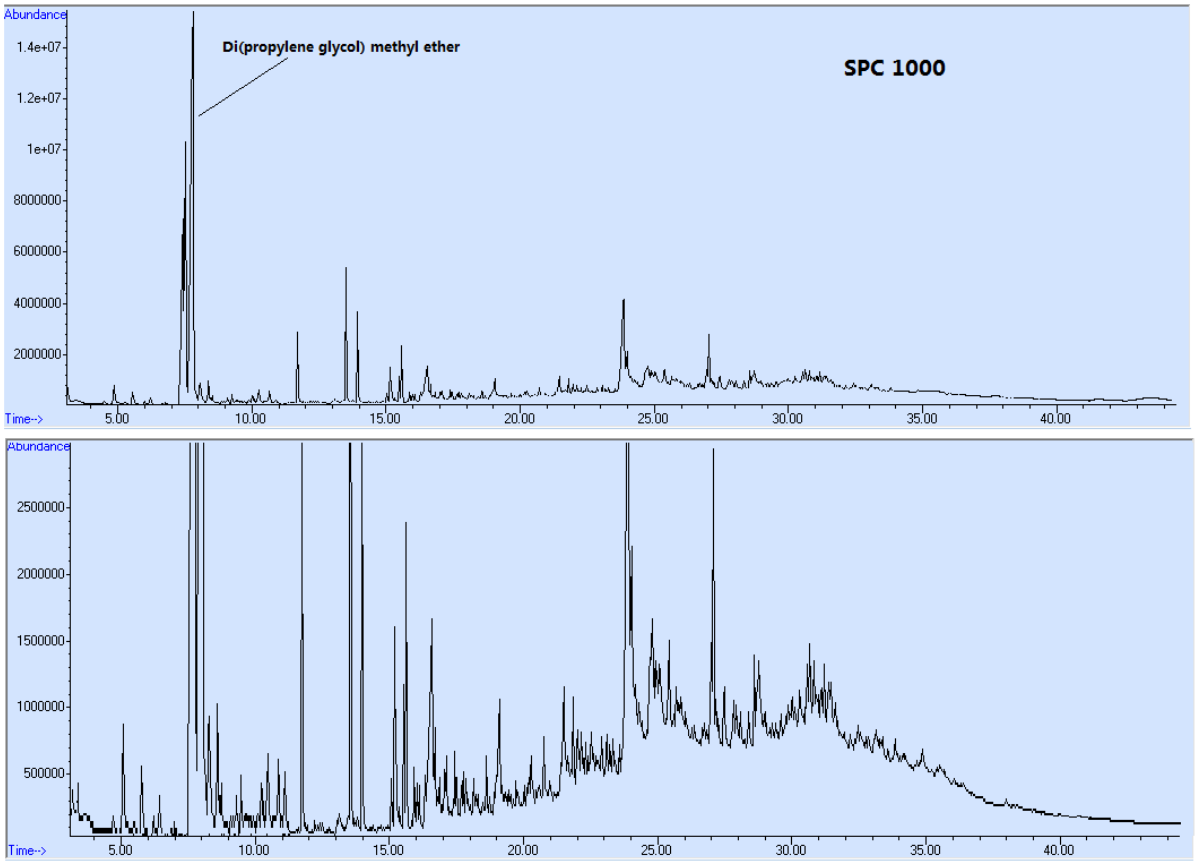

Fig. A-6. Total ion chromatogram of DWAO prepared using SPC 1000 at DOR of 1:20.

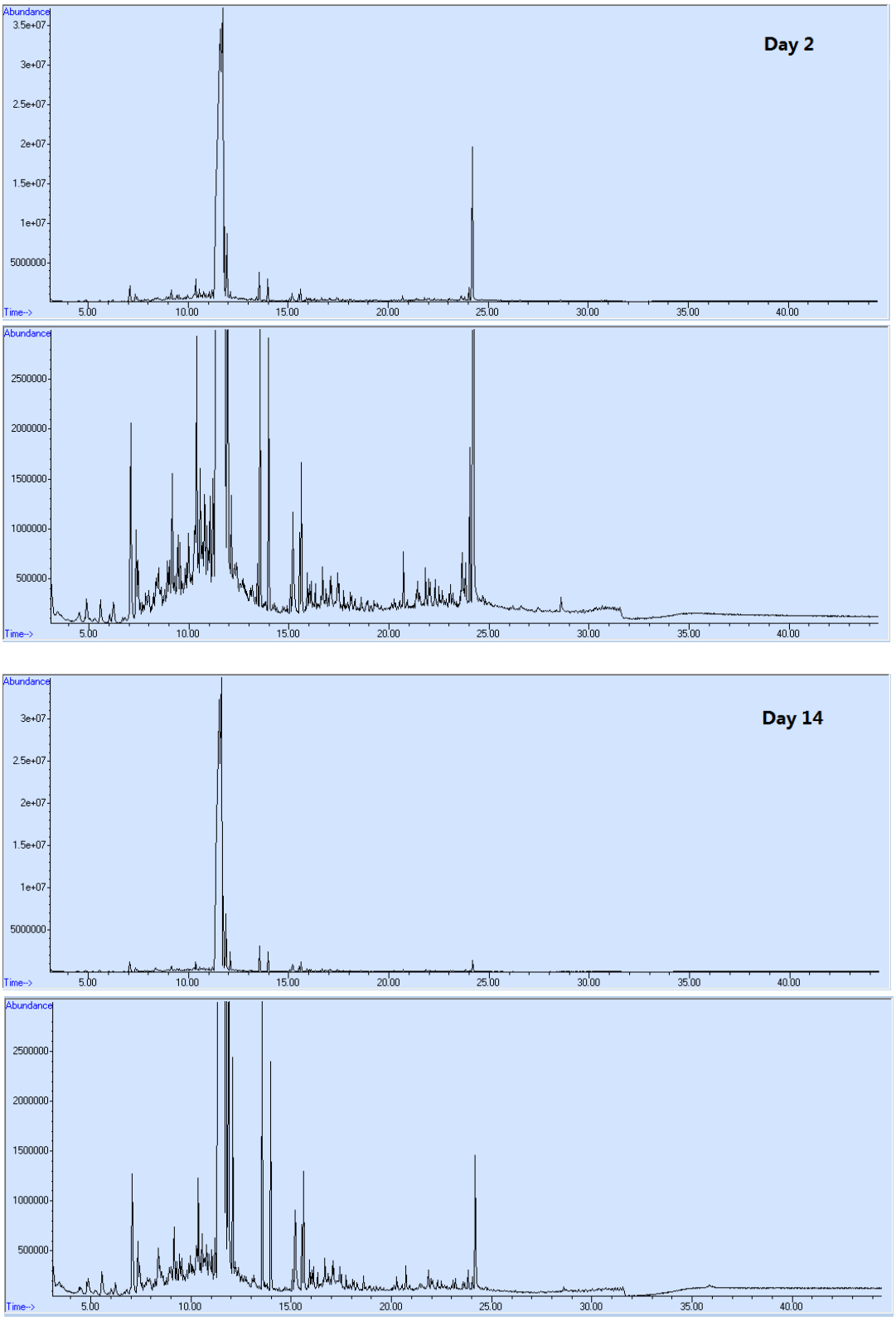

Fig. A-7. Total ion chromatogram of DWAO in Day 2 and Day 14**.**

Appendix 4. Additional data for Chapter 3: Calculations

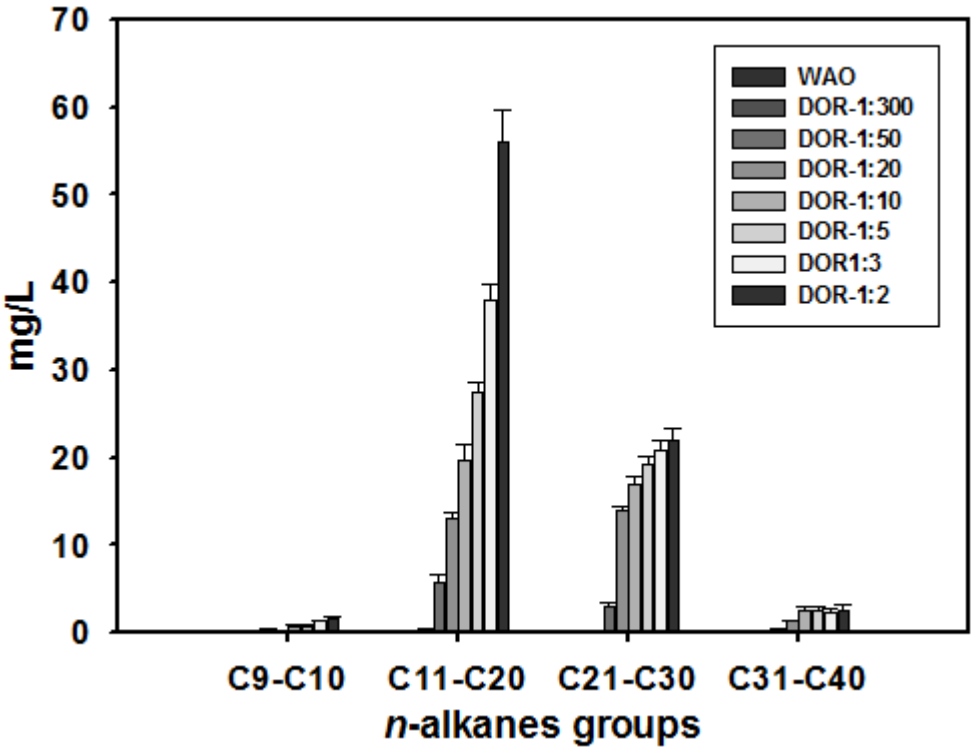

Fig. A-8. Concentrations of *n*-alkanes in four groups in the DWAO prepared at DORs from 0 to 1:2.

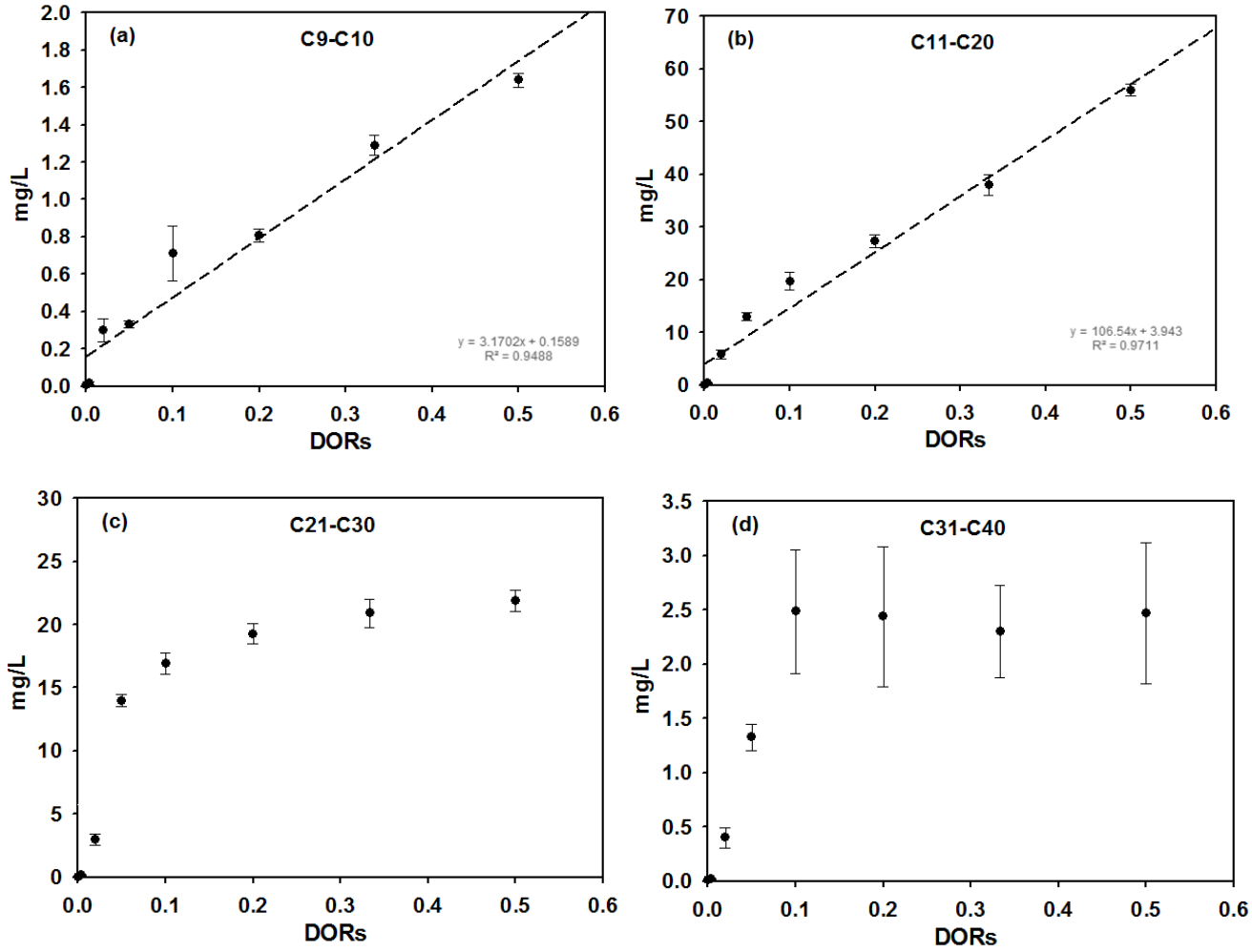

Fig. A-9. Concentrations of *n*-alkanes in four groups, C9-C10 **(a)**, C11-C20 **(b)**, C21-C30 **(c)** and C31-C40 **(d)** in the DWAO prepared at DORs from 0 to 1:2.

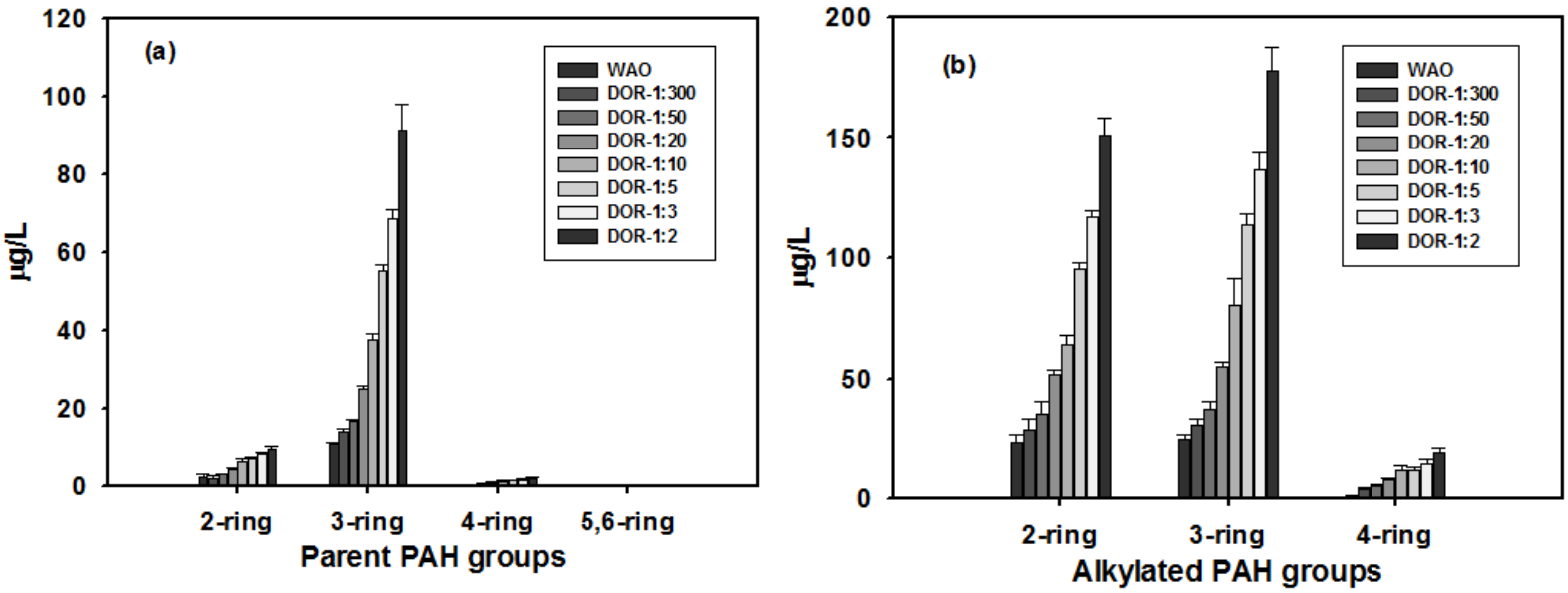

Fig. A-10. Concentrations of parent PAHs **(a)** and alkylated PAHs **(b)** in groups in the DWAO prepared at DORs from 0 to 1:2.

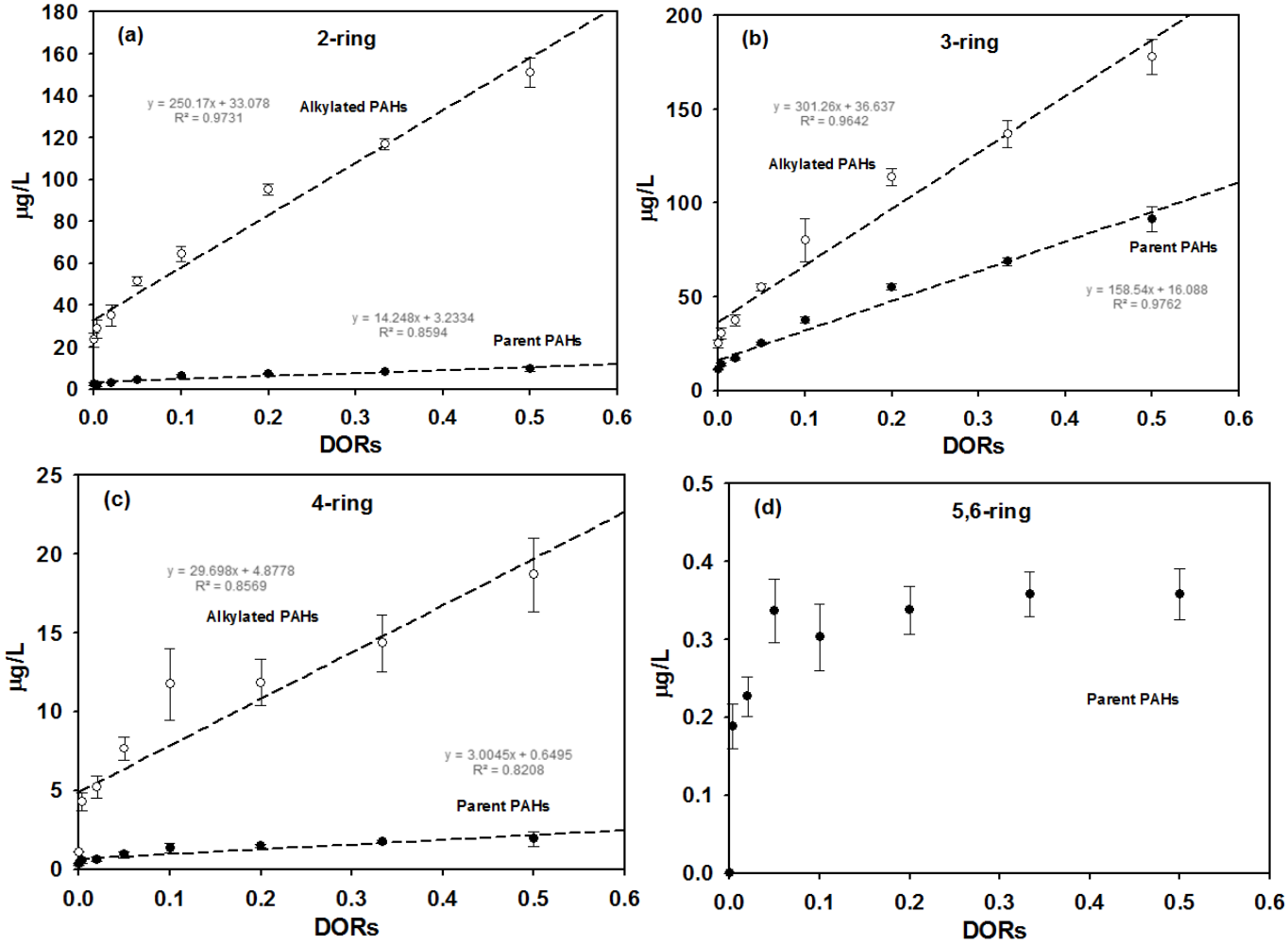

Fig. A-11. Concentrations of PAHs in four groups, 2-ring **(a)**, 3-ring **(b)**, 4-ring **(c)** and 5, 6-ring **(d)** in the DWAO prepared at DORs from 0 to 1:2.

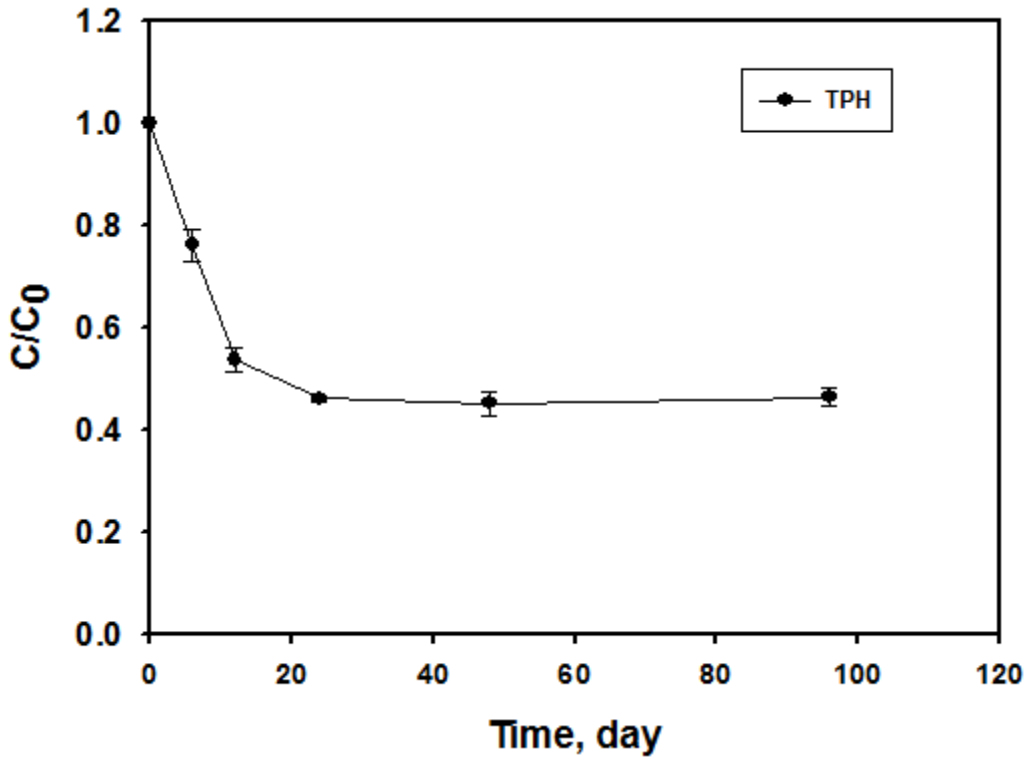

Fig. A-12. Sorption kinetics of TPH in DWAO (Corexit 9500A at DOR of 1:20) onto a loamy sand sediment (42 mL of solution with 2g of sediment)

Appendix 5. Additional data for Chapter 4

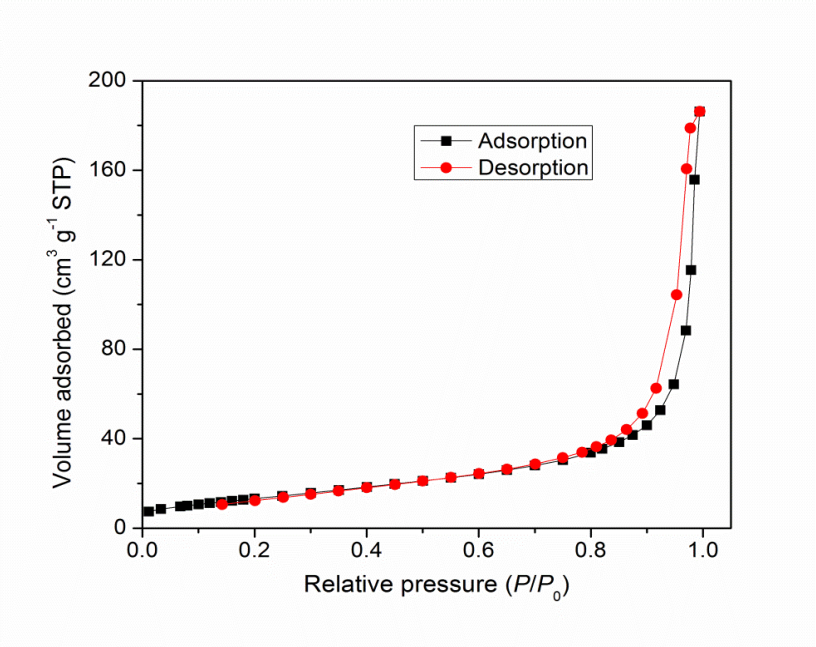

Fig. A-13. Nitrogen adsorption-desorption isothermsfor Co-TNTs-600.

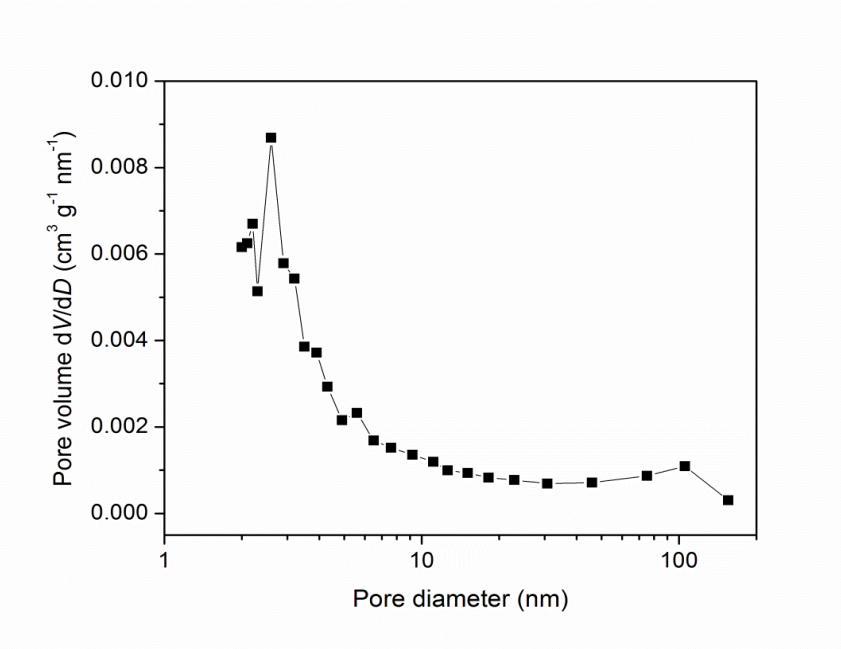

Fig. A-14. Pore size distribution of Co-TNTs-600.

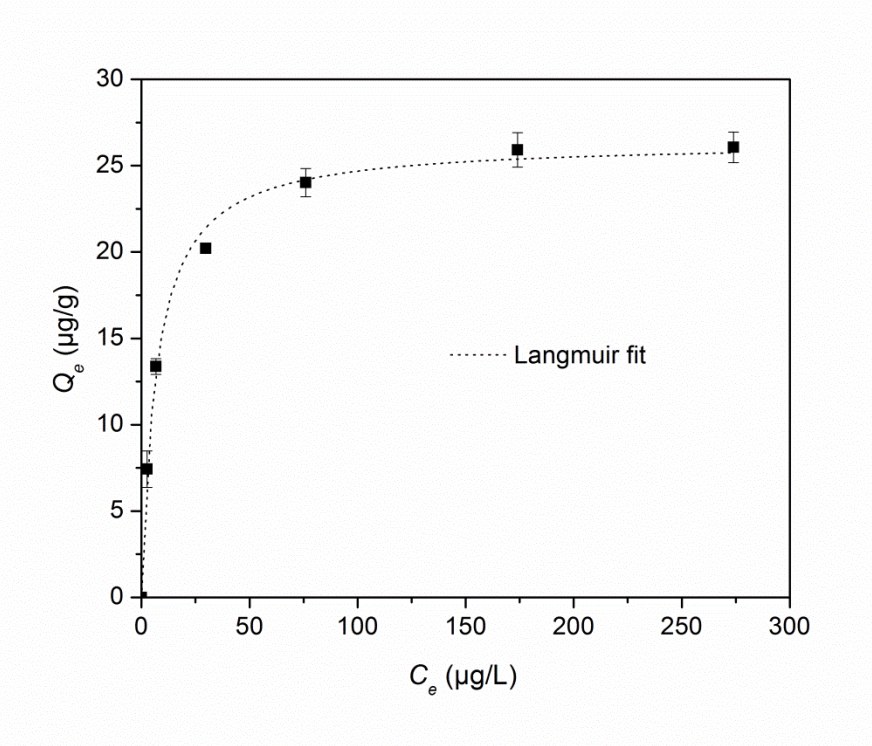

Fig. A-15. Adsorption isotherm of phenanthrene byCo-TNTs-600. (Material dosage = 1.0 g/L, pH = 7.0 ± 0.2, temperature = 25 ± 0.1°C).

Table A-1. Langmuir and Freundlich isotherm model parameters for adsorption of phenanthrene onto Co-TNTs-600.

Isotherm model	Parameter	Value
Langmuir model	Q_{max} (μg/g)	25.75
	b (L/μg)	0.15
	R^2	0.9985
Freundlich model	K_F (μg/g·(L/μg)$^{1/n}$)	7.19
	n	3.91
	R^2	0.9007

Table A-2. Apparent rate constant (k_1) and phenanthrene removal efficiency (R) by Co-TNTs-600 over 6 cycles of consecutive runs.

Cycles	k_1 (h^{-1})	R (%)
1	0.3867	98.6
2	0.3654	97.1
3	0.3310	94.8
4	0.3145	92.7
5	0.2936	89.3
6	0.2869	87.2

Table A-3. Bleeding of Co from Co-TNTs-600 over six runs.

Cycle	Co concentration in solution (mg/L)	Bleeding percent (wt%)
1	0.43	1.90
2	0.22	0.97
3	0.12	0.52
4	0.067	0.29
5	0.053	0.25
6	0.061	0.27

Table A-4. Reference standards for alkylated PAHs.

Compound	Reference standard
C1-Naph	1-methylnaphthalene
C2-Naph	1,4-Dimethylnaphthalene
C3-Naph	2,3,5-trimethylnaphthalene
C4-Naph	2,3,5-trimethylnaphthalene
C1-Fluo	1-methylfluorene
C2-Fluo	1-methylfluorene
C3-Fluo	1-methylfluorene
C1-PhenAn	1-methylphenanthrene
C2-PhenAn	9,10-dimethylanthracene
C3-PhenAn	9,10-dimethylanthracene
C4-PhenAn	9,10-dimethylanthracene
C1-FlPy	Pyrene
C2-FlPy	Pyrene
C3-FlPy	Pyrene
C1-ChryBa	Chrysene
C2-ChryBa	Chrysene
C3-ChryBa	Chrysene

Appendix 6. Copyright permission

Dear Xiao Zhao

Thank you for your email.

Please note that as one of the authors of this article, you retain the right to include the journal article, in full or in part, in a thesis or dissertation. You do not require permission to do so.

For full details of your rights as a Journal Author, please visit:

http://www.elsevier.com/wps/find/authorsview.authors/copyright#whatrights

Your retained rights allow you to submit your article in electronic format and to post this Elsevier article online if it is embedded within your thesis. You are also permitted to post your Author Accepted Manuscript online; however posting of the final published article is prohibited.

Please refer to Elsevier's Posting Policy for further information:

http://www.elsevier.com/wps/find/authors.authors/postingpolicy

Feel free to contact me if you have any queries.

Regards

Lakshmi Priya
Global Rights Department
Elsevier
(A division of Reed Elsevier India Pvt. Ltd.)

International Tech Park | Crest – 12th Floor | Taramani Road | Taramani | Chennai 600 113 | India
Tel: +91 44 42994660 | Fax: +91 44 42994701
E-mail: l.shridhar@elsevier.com | url: www.elsevier.com

From: xzz0013@auburn.edu [mailto:xzz0013@auburn.edu]
Sent: Friday, July 03, 2015 2:03 AM
To: Rights and Permissions (ELS)
Subject: Obtain Permission – Journal request

Title: Mr. Xiao Zhao
Institute/company: Auburn University
Address: 238 Harbert engineering center
Post/Zip Code: 36849
City: auburn
State/Territory: AL
Country: United States
Telephone: 3347076041
Email: xzz0013@auburn.edu

Type of Publication: Journal
Journal Title: Marine Pollution Bulletin
Journal ISSN: 0025-326X
Journal Volume: 92
Journal Issue: 1-2
Journal Year: 2015
Journal Pages: 160 to 169
Journal Author: Xiao Zhao, Yanyan Gong, S.E. O'Reilly, Dongye Zhao
Journal Article title: Effects of oil dispersant on solubilization, sorption and desorption of polycyclic aromatic hydrocarbons in sediment–seawater systems
Quality of material:
Excerpts:
Are you the author of the Elsevier material? Yes
If not, is the Elsevier author involved? No
If yes, please provide details of how the Elsevier author is involved:
In what format will you use the material? Electronic
Will you be translating the material? No
If yes, specify language:
Information about proposed use: Reuse in a thesis/dissertation
Proposed use text: The use of copyrighted materials in a thesis or dissertation requires the permission of the copyright holder. The student is responsible for securing all necessary permissions, beyond what is permitted by "fair use," and for paying any permission fees.
Additional Comments / Information:

References

Agency., U.U.E.P. (1996) Acid Digestion of Sediments, Sludges, and Soils, Method 3050B, Revision 2; USEPA. Washington, DC, USA.

Al-Ekabi, H. and Serpone, N. (1988) Kinetics studies in heterogeneous photocatalysis. I. Photocatalytic degradation of chlorinated phenols in aerated aqueous solutions over titania supported on a glass matrix. The Journal of Physical Chemistry 92(20), 5726-5731.

Blondina, G., Singer, M., Lee, I., Ouano, M., Hodgins, M., Tjeerdema, R. and Sowby, M. (1999) Influence of salinity on petroleum accommodation by dispersants. Spill Science & Technology Bulletin 5(2), 127-134.

Board, O.S. (2005) Oil Spill Dispersants:: Efficacy and Effects, National Academies Press.

Boukir, A., Aries, E., Guiliano, M., Asia, L., Doumenq, P. and Mille, G. (2001) Subfractionation, characterization and photooxidation of crude oil resins. Chemosphere 43(3), 279-286.

Bouyoucos, G.J. (1962) Hydrometer method improved for making particle size analyses of soils. Agronomy Journal 54(5), 464-&.

Bruheim, P., Bredholt, H. and Eimhjellen, K. (1999) Effects of surfactant mixtures, including Corexit 9527, on bacterial oxidation of acetate and alkanes in crude oil. Applied and environmental microbiology 65(4), 1658-1661.

Brunauer, S., Deming, L.S., Deming, W.E. and Teller, E. (1940) On a theory of the van der Waals adsorption of gases. Journal of the American Chemical Society 62(7), 1723-1732.

Camilli, R., Reddy, C.M., Yoerger, D.R., Van Mooy, B.A., Jakuba, M.V., Kinsey, J.C., McIntyre, C.P., Sylva, S.P. and Maloney, J.V. (2010) Tracking hydrocarbon plume transport and biodegradation at Deepwater Horizon. Science 330(6001), 201-204.

Chen, H.-Y., Lo, S.-L. and Ou, H.-H. (2013) Catalytic hydrogenation of nitrate on Cu–Pd supported on titanate nanotube and the experiment after aging, sulfide fouling and regeneration procedures. Applied Catalysis B: Environmental 142, 65-71.

Chen, J., Peijnenburg, W., Quan, X. and Yang, F. (2000) Quantitative structure–property relationships for direct photolysis quantum yields of selected polycyclic aromatic hydrocarbons. Science of The Total Environment 246(1), 11-20.

Chen, K., Zhu, L. and Yang, K. (2015) Acid-assisted hydrothermal synthesis of nanocrystalline TiO 2 from titanate nanotubes: Influence of acids on the photodegradation of gaseous toluene. Journal of Environmental Sciences 27, 232-240.

Chen, Q., Zhou, W.Z., Du, G.H. and Peng, L.M. (2002) Trititanate nanotubes made via a single alkali treatment. Advanced Materials 14(17), 1208-+.

Chen, W., Duan, L. and Zhu, D. (2007) Adsorption of polar and nonpolar organic chemicals to carbon nanotubes. Environmental Science & Technology 41(24), 8295-8300.

Chen, X. and Burda, C. (2008) The electronic origin of the visible-light absorption properties of C-, N-and S-doped TiO2 nanomaterials. Journal of the American Chemical Society 130(15), 5018-5019.

Chen, X., Liu, L. and Huang, F. (2015) Black titanium dioxide (TiO 2) nanomaterials. Chemical Society Reviews.

Chen, X. and Mao, S.S. (2007) Titanium dioxide nanomaterials: synthesis, properties, modifications, and applications. Chemical reviews 107(7), 2891-2959.

Choi, M. and Yong, K. (2014) A facile strategy to fabricate high-quality single crystalline brookite TiO2 nanoarrays and their photoelectrochemical properties. Nanoscale 6(22), 13900-13909.
Choi, Y., Cho, Y.-M., Gala, W.R. and Luthy, R.G. (2012) Measurement and modeling of activated carbon performance for the sequestration of parent-and alkylated-polycyclic aromatic hydrocarbons in petroleum-impacted sediments. Environmental Science & Technology 47(2), 1024-1032.
Coolbaugh, T., McElroy, A. and Guard, L.U.C. Dispersant Efficacy and Effectiveness.
Corazza, M., Lauriola, M., Zappaterra, M., Bianchi, A. and Virgili, A. (2010) Surfactants, skin cleansing protagonists. Journal Of The European Academy Of Dermatology And Venereology 24(1), 1-6.
Dahl, M., Liu, Y. and Yin, Y. (2014) Composite titanium dioxide nanomaterials. Chemical reviews 114(19), 9853-9889.
Dai, G., Liu, S., Liang, Y. and Luo, T. (2013) Synthesis and enhanced photoelectrocatalytic activity of p–n junction Co3O4/TiO2 nanotube arrays. Applied Surface Science 264(0), 157-161.
De la Pena O'Shea, V.A., Alvarez Galvan, M.C., Platero Prats, A.E., Campos-Martin, J.M. and Fierro, J.L.G. (2011) Direct evidence of the SMSI decoration effect: the case of Co/TiO2 catalyst. Chemical Communications 47(25), 7131-7133.
Desai, J.D. and Banat, I.M. (1997) Microbial production of surfactants and their commercial potential. Microbiology and Molecular biology reviews 61(1), 47-64.
Diallo, M.S., Abriola, L.M. and Weber, W.J. (1994) Solubilization of nonaqueous phase liquid hydrocarbons in micellar solutions of dodecyl alcohol ethoxylates. Environmental Science & Technology 28(11), 1829-1837.
Diercks, A.R., Highsmith, R.C., Asper, V.L., Joung, D., Zhou, Z., Guo, L., Shiller, A.M., Joye, S.B., Teske, A.P. and Guinasso, N. (2010) Characterization of subsurface polycyclic aromatic hydrocarbons at the Deepwater Horizon site. Geophysical Research Letters 37(20).
Edwards, D.A., Luthy, R.G. and Liu, Z. (1991) Solubilization of polycyclic aromatic hydrocarbons in micellar nonionic surfactant solutions. Environmental Science & Technology 25(1), 127-133.
Ehrhardt, M. and Petrick, G. (1985) The sensitized photo-oxidation of n-pentadecane as a model for abiotic decomposition of aliphatic hydrocarbons in seawater. Marine Chemistry 16(3), 227-238.
Ehrhardt, M. and Petrick, G. (1993) On the composition of dissolved and particle-associated fossil fuel residues in Mediterranean surface water. Marine Chemistry 42(1), 57-70.
Endo, S., Grathwohl, P. and Schmidt, T.C. (2008) Absorption or adsorption? Insights from molecular probes n-alkanes and cycloalkanes into modes of sorption by environmental solid matrices. Environmental Science & Technology 42(11), 3989-3995.
Faksness, L.-G., Brandvik, P.J. and Sydnes, L.K. (2008) Composition of the water accommodated fractions as a function of exposure times and temperatures. Marine Pollution Bulletin 56(10), 1746-1754.
Fasnacht, M.P. and Blough, N.V. (2002) Aqueous photodegradation of polycyclic aromatic hydrocarbons. Environmental Science & Technology 36(20), 4364-4369.
Fasnacht, M.P. and Blough, N.V. (2003) Mechanisms of the aqueous photodegradation of polycyclic aromatic hydrocarbons. Environmental Science & Technology 37(24), 5767-5772.

Feng, C., Teng, F., Liu, Z., Chang, C., Zhao, Y., Wang, S., Chen, M., Yao, W. and Zhu, Y. (2015) A newly discovered BiF3 photocatalyst with a high positive valence band. Journal of Molecular Catalysis A: Chemical 401(0), 35-40.
Fingas, M. (2012) The basics of oil spill cleanup, CRC Press.
Frysinger, G.S., Gaines, R.B., Xu, L. and Reddy, C.M. (2003) Resolving the unresolved complex mixture in petroleum-contaminated sediments. Environmental Science & Technology 37(8), 1653-1662.
Fu, J., Gong, Y., Zhao, X., O'Reilly, S. and Zhao, D. (2014) Effects of Oil and Dispersant on Formation of Marine Oil Snow and Transport of Oil Hydrocarbons. Environmental Science & Technology 48(24), 14392-14399.
Gao, H.-C., Zhao, S., Mao, S.-Z., Yuan, H.-Z., Yu, J.-Y., Shen, L.-F. and Du, Y.-R. (2002) Mixed micelles of polyethylene glycol (23) lauryl ether with ionic surfactants studied by proton 1D and 2D NMR. Journal of colloid and interface science 249(1), 200-208.
Gearing, P.J., Gearing, J.N., Pruell, R.J., Wade, T.L. and Quinn, J.G. (1980) Partitioning of no 2 fuel-oil in controlled estuarine ecosystems - sediments and suspended particulate matter. Environmental Science & Technology 14(9), 1129-1136.
George-Ares, A. and Clark, J. (2000) Aquatic toxicity of two Corexit® dispersants. Chemosphere 40(8), 897-906.
Glover, A.G. and Smith, C.R. (2003) The deep-sea floor ecosystem: current status and prospects of anthropogenic change by the year 2025. Environmental Conservation 30(3), 219-241.
Glover, C.M., Mezyk, S.P., Linden, K.G. and Rosario-Ortiz, F.L. (2014) Photochemical degradation of Corexit components in ocean water. Chemosphere 111(0), 596-602.
Gohlke, J.M., Doke, D., Tipre, M., Leader, M. and Fitzgerald, T. (2011) A review of seafood safety after the Deepwater Horizon blowout. Environmental health perspectives 119(8), 1062.
Gong, Y., Liu, Y., Xiong, Z., Kaback, D. and Zhao, D. (2012) Immobilization of mercury in field soil and sediment using carboxymethyl cellulose stabilized iron sulfide nanoparticles. Nanotechnology 23(29), 294007.
Gong, Y., Zhao, X., Cai, Z., O'Reilly, S., Hao, X. and Zhao, D. (2014a) A review of oil, dispersed oil and sediment interactions in the aquatic environment: Influence on the fate, transport and remediation of oil spills. Marine Pollution Bulletin 79(1), 16-33.
Gong, Y., Zhao, X., O'Reilly, S., Qian, T. and Zhao, D. (2014b) Effects of oil dispersant and oil on sorption and desorption of phenanthrene with Gulf Coast marine sediments. Environmental Pollution 185, 240-249.
Grandcolas, M., Cottineau, T., Louvet, A., Keller, N. and Keller, V. (2013) Solar light-activated photocatalytic degradation of gas phase diethylsulfide on WO 3-modified TiO 2 nanotubes. Applied Catalysis B: Environmental 138, 128-140.
Guiliano, M., El Anba-Lurot, F., Doumenq, P., Mille, G. and Rontani, J. (1997) Photo-oxidation of n-alkanes in simulated marine environmental conditions. Journal of Photochemistry and Photobiology A: Chemistry 102(2), 127-132.
He, Y.W., Yediler, A., Sun, T.H. and Kettrup, A. (1995) Adsorption of fluoranthene on soil and lava - effects of the organic-carbon contents of adsorbents and temperature. Chemosphere 30(1), 141-150.

Hemmer, M.J., Barron, M.G. and Greene, R.M. (2011) Comparative toxicity of eight oil dispersants, Louisiana sweet crude oil (LSC), and chemically dispersed LSC to two aquatic test species. Environmental Toxicology and Chemistry 30(10), 2244-2252.
Innocente, N., Biasutti, M., Venir, E., Spaziani, M. and Marchesini, G. (2009) Effect of high-pressure homogenization on droplet size distribution and rheological properties of ice cream mixes. Journal of Dairy Science 92(5), 1864-1875.
Jia, H., Zhao, J., Fan, X., Dilimulati, K. and Wang, C. (2012) Photodegradation of phenanthrene on cation-modified clays under visible light. Applied Catalysis B: Environmental 123–124(0), 43-51.
Jonker, M.T.O., Sinke, A.J.C., Brils, J.M. and Koelmans, A.A. (2003) Sorption of Polycyclic Aromatic Hydrocarbons to Oil Contaminated Sediment: Unresolved Complex? Environmental Science & Technology 37(22), 5197-5203.
Kanagalasara, V., Saxena, D. and Biswas, S.K. (2012) Effect of interfacial microstructure of adsorbed poly (ethylene glycol) monooleate on steel substrate on sliding friction in oil in water emulsion. The Journal of Physical Chemistry C 116(39), 20830-20838.
Khan, M.A., Jung, H.-T. and Yang, O.-B. (2006) Synthesis and characterization of ultrahigh crystalline TiO2 nanotubes. The Journal of Physical Chemistry B 110(13), 6626-6630.
Kim, S., Kim, M., Hwang, S.-H. and Lim, S.K. (2012) Enhancement of photocatalytic activity of titania–titanate nanotubes by surface modification. Applied Catalysis B: Environmental 123, 391-397.
Kirsten, W.J. (1979) Automated methods for the simultaneous determination of carbon, hydrogen, nitrogen, and sulfur, and sufur alone in organic and inorganic materials Anal. Chem. 51, 1173-1179.
Ko, S.O., Schlautman, M.A. and Carraway, E.R. (1998) Partitioning of hydrophobic organic compounds to sorbed surfactants. 1. Experimental studies. Environmental Science & Technology 32(18), 2769-2775.
Konova, P., Stoyanova, M., Naydenov, A., Christoskova, S. and Mehandjiev, D. (2006) Catalytic oxidation of VOCs and CO by ozone over alumina supported cobalt oxide. Applied Catalysis a-General 298, 109-114.
Kostka, J.E., Prakash, O., Overholt, W.A., Green, S.J., Freyer, G., Canion, A., Delgardio, J., Norton, N., Hazen, T.C. and Huettel, M. (2011) Hydrocarbon-degrading bacteria and the bacterial community response in Gulf of Mexico beach sands impacted by the Deepwater Horizon oil spill. Applied and environmental microbiology 77(22), 7962-7974.
Kou, J., Zhang, H., Yuan, Y., Li, Z., Wang, Y., Yu, T. and Zou, Z. (2008) Efficient photodegradation of phenanthrene under visible light irradiation via photosensitized electron transfer. The Journal of Physical Chemistry C 112(11), 4291-4296.
Kover, S.C., Rosario-Ortiz, F.L. and Linden, K.G. (2014) Photochemical fate of solvent constituents of Corexit oil dispersants. Water Research 52(0), 101-111.
Kujawinski, E.B., Kido Soule, M.C., Valentine, D.L., Boysen, A.K., Longnecker, K. and Redmond, M.C. (2011) Fate of dispersants associated with the Deepwater Horizon oil spill. Environmental Science & Technology 45(4), 1298-1306.
Lee, C.-K., Wang, C.-C., Lyu, M.-D., Juang, L.-C., Liu, S.-S. and Hung, S.-H. (2007) Effects of sodium content and calcination temperature on the morphology, structure and photocatalytic activity of nanotubular titanates. Journal of colloid and interface science 316(2), 562-569.

Li, Z., Lee, K., King, T., Boufadel, M.C. and Venosa, A.D. (2009) Evaluating chemical dispersant efficacy in an experimental wave tank: 2—Significant factors determining in situ oil droplet size distribution. Environmental Engineering Science 26(9), 1407-1418.
Lin, C.-H., Chao, J.-H., Liu, C.-H., Chang, J.-C. and Wang, F.-C. (2008) Effect of calcination temperature on the structure of a Pt/TiO2 (B) nanofiber and its photocatalytic activity in generating H2. Langmuir 24(17), 9907-9915.
Lin, H.K., Chiu, H.C., Tsai, H.C., Chien, S.H. and Wang, C.B. (2003) Synthesis, characterization and catalytic oxidation of carbon monoxide over cobalt oxide. Catalysis Letters 88(3-4), 169-174.
Liu, W., Ni, J.R. and Yin, X.C. (2014) Synergy of photocatalysis and adsorption for simultaneous removal of Cr(VI) and Cr(III) with TiO2 and titanate nanotubes. Water Research 53, 12-25.
Liu, W., Sun, W., Borthwick, A.G.L. and Ni, J. (2013a) Comparison on aggregation and sedimentation of titanium dioxide, titanate nanotubes and titanate nanotubes-TiO2: Influence of pH, ionic strength and natural organic matter. Colloids and Surfaces A: Physicochemical and Engineering Aspects 434(0), 319-328.
Liu, W., Wang, T., Borthwick, A.G., Wang, Y., Yin, X., Li, X. and Ni, J. (2013b) Adsorption of Pb 2+, Cd 2+, Cu 2+ and Cr 3+ onto titanate nanotubes: Competition and effect of inorganic ions. Science of the Total Environment 456, 171-180.
Liu, Y., Shu, W., Chen, K., Peng, Z. and Chen, W. (2012a) Enhanced Photothermocatalytic Synergetic Activity Toward Gaseous Benzene for Mo plus C-Codoped Titanate Nanobelts. Acs Catalysis 2(12), 2557-2565.
Liu, Z., Liu, J., Zhu, Q. and Wu, W. (2012b) The weathering of oil after the Deepwater Horizon oil spill: insights from the chemical composition of the oil from the sea surface, salt marshes and sediments. Environmental Research Letters 7(3), 035302.
Lubchenco, J. (2010) BP Deepwater Horizon Oil Budget: What Happened to the Oil?, US Department of Commerce, National Oceanic and Atmospheric Administration.
Luthy, R.G., Aiken, G.R., Brusseau, M.L., Cunningham, S.D., Gschwend, P.M., Pignatello, J.J., Reinhard, M., Traina, S.J., Weber, W.J. and Westall, J.C. (1997) Sequestration of hydrophobic organic contaminants by geosorbents. Environmental Science & Technology 31(12), 3341-3347.
Mahajan, T.B., Elsila, J.E., Deamer, D.W. and Zare, R.N. (2003) Formation of carbon-carbon bonds in the photochemical alkylation of polycyclic aromatic hydrocarbons. Origins of Life and Evolution of the Biosphere 33(1), 17-35.
Major, D., Zhang, Q., Wang, G. and Wang, H. (2012) Oil-dispersant mixtures: understanding chemical composition and its relation to human toxicity. Toxicological & Environmental Chemistry 94(9), 1832-1845.
Marin, R.P., Kondrat, S.A., Gallagher, J.R., Enache, D.I., Smith, P., Boldrin, P., Davies, T.E., Bartley, J.K., Combes, G.B., Williams, P.B., Taylor, S.H., Claridge, J.B., Rosseinsky, M.J. and Hutchings, G.J. (2013) Preparation of Fischer-Tropsch Supported Cobalt Catalysts Using a New Gas Anti-Solvent Process. Acs Catalysis 3(4), 764-772.
Mitchell, F.M. and Holdway, D.A. (2000) The acute and chronic toxicity of the dispersants Corexit 9527 and 9500, water accommodated fraction (WAF) of crude oil, and dispersant enhanced WAF (DEWAF) to< i> Hydra viridissima</i>(green hydra). Water Research 34(1), 343-348.

Mohamed, A. and Mahfoodh, A.-S.M. (2006) Solubilization of naphthalene and pyrene by sodium dodecyl sulfate (SDS) and polyoxyethylenesorbitan monooleate (Tween 80) mixed micelles. Colloids and Surfaces A: Physicochemical and Engineering Aspects 287(1), 44-50.
Nam, J.J., Thomas, G.O., Jaward, F.M., Steinnes, E., Gustafsson, O. and Jones, K.C. (2008) PAHs in background soils from Western Europe: Influence of atmospheric deposition and soil organic matter. Chemosphere 70(9), 1596-1602.
NREL (2009) United States Solar Radiation Map http://www.nrel.gov/gis/data_solar.html (http://www.nrel.gov/gis/data_solar.html).
Ou, H.-H., Liao, C.-H., Liou, Y.-H., Hong, J.-H. and Lo, S.-L. (2008) Photocatalytic oxidation of aqueous ammonia over microwave-induced titanate nanotubes. Environmental Science & Technology 42(12), 4507-4512.
Özhan, K., Miles, S.M., Gao, H. and Bargu, S. (2014) Relative Phytoplankton growth responses to physically and chemically dispersed South Louisiana sweet crude oil. Environmental monitoring and assessment 186(6), 3941-3956.
Paria, S. and Khilar, K.C. (2004) A review on experimental studies of surfactant adsorption at the hydrophilic solid–water interface. Advances in Colloid and Interface Science 110(3), 75-95.
Park, O.K. and Kang, Y.S. (2005) Preparation and characterization of silica-coated TiO2 nanoparticle. Colloids and Surfaces a-Physicochemical and Engineering Aspects 257-58, 261-265.
Pelaez, M., Nolan, N.T., Pillai, S.C., Seery, M.K., Falaras, P., Kontos, A.G., Dunlop, P.S., Hamilton, J.W., Byrne, J.A. and O'Shea, K. (2012) A review on the visible light active titanium dioxide photocatalysts for environmental applications. Applied Catalysis B: Environmental 125, 331-349.
Plata, D.L., Sharpless, C.M. and Reddy, C.M. (2008) Photochemical degradation of polycyclic aromatic hydrocarbons in oil films. Environmental Science & Technology 42(7), 2432-2438.
Qiao, R., Zhang, X.L., Qiu, R., Kim, J.C. and Kang, Y.S. (2009) Morphological Transformation of Co(OH)(2) Microspheres from Solid to Flowerlike Hollow Core-Shell Structures. Chemistry-a European Journal 15(8), 1886-1892.
Reddy, C.M., Arey, J.S., Seewald, J.S., Sylva, S.P., Lemkau, K.L., Nelson, R.K., Carmichael, C.A., McIntyre, C.P., Fenwick, J. and Ventura, G.T. (2012) Composition and fate of gas and oil released to the water column during the Deepwater Horizon oil spill. Proceedings of the National Academy of Sciences 109(50), 20229-20234.
Rivas, F.J. (2006) Polycyclic aromatic hydrocarbons sorbed on soils: A short review of chemical oxidation based treatments. Journal of Hazardous Materials 138(2), 234-251.
Rontani, J.-F. and Giral, P.-P. (1990) Significance of photosensitized oxidation of alkanes during the photochemical degradation of petroleum hydrocarbon fractions in seawater. International Journal of Environmental Analytical Chemistry 42(1-4), 61-68.
Rosenberg, E., Perry, A., Gibson, D. and Gutnick, D. (1979) Emulsifier of Arthrobacter RAG-1: specificity of hydrocarbon substrate. Applied and environmental microbiology 37(3), 409-413.
Ryerson, T.B., Camilli, R., Kessler, J.D., Kujawinski, E.B., Reddy, C.M., Valentine, D.L., Atlas, E., Blake, D.R., de Gouw, J. and Meinardi, S. (2012) Chemical data quantify Deepwater Horizon hydrocarbon flow rate and environmental distribution. Proceedings of the National Academy of Sciences 109(50), 20246-20253.

Sammarco, P.W., Kolian, S.R., Warby, R.A., Bouldin, J.L., Subra, W.A. and Porter, S.A. (2013) Distribution and concentrations of petroleum hydrocarbons associated with the BP/Deepwater Horizon Oil Spill, Gulf of Mexico. Marine Pollution Bulletin 73(1), 129-143.
Scelfo, G.M. and Tjeerdema, R.S. (1991) A simple method for determination of corexit 9527® in natural waters. Marine environmental research 31(1), 69-78.
Schick, M.J. (1963) Effect of temperature on the critical micelle concentration of nonionic detergents. thermodynamics of micelle formation1. The Journal of Physical Chemistry 67(9), 1796-1799.
Schneider, J., Matsuoka, M., Takeuchi, M., Zhang, J., Horiuchi, Y., Anpo, M. and Bahnemann, D.W. (2014) Understanding TiO2 photocatalysis: mechanisms and materials. Chemical reviews 114(19), 9919-9986.
Shankar, R., Shim, W.J., An, J.G. and Yim, U.H. (2015) A practical review on photooxidation of crude oil: Laboratory lamp setup and factors affecting it. Water Research 68, 304-315.
Shannon, M.A., Bohn, P.W., Elimelech, M., Georgiadis, J.G., Mariñas, B.J. and Mayes, A.M. (2008) Science and technology for water purification in the coming decades. Nature 452(7185), 301-310.
Singer, M., Aurand, D., Bragin, G., Clark, J., Coelho, G., Sowby, M. and Tjeerdema, R. (2000) Standardization of the preparation and quantitation of water-accommodated fractions of petroleum for toxicity testing. Marine Pollution Bulletin 40(11), 1007-1016.
Sirisaksoontorn, W., Thachepan, S. and Songsasen, A. (2009) Photodegradation of phenanthrene by N-doped TiO2 photocatalyst. Journal of Environmental Science and Health, Part A 44(9), 841-846.
Srivastava, A. and Ismail, K. (2014) Solubilization of polycyclic aromatic hydrocarbons in aqueous sodium dioctylsulfosuccinate solutions. Journal of Molecular Liquids 195(0), 105-109.
Sun, X.M. and Li, Y.D. (2003) Synthesis and characterization of ion-exchangeable titanate nanotubes. Chemistry-a European Journal 9(10), 2229-2238.
Tan, H., Zhao, Z., Niu, M., Mao, C., Cao, D., Cheng, D., Feng, P. and Sun, Z. (2014) A facile and versatile method for preparation of colored TiO 2 with enhanced solar-driven photocatalytic activity. Nanoscale 6(17), 10216-10223.
Thibodeaux, L.J., Valsaraj, K.T., John, V.T., Papadopoulos, K.D., Pratt, L.R. and Pesika, N.S. (2011) Marine oil fate: knowledge gaps, basic research, and development needs; A perspective based on the Deepwater Horizon spill. Environmental Engineering Science 28(2), 87-93.
Tjessem, K. and Aaberg, A. (1983) Photochemical transformation and degradation of petroleum residues in the marine environment. Chemosphere 12(11), 1373-1394.
Tokuoka, Y., Uchiyama, H., Abe, M. and Christian, S.D. (1995) Solubilization of Some Synthetic Perfumes by Anionic-Nonionic Mixed Surfactant Systems. 1. Langmuir 11(3), 725-729.
Tremblay, L., Kohl, S.D., Rice, J.A. and Gagne, J.P. (2005) Effects of temperature, salinity, and dissolved humic substances on the sorption of polycyclic aromatic hydrocarbons to estuarine particles. Marine Chemistry 96(1-2), 21-34.
Turner, R.E., Overton, E.B., Meyer, B.M., Miles, M.S., McClenachan, G., Hooper-Bui, L., Engel, A.S., Swenson, E.M., Lee, J.M. and Milan, C.S. (2014) Distribution and recovery

trajectory of Macondo (Mississippi Canyon 252) oil in Louisiana coastal wetlands. Marine Pollution Bulletin 87(1), 57-67.
Volkman, J.K., Holdsworth, D.G., Neill, G.P. and Bavor, H. (1992) Identification of natural, anthropogenic and petroleum hydrocarbons in aquatic sediments. Science of The Total Environment 112(2), 203-219.
Wade, T.L., Sweet, S.T., Sericano, J.L., Guinasso, N.L., Diercks, A.R.R., Highsmith, R.C., Asper, V.L., Joung, D.D., Shiller, A.M. and Lohrenz, S.E. (2011) Analyses of water samples from the Deepwater Horizon oil spill: Documentation of the subsurface plume. Monitoring and Modeling the deepwater horizon oil spill: a record-breaking enterprise, 77-82.
Walter, T., Ederer, H., Först, C. and Stieglitz, L. (2000) Sorption of selected polycyclic aromatic hydrocarbons on soils in oil-contaminated systems. Chemosphere 41(3), 387-397.
Wang, S., Li, P., Liu, H., Li, J. and Wei, Y. (2010) The structure and optical properties of ZnO nanocrystals dependence on Co-doping levels. Journal of Alloys and Compounds 505(1), 362-366.
Wang, T., Liu, W., Xu, N. and Ni, J. (2013a) Adsorption and desorption of Cd (II) onto titanate nanotubes and efficient regeneration of tubular structures. Journal of Hazardous Materials 250, 379-386.
Wang, Y.-F., Hsieh, M.-C., Lee, J.-F. and Yang, C.-M. (2013b) Nonaqueous synthesis of CoOx/TiO2 nanocomposites showing high photocatalytic activity of hydrogen generation. Applied Catalysis B: Environmental 142–143(0), 626-632.
Wang, Z. and Fingas, M. (1997) Developments in the analysis of petroleum hydrocarbons in oils, petroleum products and oil-spill-related environmental samples by gas chromatography. Journal of Chromatography A 774(1), 51-78.
Wang, Z., Fingas, M. and Li, K. (1994) Fractionation of a light crude oil and identification and quantitation of aliphatic, aromatic, and biomarker compounds by GC-FID and GC-MS, part II. Journal of chromatographic science 32(9), 367-382.
Wang, Z., Li, K., Lambert, P. and Yang, C. (2007) Identification, characterization and quantitation of pyrogenic polycylic aromatic hydrocarbons and other organic compounds in tire fire products. Journal of Chromatography A 1139(1), 14-26.
Wangl, C., Yediler, A., Peng, A. and Kettrup, A. (1995) Photodegradation of phenanthrene in the presence of humic substances and hydrogen peroxide. Chemosphere 30(3), 501-510.
Wen, S., Zhao, J., Sheng, G., Fu, J. and Peng, P.a. (2002) Photocatalytic reactions of phenanthrene at TiO 2/water interfaces. Chemosphere 46(6), 871-877.
White, J.C. and Pignatello, J.J. (1999) Influence of bisolute competition on the desorption kinetics of polycyclic aromatic hydrocarbons in soil. Environmental Science & Technology 33(23), 4292-4298.
Whitehead, A., Dubansky, B., Bodinier, C., Garcia, T.I., Miles, S., Pilley, C., Raghunathan, V., Roach, J.L., Walker, N. and Walter, R.B. (2011) Genomic and physiological footprint of the Deepwater Horizon oil spill on resident marsh fishes. Proceedings of the National Academy of Sciences, 201109545.
Xia, K., Hagood, G., Childers, C., Atkins, J., Rogers, B., Ware, L., Armbrust, K., Jewell, J., Diaz, D. and Gatian, N. (2012) Polycyclic aromatic hydrocarbons (PAHs) in Mississippi seafood from areas affected by the Deepwater Horizon oil spill. Environmental Science & Technology 46(10), 5310-5318.

Xiong, L., Chen, C., Chen, Q. and Ni, J. (2011a) Adsorption of Pb(II) and Cd(II) from aqueous solutions using titanate nanotubes prepared via hydrothermal method. Journal of Hazardous Materials 189(3), 741-748.
Xiong, L., Sun, W., Yang, Y., Chen, C. and Ni, J. (2011b) Heterogeneous photocatalysis of methylene blue over titanate nanotubes: Effect of adsorption. Journal of colloid and interface science 356(1), 211-216.
Xiong, L., Yang, Y., Mai, J., Sun, W., Zhang, C., Wei, D., Chen, Q. and Ni, J. (2010) Adsorption behavior of methylene blue onto titanate nanotubes. Chemical Engineering Journal 156(2), 313-320.
Yamada, M., Takada, H., Toyoda, K., Yoshida, A., Shibata, A., Nomura, H., Wada, M., Nishimura, M., Okamoto, K. and Ohwada, K. (2003) Study on the fate of petroleum-derived polycyclic aromatic hydrocarbons (PAHs) and the effect of chemical dispersant using an enclosed ecosystem, mesocosm. Marine Pollution Bulletin 47(1–6), 105-113.
Yin, F., Hayworth, J.S. and Clement, T.P. (2015a) A tale of two recent spills-comparison of 2014 galveston bay and 2010 deepwater horizon oil spill residues. PloS one 10(2).
Yin, F., John, G.F., Hayworth, J.S. and Clement, T.P. (2015b) Long-term monitoring data to describe the fate of polycyclic aromatic hydrocarbons in Deepwater Horizon oil submerged off Alabama's beaches. Science of The Total Environment 508, 46-56.
Yu, H., Huang, G.H., An, C.J. and Wei, J. (2011) Combined effects of DOM extracted from site soil/compost and biosurfactant on the sorption and desorption of PAHs in a soil-water system. Journal of Hazardous Materials 190(1-3), 883-890.
Yu, H., Yu, J., Cheng, B. and Zhou, M. (2006a) Effects of hydrothermal post-treatment on microstructures and morphology of titanate nanoribbons. Journal of Solid State Chemistry 179(2), 349-354.
Yu, J., Yu, H., Cheng, B., Zhao, X. and Zhang, Q. (2006b) Preparation and photocatalytic activity of mesoporous anatase TiO 2 nanofibers by a hydrothermal method. Journal of Photochemistry and Photobiology A: Chemistry 182(2), 121-127.
Yu, J.G., Yu, H.G., Cheng, B. and Trapalis, C. (2006c) Effects of calcination temperature on the microstructures and photocatalytic activity of titanate nanotubes. Journal of Molecular Catalysis a-Chemical 249(1-2), 135-142.
Zhang, G., Huang, H., Li, W., Yu, F., Wu, H. and Zhou, L. (2012) Enhanced photocatalytic activity of CoO/TiO2 nanotube composite. Electrochimica Acta 81(0), 117-122.
Zhang, J., Zeng, J. and He, M. (2009) Effects of temperature and surfactants on naphthalene and phenanthrene sorption by soil. Journal of Environmental Sciences 21(5), 667-674.
Zhang, J., Zhang, Y., Lei, Y. and Pan, C. (2011) Photocatalytic and degradation mechanisms of anatase TiO2: a HRTEM study. Catalysis Science & Technology 1(2), 273-278.
Zhao, B., Zhu, L., Li, W. and Chen, B. (2005) Solubilization and biodegradation of phenanthrene in mixed anionic–nonionic surfactant solutions. Chemosphere 58(1), 33-40.
Zhao, D., Hunter, M., Pignatello, J.J. and White, J.C. (2002) Application of the dual-mode model for predicting competitive sorption equilibria and rates of polycyclic aromatic hydrocarbons in estuarine sediment suspensions. Environmental Toxicology and Chemistry 21(11), 2276-2282.
Zhao, D.Y., Pignatello, J.J., White, J.C., Braida, W. and Ferrandino, F. (2001) Dual-mode modeling of competitive and concentration-dependent sorption and desorption kinetics of polycyclic aromatic hydrocarbons in soils. Water Resources Research 37(8), 2205-2212.

Zhao, X., Gong, Y., O'Reilly, S. and Zhao, D. (2015) Effects of oil dispersant on solubilization, sorption and desorption of polycyclic aromatic hydrocarbons in sediment–seawater systems. Marine Pollution Bulletin.
Zheng, X., Shen, G., Li, Y., Duan, H., Yang, X., Huang, S., Wang, H., Wang, C., Deng, Z. and Su, B.-L. (2013) Self-templated synthesis of microporous CoO nanoparticles with highly enhanced performance for both photocatalysis and lithium-ion batteries. Journal of Materials Chemistry A 1(4), 1394-1400.
Zhou, W. and Zhu, L. (2005) Distribution of polycyclic aromatic hydrocarbons in soil–water system containing a nonionic surfactant. Chemosphere 60(9), 1237-1245.